

Molecular and functional
characterization of
inflammation-induced cell state
transitions in
malignant-transformed
melanocytes

Dissertation

zur

Erlangung des Doktorgrades (Dr. rer. nat.)

der Mathematisch-Naturwissenschaftlichen Fakultät
der Rheinischen Friedrich-Wilhelms-Universität Bonn

vorgelegt von

Julia R. Reinhardt

aus Ludwigsburg

Bonn, November 2018

Angefertigt mit Genehmigung der Mathematisch-Naturwissenschaftlichen Fakultät der
Rheinischen Friedrich-Wilhelms-Universität Bonn

1. Gutachter: Prof. Dr. Michael Hölzel

2. Gutachter: Prof. Dr. Waldemar Kolanus

Tag der Promotion: 17.09.2019

Erscheinungsjahr: 2019

Contents

List of Figures	x
List of Tables	xi
1 Summary	1
2 Zusammenfassung	3
3 Introduction	5
3.1 Melanoma - causes and consequences	5
3.1.1 Origin and development of melanoma	5
3.1.2 Risk factors for melanoma	6
3.1.3 The genetics of melanoma	7
3.2 Therapy of melanoma	9
3.2.1 Targeted therapy	9
3.2.2 Cancer immunoediting and checkpoint immune blockade	11
3.2.3 Therapy resistance and tumor heterogeneity	12
3.3 Melanoma phenotype switching	13
3.3.1 Concepts of phenotypic heterogeneity	13
3.3.2 Phenotypic plasticity in melanoma	14
3.3.3 The tumor microenvironment shapes melanoma cell states	15
3.3.4 A regulatory network of melanoma phenotype switching	18
4 Objectives of this study	21
5 Material and methods	23
5.1 General laboratory equipment	23
5.1.1 Instruments and equipment	23
5.1.2 Software	24
5.1.3 Consumables and plasticware	24
5.1.4 Chemicals	25
5.1.5 Cell culture substances	27
5.1.6 Recombinant proteins and peptidases	27
5.1.7 Cell culture stimulants and inhibitors	27
5.1.8 Commercially available kits, reagents and enzymes	28
5.1.9 Primary antibodies for immunoblot	29
5.1.10 Secondary antibodies for immunoblot	29

5.1.11	Antibodies for flow cytometry	30
5.1.12	Molecular biology - buffers, media and agar	30
5.1.13	Cell culture media and buffers	32
5.1.14	Lysis buffers	33
5.1.15	Immunoblot buffers and preparation of SDS PAGE gels	34
5.1.16	Cell lines and bacteria	36
5.1.17	Primer sequences	36
5.2	Experimental procedures	41
5.2.1	Generation of expression vectors	41
5.2.2	Cell culture and generation of cell lines	44
5.2.3	Stimulation and manipulation of cells	47
5.2.4	RNA isolation, cDNA synthesis and qPCR	48
5.2.5	ChIP qPCR	49
5.2.6	Immunoblotting	50
5.2.7	Flow cytometry based methods	51
5.2.8	Bisulfite conversion based methylation analysis by deep sequencing	52
5.2.9	Sample preparation and running deep sequencing	53
5.2.10	Bioinformatic analyses	55
5.2.11	Statistics	58
6	Results	59
6.1	CD73 is a marker for melanoma cell plasticity	59
6.1.1	Bioinformatic analysis on a large panel of melanoma cell lines reveals CD73 as a marker expressed upon <i>nascent invasiveness</i>	59
6.1.2	Established <i>invasive</i> phenotype markers in melanoma are not suitable for describing a <i>nascent invasive</i> phenotype	63
6.1.3	A <i>nascent invasive</i> phenotype is primed to phenotype switching	63
6.1.4	CD73 expression in <i>nascent invasive</i> melanoma cells is associated with mitogenic and inflammatory signaling pathways	64
6.2	Mitogenic inflammatory signaling drives CD73 expression in melanoma through the MAPK pathway	66
6.2.1	A melanoma cell line panel as a model to study CD73 regulation <i>in vitro</i>	66
6.2.2	Inflammatory and mitogenic signaling cooperatively induce CD73 expression	67
6.2.3	Epigenetic remodeling at the <i>NT5E</i> locus is required for induction of CD73	68
6.2.4	CD73 induction in melanoma by both mitogenic and inflammatory stimuli depends on MAPK signaling cascade activation	69
6.2.5	Inflammatory macrophage supernatant constitutes a source for melanoma cell CD73 induction	71
6.2.6	Baseline CD73 expression depends on MAPK signaling in melanoma	72

6.3	JUN/ AP1 complexes control transcription of <i>NT5E</i> in dependence on MAPK activation	75
6.3.1	The search for transcription factors that correlate with CD73 expression in melanoma points to JUN	75
6.3.2	Cooperative upregulation of CD73 is accompanied by the induction of JUN/ AP1 family members	76
6.3.3	JUN strongly induces melanoma cell CD73 in dependence of MAPK activation	77
6.3.4	A conditional expression system to study defined JUN transcriptional activity on the <i>NT5E</i> genomic locus	79
6.3.5	Transient JUN induction establishes a MTF ^{high} / CD73 ^{high} phenotype in melanoma	80
6.3.6	ChIP qPCR reveals prominent binding of JUN to AP1 consensus sites located in <i>NT5E</i>	81
6.4	A CRISPR/Cas9-FACSsorting enhancer screening approach for functional validation of AP1 binding sites in <i>NT5E</i>	82
6.4.1	Development of the CRISPR/Cas9-FACSsorting enhancer screen	82
6.4.2	JUN induces CD73 by binding to a specific AP1 consensus site in <i>NT5E</i>	83
6.4.3	Positional mutation analysis constitutes a method for the identification of previously unknown enhancer elements with single base pair resolution	85
6.4.4	CD73 baseline expression depends on JUN binding to the first intronic AP1 #5 site in <i>NT5E</i>	86
6.4.5	Disruption of the first intronic AP1 #5 site in <i>NT5E</i> leads to long term depletion of CD73	89
7	Discussion	91
7.1	The trajectory of melanoma cell state transitions	91
7.2	CD73, a melanoma plasticity marker with an important role in tumor immunosuppression	97
7.3	Survey on the functional relevance of CD73 expression for EMT and inflammatory phenotype switching	99
7.4	Melanoma CD73 expression links to primary and acquired resistance towards cancer immunotherapy	100
7.5	Prognostic implications of CD73 marker expression on <i>nascent invasive</i> melanoma	102
7.6	The relevance of MAPK signaling for CD73 expression on melanoma cells	102
7.7	Conclusion	104
	Abbreviations	107
	Bibliography	111

Acknowledgment / Danksagung	139
List of publications	141

List of Figures

3.1	Melanocyte function and the <i>Clark Model</i> for development and progression of melanoma	6
3.2	Risks factors for melanoma	7
3.3	Genetic drivers of melanoma	8
3.4	Melanoma therapy	10
3.5	Melanoma plasticity is a result of tumor cell - microenvironment interactions	16
3.6	A signaling network regulating melanoma cell phenotype switching . . .	19
6.1	CD73 marks a <i>nascent invasive</i> phenotype in melanoma	61
6.2	Common <i>invasive</i> markers fail to indicate early phenotype switching . .	62
6.3	A <i>nascent invasive</i> phenotype is primed to phenotype switching	64
6.4	GSEA identifies mitogenic and inflammatory pathways in the regulation of melanoma CD73 expression	65
6.5	A melanoma cell line panel confirms <i>in silico</i> plasticity analyses <i>in vitro</i>	67
6.6	Cooperative CD73 induction by mitogenic and inflammatory stimuli . .	68
6.7	Epigenetic remodeling induces CD73 expression and susceptibility to mitogenic inflammatory stimulation	69
6.8	MAPK cascade signaling orchestrates mitogenic inflammatory CD73 induction in melanoma	70
6.9	THP1 macrophage secretome induces melanoma cell CD73 expression .	71
6.10	Baseline CD73 expression is decreased by MAPK inhibition	72
6.11	Cell cycle arrest does not account for the reduction of CD73 expression	73
6.12	Prolonged MAPK blockade further decreases - rehabilitating MAPK activity restores CD73 expression	73
6.13	Testing an inhibitor panel for CD73 regulation beyond MAPK signaling	74
6.14	JUN is a transcription factor with ENCODE annotated binding in <i>NT5E</i> and highly correlates with melanoma cell CD73 expression	75
6.15	<i>Invasive</i> cell state correlates with CD73 / JUN and induction of CD73 is accompanied by accumulation of JUN/ AP1 factors	77
6.16	Ectopic JUN induces CD73 in MaMel.15 upon stabilization by mitogenic stimulation	78
6.17	Ectopic JUN boosts CD73 expression in <i>nascent invasive</i> melanoma cells	78
6.18	Establishment of a JUN conditional cell line system in MaMel.79b _{late} .	79
6.19	Transient JUN in MaMel.79b _{late} JUN-CitrineDOX establishes a MITF ^{high} CD73 ^{high} phenotype	80

6.20	Prominent binding of JUN to <i>NT5E</i> intronic enhancer region in ChIP qPCR	81
6.21	Design of the CRISPR/Cas9-FACSorting enhancer screening approach	83
6.22	CRISPR/Cas9-based FACSorting approach for enhancer screening identifies AP1 #5 site for CD73 induction by JUN	84
6.23	Proof of principle positional mutation analysis identifies the canonical AP1 #5 site motif for CD73 regulation by JUN	86
6.24	The AP1 #5 site is relevant for CD73 expression in SK.Mel28, MaMel.85, MaMel.54a, and MaMel.65	87
6.25	Positional mutation analysis confirms the relevance of AP1 #5 for baseline CD73 expression	89
6.26	SK.Mel28 show long term depletion of CD73 when enriching on AP1 #5 site disruption by FACSorting	90
7.1	<i>Nascent invasive</i> phenotype switching becomes apparent in single cell RNAseq data by Aibar <i>et al.</i> for coinciding MITF and invasive regulon activity	95
7.2	<i>Nascent invasive</i> phenotype switching in comparison to the plasticity model proposed by Tsoi <i>et al.</i>	96
7.3	A model of <i>Nascent invasive</i> phenotype switching in melanoma in comparison to the <i>Waddington's landscape</i> of partial EMT	105

List of Tables

5.1	Instruments and equipment	23
5.2	Software	24
5.3	Consumables and plasticware	24
5.4	Chemicals	25
5.5	Cell culture substances	27
5.6	Recombinant proteins and peptidases	27
5.7	Cell culture stimulants and inhibitors	27
5.8	Commercially available kits, reagents and enzymes	28
5.9	Primary antibodies for immunoblot	29
5.10	Secondary antibodies for immunoblot	29
5.11	Antibodies for flow cytometry	30
5.12	Preparation of EtBr agarose gels	31
5.13	Preparation of SDS PAGE gels	35
5.14	Cell lines and bacteria	36
5.15	Primers for cloning	36
5.16	Primers for analyzing mRNA expression in qPCR	37
5.17	Primers for ChIP qPCR	37
5.18	sgRNA oligonucleotide sequences	38
5.19	Primers for first level MiSeq PCR	38
5.20	Barcoding fwd-primers for second level MiSeq PCRs	39
5.21	Barcoding rev-primers for second level MiSeq PCRs	39
5.22	Passaging ratios and schemes for the individual cell lines	45

1 Summary

Cellular phenotype plasticity is a hallmark of embryonic development in order to achieve cell type specification from precursor populations. The molecular mechanisms orchestrating phenotypic plasticity are of interest because they may also help to understand how its dysregulation contributes to disease development, in particular cancer. The neural crest is an embryonic cell population that is well known for its migratory capacity and phenotypic plasticity. Malignant melanoma, an aggressive type of skin cancer, is a neural crest-related malignancy originating from the pigment producing melanocytes in the epidermis. In the recent years, it became clear to the field of neural crest biologists that melanoma is an ideal model system to study basic principles of phenotype plasticity of the neural crest cell lineage. Melanoma cells are highly prone to phenotype switching and this is linked to the expression level of MITF (Microphthalmia-associated transcription factor), the master transcription factor of the melanocyte cell lineage that induces the expression of pigmentation-related genes among other effects. On this basis, melanoma cell state transitions have been classified as a binary switch between a differentiated MITF^{high} *proliferative* phenotype and a dedifferentiated MITF^{low} *invasive* phenotype. However, intermediate melanoma cell states, as well as the detailed molecular mechanisms concerting the transitions remain elusive.

In this study we identified a novel *nascent invasive* cell state in melanoma. This phenotype exhibits early inflammatory and early invasive signaling programs although keeping the differentiation signature. Expression of the cell surface 5'ectonucleotidase CD73 was revealed as a marker for *nascent invasiveness* and further increased upon full dedifferentiation. Interestingly, CD73 is not only known as a mesenchymal stem cell marker, but also involved in tumor immunosuppression and therefore emerges as a target for cancer immunotherapy. Computational and *in vitro* studies confirmed a critical cooperation of mitogenic growth factors and pro-inflammatory cytokines inducing CD73 expression. This was dependent on the MEK-ERK signaling cascade and coordinated by the transcription factor c-Jun, which critically bound to an intronic enhancer within the CD73 genomic locus. The findings reported in this thesis provide novel mechanistic insight into neural crest plasticity, melanoma cell state transitions and the regulation of a CD73-dependent immunosuppressive tumor microenvironment.

2 Zusammenfassung

Phänotypische Plastizität ist ein entscheidender Mechanismus in der Embryonalentwicklung um die Vielzahl von Zelltypen aus Vorläuferpopulationen zu erzeugen. Die zugrunde liegenden molekularen Mechanismen sind von großer Bedeutung, da sie auch unser Verständnis von Pathomechanismen verbessern wie z.B. bei Krebs. Die Neuralleiste ist eine embryonale Vorläuferzellpopulation, bekannt für eine hohe Migrationsaktivität und phänotypische Plastizität. Das maligne Melanom, ein aggressiver Hautkrebs, ist ein Abkömmling der Neuralleiste und entsteht aus den Melanozyten in der Epidermis. Im Feld der Neuralleistenbiologie ist es in den letzten Jahre klar geworden, dass das Melanom ein ideales Modell ist für die Untersuchung der phänotypischen Plastizität. Melanomzellen neigen stark zu Phänotypveränderungen und zentral ist dabei die Expression von MITF (Mikrophthalmie-assoziiertes Transkriptionsfaktor), dem Schlüsseltranskriptionsfaktor der melanozytären Zellreihe. Bisher wurden Zellzustände in Melanomzellen daher binär in einen differenzierten MITF-reichen und *proliferativen* Phänotyp sowie einen de-differenzierten MITF-armen und *invasiven* Phänotyp eingeteilt. Jedoch verbleiben Zwischenzustände sowie die genauen molekularen Mechanismen, die diese Übergänge kontrollieren, unzureichend erforscht.

In dieser Studie konnten wir einen neuartigen *früh-invasiven* Zellzustand in Melanomzellen identifizieren, der durch einen Anstieg entzündlicher und invasiver Signalprogramme in einer Subpopulation von differenzierten Melanomzellen gekennzeichnet ist. Wir fanden heraus, dass die membranständige 5'Exonukleotidase CD73 einen Marker für diese *früh-invasive* Zellpopulation darstellt und bei vollständiger *invasiver* Phänotypumschaltung von Melanomzellen weiter hochreguliert wird. CD73 nicht nur als Marker mesenchymaler Stammzellen bekannt, sondern auch bedeutsam für Tumor-Immunsuppression und damit ein potentielles Ziel für Immuntherapien gegen Krebs. Bioinformatische Analysen und *in vitro* Studien wiesen auf ein kritisches Zusammenspiel von mitogenen Wachstumsfaktoren und pro-inflammatorischen Zytokinen bei der Induktion von CD73 hin. Die Induktion von CD73 war dabei abhängig von der MEK-ERK-Signalkaskade und wurde koordiniert von dem Transkriptionsfaktor c-Jun über Bindung an einen intronischen Enhancer im CD73 Gen. Die Ergebnisse dieser Arbeit bieten neue Einblicke in Prozesse welche Plastizität der Neuralleiste und im Melanom steuern, insbesondere in die Regulation eines CD73-abhängigen immunsuppressiven Tumormikromilieus, und erleichtern damit die rationale Entwicklung zukünftiger kombinatorischer Immuntherapien.

3 Introduction

3.1 Melanoma - causes and consequences

3.1.1 Origin and development of melanoma

Melanoma arises from malignant transformation of melanocytes, the pigment producing cells of the skin. Because of its neural crest origin it forms an highly aggressive and early metastasizing form of cancer. Melanoma cells display high invasiveness, adaptivity and chemoresistance leading to poor clinical outcome and death if not diagnosed at an early stage. In contrast to local restricted and early stage melanoma, which can be cured by surgical excision in most cases [227], advanced melanoma leads to death within 6-12 months [254]. Hence, even though melanomas make up only about 5% of skin cancers, they cause most of skin cancer related death [188]. Alarmingly, in contrast to other cancer entities, melanoma incidence in the western world is still rising and expected to double every 10 - 20 years [154, 85].

During development, transitory and highly invasive cells of the neural crest migrate throughout the body to build the peripheral nervous system as neurons and Schwann cells, and constitute cells of the endocrine system, facial cartilage and smooth muscle [244]. Within hair follicles and the basal layer of the skin, they form melanocytes [247, 94]. The function of melanocytes is to protect the DNA at those outer parts of the body from DNA damage by highly energetic ultraviolet (UV) radiation (Figure 3.1). Damaged DNA from keratinocytes stimulates the production and secretion of melanosome vesicles in melanocytes, which contain the pigment molecule melanin. Melanin protects cellular DNA from reactive oxygen species (ROS) and functions like a shield around the nucleus of keratinocytes in the skin, causing the effect of tanning [247, 94].

The *Clark Model* on melanoma development proposes several sequential steps during melanocyte transformation (Figure 3.1) [43]: A cell that is encountering DNA damage accumulates errors during DNA repair, leading to an increase in mutational load. In case tumor-suppressor genes or proto-oncogenes become affected, this results in aberrant proliferation and the development of a hyperplastic lesion. Still, cell cycle control mechanisms curtail uncontrolled growth and mediate oncogene-induced cellular senescence, resulting in a benign melanocytic nevus that may remain dormant or progress

after prolonged time [165]. In contrast, dysplastic nevi are associated with rapid, irregular growth and contingent malignant progression [95]. Bypass of senescence is the consequence of further somatic mutations or genetic predispositions leading to cell cycle deregulation [20]. Melanoma first spreads horizontally within the epidermis, termed radial growth phase (RGP). Upon progression it comes to loss of adhesion and gain of migratory capacities initiating a vertical growth phase (VGF) that allows escape from tight control by keratinocytes. Vertical migration via stromal cell interactions into the dermis passes the basement membrane, and eventually leads to metastatic dissemination [93]. Today we know that only about 20-30% of melanoma arise from transformation of benign melanocytic or dysplastic nevi, yet the majority of 70-80% develop *de novo* from melanocytes with no previously detected hyperplastic lesion [16] (Figure 3.1, blue dotted lines). Transformation from RGP to VGF has major impact on melanoma malignancy, hence tumor thickness as measured by *Breslow Depth* is still the best prognostic parameter [28, 254].

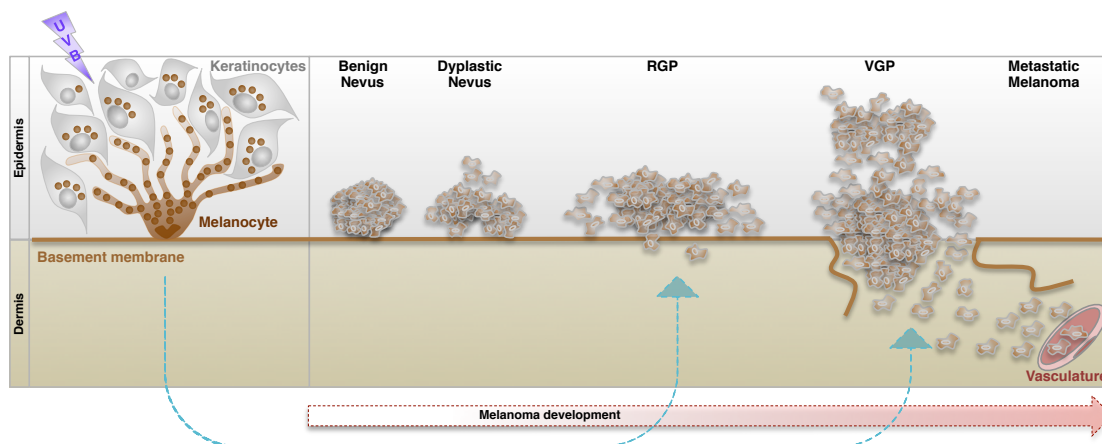


Figure 3.1: **Melanocyte function and the Clark Model for development and progression of melanoma** Melanocytes are located in the basement membrane and, upon UV radiation transfer melanin pigment to keratinocytes via dendrite processes. Melanin located around the nucleus is scattering energetic light in order to protect from DNA damage. Oncogenic mutations cause hyperplastic proliferation of melanocytes, resulting induction of senescence and benign melanocytic or dysplastic nevi. Upon cell cycle deregulation horizontal spreading in a radial growth phase (RGP) follows. Malignancy of melanoma is achieved upon progression to a vertical growth phase (VGF), eventually resulting in metastasis. Dotted arrows indicate potential conversions in melanoma development.

3.1.2 Risk factors for melanoma

The major known risk factor for the development of melanoma is intermittent and heavy UV radiation, especially during childhood [150]. Especially UVB radiation is highly genotoxic by causing cyclobutane pyrimidine dimers (CPDs) between adjacent cytosine (C) and thymine (T) residues. Those alterations are error-prone in repair, and lead to the

characteristic UVB signature mutations CT or CC into TT. Therefore melanomas exhibit the highest mutational load across all tumor entities with more than 10 mutations per DNA megabase [156, 6]. UV radiation also provokes microenvironmental changes such as the release of growth hormones and immune remodeling factors by keratinocytes, shaping and impairing proper immune cell functions and *vice versa* provoking gain of an embryonic, aggressive phenotype in the transforming melanocytes [13, 156]. Additional risk factors for the development of melanoma are summarized in Figure 3.2, and include a family history of melanoma [16], personal history of melanoma [95], increased occurrence of nevi [84] as well as drug-related [153] and age-related immunosuppression [253]. Pale, fair-skinned and, most of all, red-haired individuals are at highest risk of developing cutaneous melanoma [82]. Accordingly, in Australian and New Zealand inhabitants melanoma manifests with an incidence rate of approximately 60 cases per 100,000 in a year, whereas 1 in 100,000 dark-skinned African people develops cutaneous melanoma [67]. Additionally, there is a gender dependent preferential location of cutaneous melanoma: Males are more likely to develop melanoma on the back, melanomas in females are more often found on the legs [210].

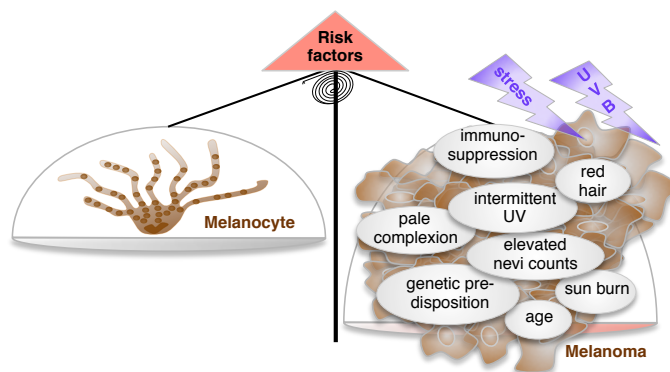


Figure 3.2: **Risks factors for melanoma** Schematic overview on the major risk factors for melanoma development.

3.1.3 The genetics of melanoma

Genetic alternations promoting melanoma development can be splitted into germline and somatic mutations and are depicted in Figure 3.3, A. About 10% of melanoma cases trace back to familiar genetic defects in the *CDKN2A* or *CDK4* genes leading to a deregulated cell cycle or in the *MC1R* locus disturbing central melanocytic signaling cascades and leading to impaired pigmentation, pale skin and red hair [40]. Interestingly, individuals with germline mutations in *p53*, who are highly prone to cancer development, are only rarely affected by melanoma [158]. About 50% of familiar melanoma lack a clear genetic basis so far [16]. Sporadic somatic mutations in combination with environmental factors account for 90% of cutaneous melanomas in individuals with no familiar

predisposition (Figure 3.3, A). In 85% of those melanomas, primary driver mutations are found to alter mitogen-activated protein kinases (MAPK) pathway activity [5, 132]. The MAPK signaling cascade is essential for melanoma growth and progression [72]. It mediates signaling downstream of receptor tyrosine kinases (RTKs), i.e. cMET, FGFR and cKIT in melanoma, as well as G protein coupled receptors (GPCRs) [72]. It is composed of several sequential kinase modules that specify, modify and amplify signaling transmission for regulation of target gene transcription as schematically illustrated in Figure 3.3, B. Ligand induced receptor trans-phosphorylation promotes RAS activation by GDP to GTP exchange. RAS-GTP, if not instantly inactivated by NF1, activates kinase signal transmission by phosphorylation of RAF, which in turn phosphorylates MEK, that phosphorylates ERK. pERK finally translocates to the nucleus and modulates target transcription factor (TF) activity. About 50% of melanoma harbor alterations in the rapidly accelerated fibrosarcoma protein kinase B (*BRAF*) gene causing constitutive signaling activation independent from RAS [50]. BRAFV600E accounts for 90% of those genetic aberrations, overall leading to an 600x hyper-activation in comparison to wildtype (WT) BRAF [266]. Mutually exclusive to deregulated BRAF are MAPK hyper-activating mutations in the neuroblastoma RAS viral oncogene homolog (*NRAS*) gene, which occur in 20% of melanoma and most commonly affect the position Q61 [115]. Interestingly, common BRAF and NRAS mutations do not exhibit a characteristic UV signature and are believed to result from UV induced genotoxic stress, such as ROS [105, 63]. Recently, the era of deep sequencing revealed *NF1* inactivation mutations in about 15% of melanomas to constitute the third frequent driver mutation, leaving 15% BRAF/NRAS/NF1 triple WT melanomas that harbor rare, or so far unknown primary driver mutations [132, 105].

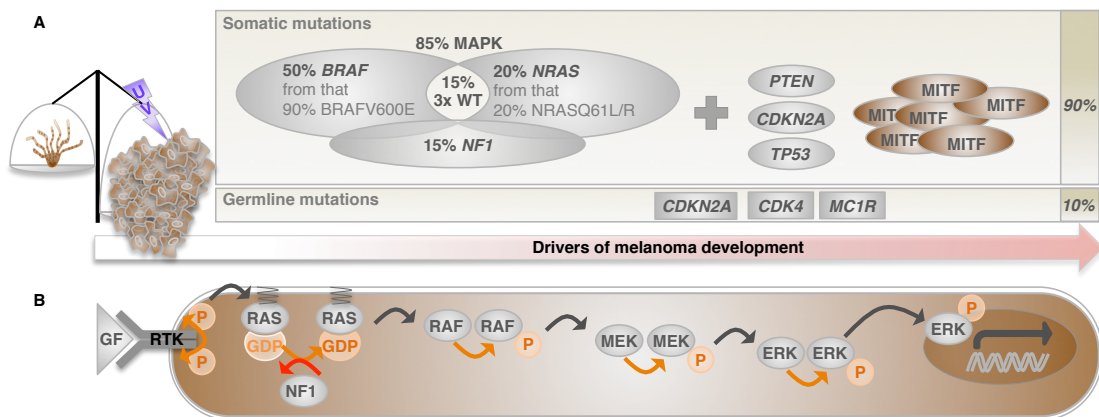


Figure 3.3: **Genetic drivers of melanoma.** **(A):** Illustration on the genetics of melanoma development, with primary somatic driver mutations leading to MAPK hyper-activation and main secondary driver mutations, which are important for overcoming oncogene-induced senescence. Germline mutations which predispose for melanoma are indicated below. 3x WT = BRAF/NRAS/NF1 triple wildtype. Right side: 90% of melanoma sporadic, 10% of familial predisposition. **(B):** Schematic overview on molecular signal transduction by the MAPK cascade. P = phosphorylation.

Sole constitutive MAPK pathway activation causes oncogene-induced senescence [54], which is giving an explanation for about 80% of benign melanocytic nevi harboring BRAF mutations [187]. Secondary driver mutations in melanoma that bypass senescence cause the loss of p16^{INK4a}, p14^{ARF} or p53 [184]. Also, an hyper-activation of AKT / phosphatidylinositol-3-kinases (PI3K) signaling is observed in up to 40% of melanoma, predominately due to inactivating mutations in the negative regulator *PTEN*, but also due to amplification of *AKT* [228]. Besides *MITF* amplification and overexpression is found in 4-21% of melanoma patients [105, 86].

3.2 Therapy of melanoma

Prognosis and therapy of melanoma largely depends on its stage. As long as melanoma growth is locally restricted surgical excision presents the first choice of treatment and a 5 year survival rate of 98% is encouraging [227] (Figure 3.4, A). However, metastasizing melanomas evolve rapidly and unnoticed due to their small size, leading to a rapid drop of the 5 year survival rate with less than 10% for treated patients [83]. Poor survival was also a result of the limited and poorly effective options for treatment. Only 10-15% of patients benefit from DNA-alkylating chemotherapy by Dacarbazine, which for a long time represented the only FDA approved treatment for advanced melanoma, but still did not improve the overall survival [254]. Also, high dose IFN therapy, that was introduced as adjuvant treatment after surgery, did not show a clear improvement of overall survival, while substantial side-effects had to be tolerated [128, 127]. High dose of IL2, that was introduced subsequently, achieved significant responses in a small subset of patients, yet showed high toxicity [12]. After a long time of fruitless research, therapy of advanced melanoma was revolutionized twice by the introduction of targeted therapy and immune checkpoint blockade in the early 2010s (Figure 3.4, B and C).

3.2.1 Targeted therapy

In the year 2002, the discovery of mutant BRAF driving melanoma proliferation and survival in half of all patients pushed the development of targeted therapy by MAPK cascade small molecule inhibitors [269, 50]. In 2011, Vemurafenib was the first FDA approved inhibitor targeting mutant BRAF, leading to rapid remission of multiple metastases in patients suffering from metastatic melanoma with significant improved overall survival and response rates of 84% and 48% after 6 month, respectively. In comparison, in the Dacarbazine control arm, only 5% of patients responded to the treatment and after 6 months only 64% were still alive [37, 124]. In 2013, Dabrafenib as a further inhibitor of mutant BRAF and Trametinib as a non-competitive inhibitor of MEK1/2, were approved for the treatment of advanced melanoma, both showing similar benefits

like Vemurafenib [97, 78]. ERK inhibitors, such as SCH772984, are under clinical investigation currently. Despite the great enthusiasm from initial therapeutic responses, major drawback occurred by the nearly imperative acquired resistance after 5-12 months and the development of additional metastases [37, 97, 157]. Several targeted therapy combinatorial treatment approaches were tested in clinical trails with the hope to circumvent common resistance pathways. Even though achieving an increased overall and progression free survival, therapy resistance, relapse and death of patients occurred eventually [137, 145, 77].

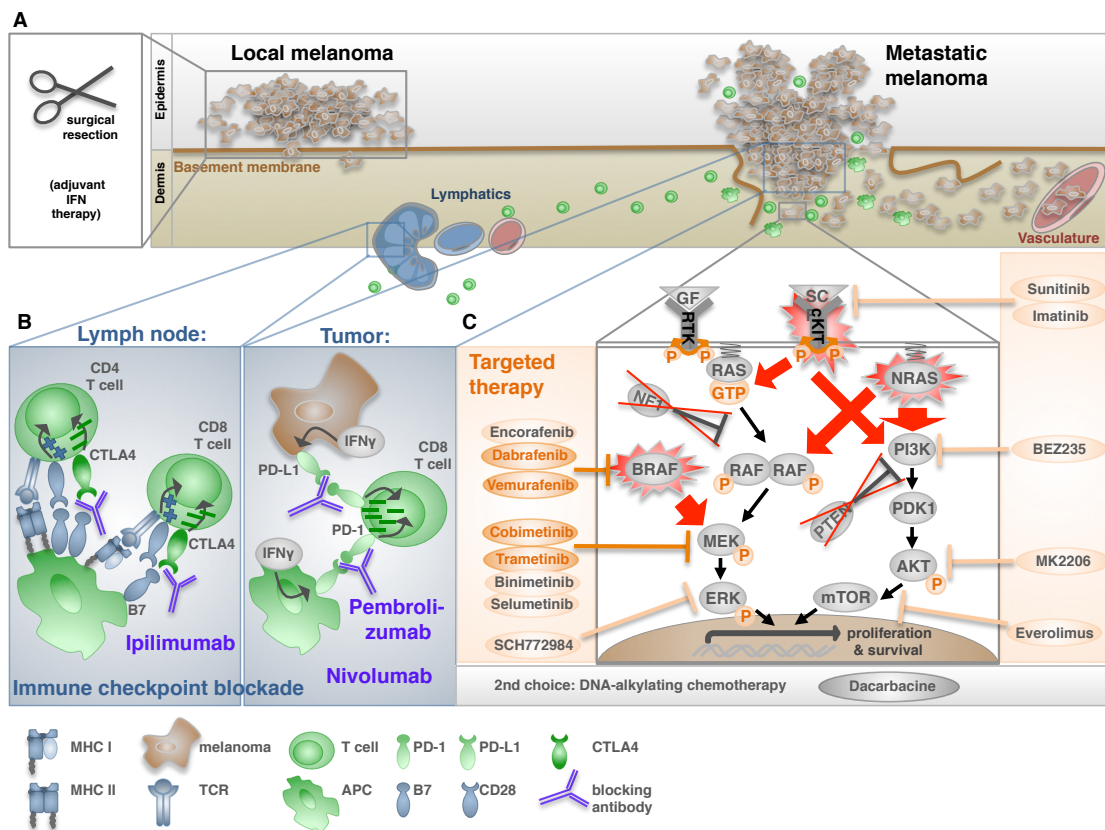


Figure 3.4: **Melanoma therapy (A):** Schematic illustration on low grade, local restricted melanoma and advanced, metastatic melanoma. **(B):** Close up of immune checkpoint regulation in lymph node and tumor. CTLA-4 ligation inhibits naïve T cell activation in the lymph node, PD-1/ PD-L1 interaction terminates T cell response in the tumor, which occur in response to induction of PD-L1 on tumor and APCs by IFN γ . Monoclonal antibodies Ipilimumab and Pembrolizumab / Nivolumab block CLTA4 and PD-1 ligation, respectively. **(C):** Intracellular signaling cascades that are commonly deregulated in melanoma and respective proteins addressed by targeted therapy. Black arrows indicate physiological signaling cascades. Red accentuations and red arrows illustrate the various oncogenic aberrations that drive melanoma cell proliferation and survival. Orange inhibitors are FDA approved for melanoma therapy, beige inhibitors are currently tested in clinical trials. P = phosphorylation.

Further options of targeting PI3K-AKT-mTOR signaling in melanoma are of high interest, especially for patients suffering from NRAS mutant melanoma with so far no

established targeted therapy and for patients suffering from BRAF mutant melanoma with primary resistance to BRAF inhibition (BRAFi) by loss of *PTEN* [254]. Combining MAPK inhibition (MAPKi) and PI3K inhibition (PI3Ki) has achieved promising results, overcoming resistance development *in vitro* [92] and clinical trials are under development. Even though targeting cKIT by Imatinib in previously unselected advanced melanoma has failed to achieve significant results in clinical trials [258], ongoing studies on patients selected on melanoma with rare *KIT* mutations are promising [35]. An overview on currently available targeted therapies for advanced melanoma and drugs that are in clinical testing is given in Figure 3.4, C.

3.2.2 Cancer immunoediting and checkpoint immune blockade

The idea that the immune system detects and fights malignant transformation has been proposed already in 1957 by Paul Ehrlich and MacFarlane Burnet [65, 30]. In the following decades, evidence on the existence of tumor-associated antigens and tumor-specific immune cells accumulated. The identification of melanoma-associated-antigens provided suitable targets for therapeutical stimulation of an anti-tumor immune response. Melanoma-associated-antigens include melanocytic proteins that are expressed in high abundance in melanoma, such as Melan-A, gp100, TRP1 and TRP2, and the cancer testis antigens MAGE-1, MAGE-2 and NY-ESO-1. With respect to these findings, highly personalized and labor-intensive adoptive T cell transfer (ACT) therapies have been developed. ACT involves the *ex vivo* activation and expansion of a patient's tumor-specific T cells, for strengthening anti-tumor immune responses upon re-infusion and has displayed durable clinical effects in a fraction of melanoma patients [204]. Latest research focusses on the development of genetically engineered chimeric antigen receptor (CAR) T cells, allowing the bypass of tumor immunosuppression and HLA restricted antigen detection [61].

Immune checkpoint blockade brought major advances for the therapy of advanced melanoma and for the first time, long term effective responses and durable remissions were seen [104, 212]. It is based on Schreiber's model, which proposes a pre-existing anti-tumor immune response that has been shut off by the tumor in a co-evolutionary process of tumor immunoediting [60, 59]. Tumor immunoediting harnesses the versatile mechanisms of the immune system to control excess inflammation and prevent auto-immunity, in order to hide from immune recognition [60, 59]. Blocking negative immune checkpoints aims on intrinsic reactivation of the patient's own anti-tumor immune response, as summarized in Figure 3.4, B [200]. The first immune checkpoint inhibitor for melanoma therapy was Ipilimumab, a fully humanized blocking antibody against cytotoxic T-lymphocyte-associated protein 4 (CTLA-4), which is a negative immune checkpoint receptor highly expressed on dysfunctional T cells in the tumor [104]. Under physiological conditions, CTLA-4 prevents self-recognition of T cells after thymus maturation. With respect to this, it prohibits the activation of naïve T-cells in the

lymph node by interfering with co-stimulatory CD28-B7 signaling during T cell - antigen presenting cells (APC) interactions and leading to T cell anergy (Figure 3.4, B left side) [134, 265]. Subsequent clinical studies directed against the programmed cell death protein 1 (PD-1) / programmed cell death protein 1 ligand 1 (PD-L1) axis, achieved even more remarkable results and lead to accelerated FDA approval of the PD-1 monoclonal blocking antibodies Nivolumab and Pembrolizumab [202, 203, 251, 42]. PD-1 is expressed on activated T cells, B cells and myeloid cells and operates in the effector phase of an immune response within peripheral tissues by ligation to either PD-L2 on B cells and macrophages, or PD-L1, which can be induced by $IFN\gamma$ during inflammation in a variety of tissues, including tumors (Figure 3.4, B right side) [17]. PD-1 - PD-L1/PD-L2 interaction terminates T cell responses and leads to an exhausted phenotype, which is important for the establishment of peripheral tolerance and at the same time a mechanism commonly harnessed by tumor cells [76, 270].

With the FDA approval of Ipilimumab, Nivolumab and Pembrolizumab the treatment scheme of advanced melanoma was restructured and immune checkpoint therapy was set as the new frontline, replacing Dacarbazine chemotherapy [202, 203, 251, 104, 42]. Considering the immunogenic effects that have been attributed to MAPK blockade in melanoma, a combination of targeted therapy and checkpoint immune therapy seems highly promising [31, 26]. However, first approaches in this direction, combining BRAFi and CTLA-4 blockade were unsuccessful in clinical trials due to toxicity issues [199]. Further attempts, combining MEKi and PD-1 blockade seems to be able to circumvent BRAFi-mediated paradoxical T cell reactivation and associated toxicity [21]. Investigations on a triple blockade of MEK, BRAF and PD-1 are currently ongoing [198]. Long-term follow-up studies on immune checkpoint inhibitors reveal enduring complete remission in a fraction of metastatic melanoma patients [212]. The ongoing success of immune checkpoint blockade has unleashed the dream of curing advanced melanoma and current research focusses on the evaluation of further immunomodulatory molecules as targets for combinatorial immunotherapy.

3.2.3 Therapy resistance and tumor heterogeneity

Tumor heterogeneity is the main obstacle during cancer therapy and a major cause for therapy resistance [75]. In melanoma both, spatial and temporal heterogeneity, have been described [219, 141]. On a histomorphological level melanoma heterogeneity is readily observable by the presence or absence of pigmentation [14]. Moreover, the broad histomorphological spectrum can complicate diagnosis, as melanomas can even adopt morphologies of schwannomas or neurofibromas [211, 109].

One part of tumor heterogeneity and resulting consequences for therapy resistance is explained by the gene-centric theory of clonal evolution, which follows the darwinistic principle "survival of the fittest". During cancer development genomic instability together with unlimited proliferation facilitates the accumulation of mutations [75, 161, 173]. This leads to high genetic diversification of the offspring and establishes the basis of an

iterative selection process in favor of cancer cells with optimal environmental adaptation [75, 161, 173]. Branching of clones rather than linear clonal evolution generates high diversity in coexisting tumor cell clones with individual mutational signatures [89]. According to this concept, therapy resistance is the result of selection for tumor cell clones with genetic aberrations enabling the bypass of treatment.

One can discriminate between primary therapy resistance, defined by a given predisposition of a tumor to escape from therapy, and acquired therapy resistance, that describes *de novo* changes arising under therapy. As an example, primary resistance against targeted therapy in melanoma is associated with the expression of BCL2A1 [96], loss of PTEN [183], activation of CCND1 [229] or mutations in *CDKN2A* and *CDK4* [40]. Acquired therapy resistance is caused by MAPK signaling re-activating mutations in about 70% of cases, and in 22% by mutations activating the PI3K/AKT pathway [225].

Clearly, selection on cancer cells with survival benefits due to genetic traits is decisive for therapy resistance, yet not sufficient to explain the complete spectrum of treatment responses, in both targeted therapy and immunotherapeutic approaches. In the recent years, we have realized that both, phenotypic and genetic diversity contributes to tumor heterogeneity. Reciprocal interactions between tumor cell subpopulations and cells of the tumor microenvironment impact on the phenotype and behavior of a tumor, enabling rapid adaptation to environmental changes during therapeutic interventions [159]. Non-genetic heterogeneity relates to differences in tumor cell differentiation, metabolic and transcriptional programs, tumor cell immunogenicity and composition of the tumor microenvironment [155]. Today we know that such phenotypic heterogeneity explains up to 40% of existence or emergence of therapy resistance [225, 260, 264]. In this regard, it has been shown that a dedifferentiated gene expression signature is associated with resistance to targeted therapy in melanoma [167, 129] and melanoma escape from immunotherapy by undergoing inflammation-induced dedifferentiation [136]. On the contrary, the melanocytic lineage program has also emerged in promoting therapy resistance [117], hinting on complex phenotype - therapy resistance relations.

3.3 Melanoma phenotype switching

3.3.1 Concepts of phenotypic heterogeneity

Initially, a rare slow-cycling cancer stem cell (CSC) within the rapidly proliferating bulk of cancer cells has been highlighted in non-genetic heterogeneity causing therapy resistance. Therapy resistant CSCs are believed to populate the tumor bulk in a hierarchical manner by giving rise to highly proliferative and more differentiated offsprings [155]. In melanoma, the expression of several neural-crest associated markers has been suggested for the identification of CSCs. Among them are nerve growth factor receptor (NGFR)

/ CD271 [25], CD133 [164], ALDH1 [27], ABCB5 [213] and the B cell marker CD20 [71]. Estimates on the frequency suggested stem cell properties in a highly rare fraction of 0.0001% of melanoma cells [213]. An interesting study by Quintana *et al.* showed that about 25% of melanoma cells were able to initiate tumor growth irrespective of CSC marker expression when injected into highly immunocompromised mice, thereby questioning the hierarchical concept of CSCs [191]. Another study by Shackleton and colleagues showed that both CD133 positive and CD133 negative melanoma cell subpopulations are equally tumorigenic and recapitulate the initial spectrum of CD133 expression in developing tumors [220]. The unidirectional CSC model was revised and more emphasis was set on reciprocal interactions between tumor cells and cells of the tumor microenvironment. Presently, CSCs are rather seen as distinct cancer cell phenotypes that arise non-hierarchically by stochastic fluctuation.

Differentiated cells, which revert their phenotype and temporarily switch back to a pluripotent cell state in physiological processes, have been first observed in the phenomenon of epithelial to mesenchymal transition (EMT) or in the other direction in mesenchymal to epithelial transition (MET) [99]. Epithelial cells that undergo EMT reorganize signaling programs, lose apical-basal polarity and adhesion. In parallel, they acquire features of motile invasive mesenchymal cells. This process is essential during development and wound healing, but also an integral feature during fibrosis and cancer progression [246, 245]. The capacity to revert differentiation in response to microenvironmental cues is especially manifest for cells of neuroectodermal origin, as they are determined to undergo EMT-like changes during development in order to leave the neural crest and invade the body. As an example, it has been shown that activation of NOTCH signaling in terminally differentiated melanocytes initiated reprogramming to a neural-crest like stem cell state [185]. Furthermore, expression of EMT-related TFs, such as ZEB2 and SLUG as well as the mesenchymal related markers CDH2 and Vimentin, can still be detected in terminally differentiated melanocytes to some extent [126].

3.3.2 Phenotypic plasticity in melanoma

Gene expression analyses in large collections of melanoma cell lines and cohorts of primary and metastatic tumors from melanoma patients yielded substantial insights into the taxonomy of melanoma phenotypes [24, 107]. Two distinct, mutually exclusive transcriptional profiles of melanoma cells emerged, which set the basis for classification of the MITF^{high} *proliferative* and MITF^{low} *invasive* phenotypes in melanoma [107, 34]. MITF^{high} *proliferative* cells are attributed with a high rate of proliferation and a high degree of differentiation, including expression of melanocytic antigens, which usually enables identification already on a visual level by the black pigment melanin [34]. On the contrary, MITF^{low} *invasive* cells are missing pigmentation, and adapt a slow-cycling de-differentiated cell state with an increased migratory potential. This phenotype is prone to invasion and metastatic dissemination [34]. Importantly, MITF has evolved

not only as a marker the *proliferative* phenotype, but has also been assigned the central regulator of melanoma phenotypic plasticity [39]. MITF comprises nine isoforms and belongs to the Myc-related family of basic helix-loop-helix (bHLH) leucine zipper TFs [139]. MITF-M (in the following termed MITF) is the shortest isoform and exclusively expressed in melanocytes [34]. During melanocyte differentiation MITF promotes melanoblast survival and proliferation and prevents trans-differentiation into glial and neuronal lineages [179]. In melanoma, MITF is termed the melanoma lineage oncogene, as it is overexpressed in many melanomas and induction of MITF in melanocytes has been shown to overcome oncogene induced senescence [52]. The *Rheostat Model* explains lineage dependent expression in melanoma and compensation for loss of MITF expression [34]. It proposes that melanomas with high levels of MITF are differentiated though highly proliferative. However, cells will initiate final differentiation upon enforced elevation of MITF. Low levels of MITF are only tolerated when a stem cell like phenotype is acquired, on the contrary acute MITF depletion is leading to senescence and cell death [86].

Direct evidence for *in vivo* melanoma cell phenotype switching came from a study by Hoek *et al.*, who showed that both *proliferative* and *invasive* melanoma cell lines were capable to form tumors in immunocompromised mice [106]. Additionally, tumors of both MITF^{low} *invasive* and MITF^{high} *proliferative* cell lines revealed similar heterogenous expression of MITF and the proliferation marker Ki67 in immunohistochemical analyses of the established tumors [106]. Importantly, single cell RNA sequencing (scRNA-seq) of melanoma cells derived from human melanoma revealed that even within a single tumor of the *proliferative* phenotype, cells with an *invasive* signature coexist, indicating that stochastic phenotype switching is present *in vivo* [248, 88]. While MITF expression clearly defines a *proliferative* phenotype in melanoma, several markers have been proposed to identify an *invasive* melanoma cell state. Most research has been performed on the neural crest marker NGFR, which was first assigned to play a role as a CSC marker in melanoma [25]. The RTK AXL is frequently over-expressed in *invasive* melanoma cell lines and plays a direct role for melanoma cell migration and survival [218, 167]. A switch from CDH1 to CDH2 is a well accepted feature of disseminating melanoma cells during formation of metastasis, and hence CDH2 expression has been used to study melanoma cell dedifferentiation.

3.3.3 The tumor microenvironment shapes melanoma cell states

Reciprocal interactions between tumor cells and their microenvironment had already been noticed by Paget in 1889, when he postulated his theory on "Seed and Soil" for cancer cell dissemination: A cancer cell seed will only survive and form metastasis at a distant site when the site of implantation provides adequate soil for its nidation and growth [180]. Initial evidence for microenvironmental driven metastatic phenotype

switching in melanoma was provided by a study which showed reversible transdifferentiation and acquisition of invasive features in melanocytes, which were cultured side by side with metastatic melanoma cells [217]. Since then, data showing the importance of the tumor microenvironment for shaping cancer cell phenotypes has accumulated [2]. An overview on microenvironmental stress triggers, cell type interactions and signaling molecules involved in reciprocally shaping tumor and bystander cell phenotypes is given in Figure 3.5, and will be described in detail below.

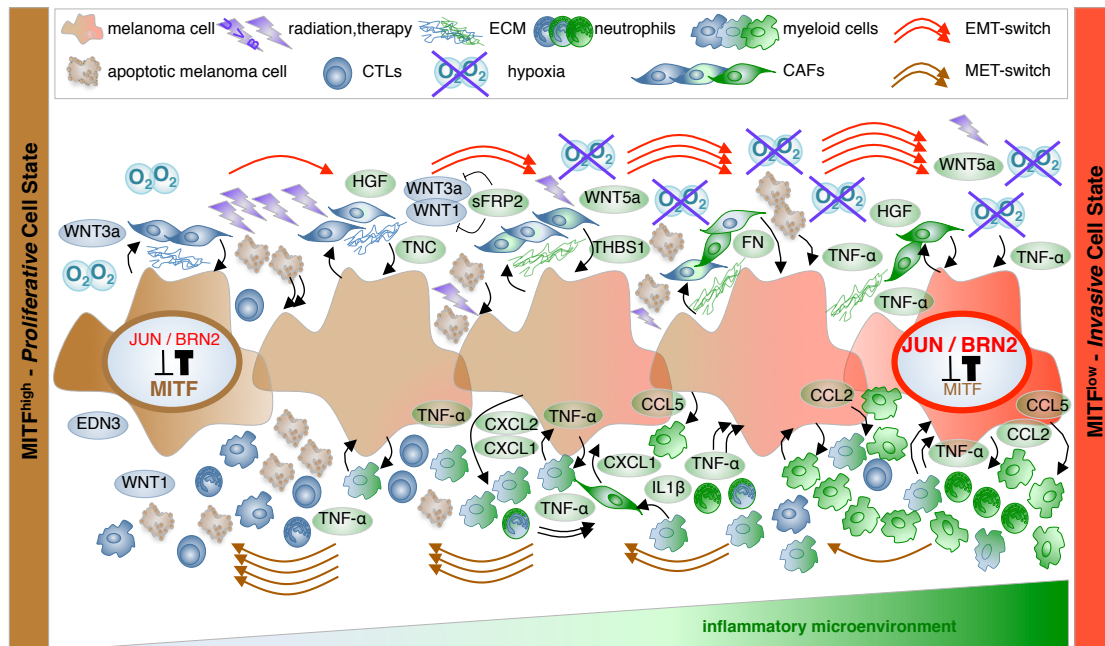


Figure 3.5: **Melanoma plasticity is a result of tumor cell - microenvironment interactions** Figure adapted from Reinhardt *et al.* [194]. Mediators of inflammation and therapy-induced stress are depicted that change the tumor-microenvironment, melanoma cell characteristics, and reciprocally influence cancer and cancer-associated-cells' phenotypes. Inflammation promotes phenotype switching from a MITF^{high} proliferative melanoma cell state (brown) to a MITF^{low} invasive phenotype (red). An anti-tumoral immune response (blue immune and stromal cells) is remodeled to chronic pro-tumorigenic inflammation (green immune and stromal cells). Red and brown arrows highlight reversible phenotype switching. CTLs: Cytotoxic T lymphocytes, CAFs: Cancer-associated fibroblasts, ECM: extracellular matrix, EMT: Epithelial-mesenchymal transition, MET: Mesenchymal-epithelial transition.

During phenotype switching melanoma cells respond and adapt to cellular stress in order to cope with intracellular imbalance and ensure survival. Stress can be caused by many triggers, such as energy shortage that requires modulation of metabolism, genotoxic stress induced by DNA damage, toxic stress affecting proper protein functions and inflammation [70, 175, 136, 38]. Hypoxia represents a further stress condition and a hallmark of the developing tumor. Phenotype switching of melanoma cells towards an *invasive* cell state and metastatic dissemination in response to hypoxia has been repetitively shown [38, 271, 74]. On the contrary, oxidative stress is a main burden during metastatic dissemination. Melanoma cells have been shown to adopt to hostile

conditions while circulating by changing metabolic pathways [186]. An effective therapy represents a strong impulse for phenotype switching, as it involves all kinds of stress triggers. Stress impulses that promote phenotype switching are not only provided by environmental triggers, but also by tumor cells, which has been recently demonstrated in a study by Obenauf *et al.*, who found that melanoma cells protect neighboring melanoma cells by a therapy-induced secretome [175].

Within the tumor microenvironment altered stromal cells constitute an important source of factors that shape melanoma cell states (Figure 3.5, upper part). For example, it has been shown that components of the extracellular matrix (ECM), which are secreted by cancer-associated fibroblasts (CAFs), such as Fibronectin, TenascinC and THBS1, can modulate and activate melanoma cell PI3K signaling and the focal adhesion kinase (FAK) via integrins, thereby leading to transcriptional rewiring and conferring therapy resistance [73, 103]. Fibroblasts that secrete HGF are involved in remodeling melanoma signaling programs upon BRAFi [238]. HGF derived from keratinocytes has been demonstrated to down-regulate melanoma cell CDH1 expression, thereby increasing invasiveness [140]. Another way keratinocytes are promoting melanoma cell *invasive* phenotype switching involves NOTCH signaling and subsequent down-regulation of MITF in melanoma [90]. Furthermore, fibroblasts in an aged microenvironment were found to promote melanoma cell invasiveness by secretion of sFRP2, an inhibitor of canonical WNT signaling [121, 123]. Of note, this finding provides an explanation for the poor prognosis observed for melanoma in the elderly [149]. In return, phenotype switching from *invasive* to *proliferative* is required during seeding of metastasis. Addressing this aspect, a recent study in a zebrafish model provided interesting results on the involvement of Endothelin-3 at the site of metastasis to promote MET-like switching in melanoma cells and thus allowing metastatic dissemination [125].

Understanding inflammation-induced phenotype switching during the development of therapy resistance has come into focus by the recent advances in targeted therapy and anti-cancer immunotherapy. Effective immunotherapies elicit a strong anti-tumoral inflammatory response within the tumor accompanied by infiltration of myeloids, neutrophils, cytotoxic T cells and NK cells that promote high tumoral concentrations of $\text{IFN}\gamma$ and $\text{TNF}\alpha$. Long lasting tumoral inflammation initiates remodeling processes and converts an acute into a chronic pro-tumorigenic inflammation [47]. As an example, in a syngeneic melanoma mouse model for ACT, $\text{TNF}\alpha$ promoted reversible dedifferentiation of melanoma cells, accompanied by loss of target antigen, leading to ablated anti-tumor T cell recognition and therapy resistance [136]. A recent study found that besides T cells, NK cells provide a source of $\text{TNF}\alpha$ within the tumor microenvironment, mediating *invasive* phenotype switching of melanoma cells [280]. In another model, $\text{TNF}\alpha$ released in the course of neutrophilic inflammation in response to intermittent UV exposure promoted melanoma cell switching to an angiotrophic phenotype and perivascular metastatic invasion [13]. Additionally, $\text{TNF}\alpha$ mediated melanoma cell dedifferentiation has been implicated in resistance to targeted therapy [129]. *Vice versa*, *invasive* phenotype switching in melanoma counter-impacts on the composition of immune cells within

the tumor microenvironment. A summary of tumor-immune cell interactions that reciprocally shape the tumor microenvironment is illustrated in the lower part of Figure 3.5. Melanoma cell *invasive* phenotype switching is accompanied by up-regulation of NF κ B target genes in melanoma cells and recruitment of pro-tumorigenic myeloid cells via CCL2, CCL5 and CXCL1/2 chemokine secretion [201]. Inflammation-associated phenotype switching has been associated with inflammatory niches build by CAFs and myeloid cells that secrete CXCR2 ligands and Il1 β , respectively [278]. In line with experimental evidence for the importance of inflammation in phenotype switching and therapy resistance, clinical data show failure of immune checkpoint blockade to correlate with an *invasive* phenotype in melanoma [113].

3.3.4 A regulatory network of melanoma phenotype switching

An important mechanism in melanoma phenotype switching is the reciprocal antagonism of *proliferative* and *invasive* signaling hubs, which are controlled by a plentitude of stress triggers. An overview on the main stress triggers that comprise hypoxia, starvation, cellular stress, inflammation, therapeutic intervention, molecular mediators, and antagonistic signaling pathways is given in Figure 3.6.

MITF in melanocytes is regulated by α MSH binding to MC1R, which leads to accumulation of cAMP and induction of MITF expression via CREB in cooperation with the neural-crest specific TF SOX10 [189, 112]. Furthermore, canonical WNT signaling via WNT1/3a and stabilization of β catenin is driving MITF expression [241]. Constitutive expression of MITF promotes melanoma cell proliferation, survival and is orchestrating differentiation genes, altogether driving the *proliferative* phenotype [139]. At the same time, MITF expression is inhibiting *invasive* phenotype switching [39, 34]. Carreira *et al.* have shown Dia1 as a central regulator in that process [34]. More recent studies reveal metabolic remodeling by MITF leading to an impairment of RHO-GTPases, which are essential for invasion [23]. Importantly, in previous work we could show that MITF directly antagonizes JUN, central player of inflammation- and stress-triggered phenotype switching through binding in the *JUN* enhancer region [201]. Furthermore, there is evidence, that CDH1 impairs JUN at post-translational level [234].

In return, *invasive* signaling hubs antagonize MITF and a *proliferative* cell state in many ways. Several stem cell-associated and neural crest signaling pathways have been implicated. Most relevant are WNT5a mediating non-canonical WNT signaling, TGF β signaling and inflammatory pathway activation [176]. Hypoxia leads to stabilization of HIF1 α inducing BHLHB2 expression which in return represses MITF [38, 271]. Furthermore, hypoxia augments an *invasive* phenotype by a switch from ROR1 to ROR2 expression, thereby promoting non-canonical WNT signaling via WNT5a [176]. Repression of MITF by non-canonical WNT signaling is mediated by activation of Stat3, that represses

Pax3, which is an inducer of MITF expression, in summary lowering MITF expression [56]. In addition, non-canonical WNT signaling leads to the induction of invasive signature genes and EMT TFs, such as Vimentin and Snail [57].

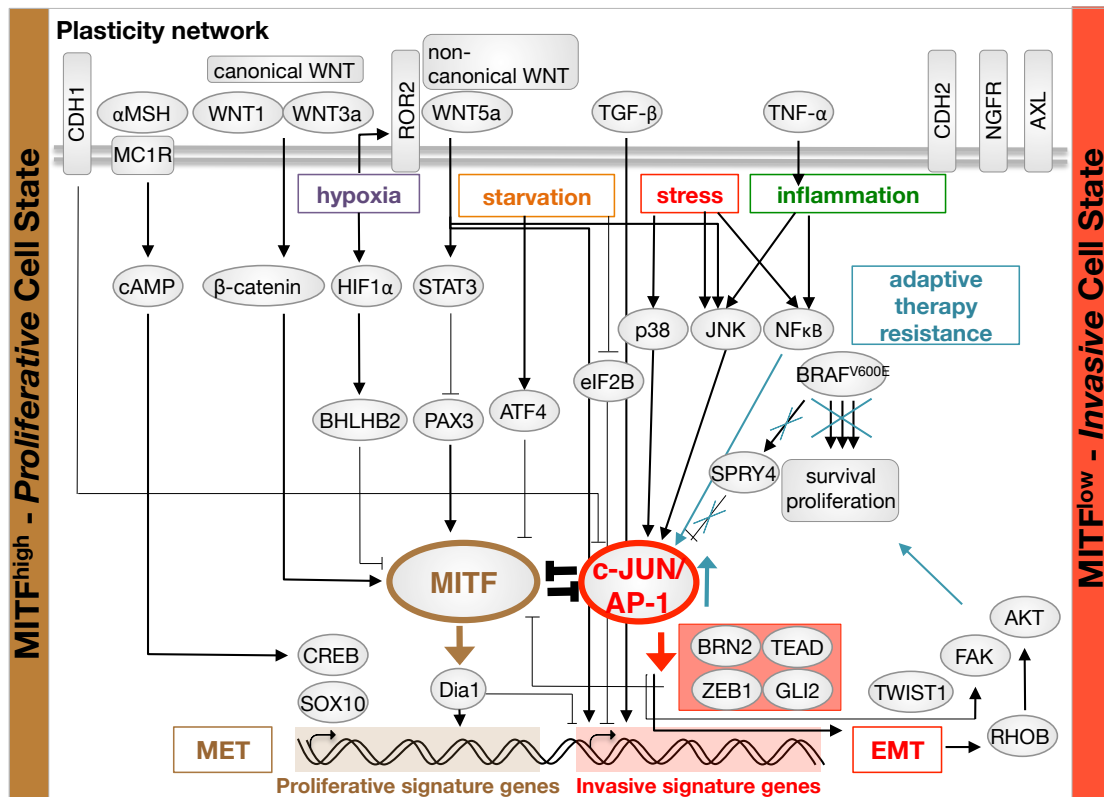


Figure 3.6: **A signaling network regulating melanoma cell phenotype switching** Figure adapted from Reinhardt *et al.* [194]. Schematic overview adapted from Reinhardt *et al.* depicting known molecular mechanisms involved in melanoma phenotype switching due to environmental stress triggers as indicated.

We recently showed that JUN induces *invasive* phenotype switching, while at the same time counteracting MITF on a transcriptional and translational level by so far unknown mechanisms [201]. Various stress impulses via p38, JNK, and NF κ B signaling can converge on, or cooperate with AP1/ JUN to orchestrate melanoma cell plasticity. Additionally, under MAPKi therapy, elevated JUN levels have been repetitively observed causing phenotype switching, resulting in therapy resistance [51, 69, 192, 249]. So far, JunB/ATF2 heterodimers have been reported to down-regulate MITF expression by interfering with SOX10 [222]. Another study, that performed transcriptomic and epigenetic analyses on melanoma culture panels, confirmed MITF/SOX10 and AP1/TEAD as regulators for *proliferative* and *invasive* melanoma cells, respectively [262]. In addition to JUN, the TFs Brn-2, Gli-2, Zeb1 have been identified to oppose MITF and a *proliferative* phenotype, while inducing *invasive* signature genes [91, 116, 33, 192, 201]. In detail, Brn-2 has been shown to repress MITF, while at the same time promoting

melanoma cell dedifferentiation [91].

Translational reprogramming represents another recently highlighted feature of melanoma phenotype switching. Rapid growth of tumor cells imperatively leads to nutrient deprivation. With respect to this, Falletta and colleagues showed massive translational reprogramming in melanoma cells in a situation of glutamine starvation, which was initiated by blockade of the translation initiation factor eIF2B and led to *invasive* phenotype switching. In parallel, an integrated stress response was observed to block MITF via ATF4. Intriguingly, the group was able to show similar effects when treating the cells with $TNF\alpha$ providing further insides on the mechanisms of inflammation-induced dedifferentiation of melanoma cells [70].

4 Objectives of this study

Phenotypic plasticity endows cancer cells to rapidly adapt to and bypass potential harmful conditions, impacting on cell survival, tumor growth, metastasis and mediating therapy resistance. However, despite all the progress made in recent years, we are only beginning to decode the regulatory network of melanoma phenotype switching. Inflammation and stress signaling in the tumor represent key determinants of an effective therapeutic response [2]. The fact that both are also key triggers for melanoma phenotype switching bridges the gap to plasticity-related therapy resistance and underlines the importance for understanding inflammation-induced cell state transitions in melanoma on a functional and molecular level. Enhanced understanding of the underlying molecular mechanisms eventually provides control of phenotype switching with the goal to forestall therapy resistance and prevent metastatic spread. Initial attempts for directed phenotype switching during melanoma therapy have already shown promising results [208, 230].

The central hypothesis of this thesis claims the existence of additional transition cell states in melanoma between the well characterized opposing phenotypes defined by the presence or absence of melanocytic differentiation programs or invasive dedifferentiation signatures. In order gain a more detailed understanding on the trajectory of melanoma phenotypes and to allow insights into process of interconversion, three specific aims are defined:

1. To identify transitory cell states by bioinformatic investigation of inflammatory signature marks on large melanoma expression data and to evaluate markers for molecular and functional characterization of transition cell states (see chapter 6.1).
2. To characterize molecular pathways that are orchestrating intermediate cell state interconversion and that are regulating intermediate cell state marker expression (see chapter 6.2).
3. To dissect transcription factor binding sites controlling melanoma phenotype switching using functional genomics (see chapter 6.3 and 6.4).

5 Material and methods

5.1 General laboratory equipment

5.1.1 Instruments and equipment

Table 5.1: Instruments and equipment

Instrument	Company
Axio Vert A1 Microscope	Biorad
BD FACS ARIA III cell sorter	BD Biosciences
BD FACS Canto II flow cytometer	BD Biosciences
Branson analog sonifier 250	Branson Ultrasonics
Centrifuges (5417R, 5424, 5810K)	Eppendorf
Excella [®] E24 incubator shaker	New Brunswick Scientific
Freezer -80°C MDF-U55V-PE	Panasonic
HERAcell [®] 240 CO2 incubator	Thermo Fisher Scientific
HERAsafe [®] KS laminar air flow cabinet	Thermo Fisher Scientific
Heraeus [®] microbiological incubator	Thermo Fisher Scientific
Julabo TW8 waterbath	Julabo
InGenius3 gel documentation system	Syngene
Light Cycler [®] 480 II	Roche
Magnetic stirrer Stuart [™] stirplate SB161	Sigma-Aldrich
Mini-PROTEAN [®] electrophoresis cell	Biorad
Micropipettes Pipet-Lite LTS	Rainin/ Mettler-Toledo
MiSeq sequencer	Illumina
Mr Frosty [™] freezing container	Thermo Fisher Scientific
Multistep pipettor	VWR
NanoDrop 2000 spectrophotometer	Thermo Fisher Scientific
Odyssey [®] SA imaging system	LI-COR [®] Bioscience
PerfectBLUE [™] gel system	Peqlab
pH meter Hanna [®] pH 21	Woonsocket
Pipetboy pipetting aid	Integra Biosciences
Power Source	VWR, Radnor, PA, USA
Scale TE601	Sartorius
Spectrometer Ultrospec 10	Amersham Biosciences

Table 5.1: Instruments and equipment

TC10™ automated cell counter	Biorad
ThermoMixer® R	Eppendorf
T100 thermal cycler	Biorad, Hercules
Ultraviolet transilluminator GelVue	Syngene
VV3 vortexer	VWR

5.1.2 Software

Table 5.2: Software

Software	Developer/ Company
ApE V2.0.50	M. Wayne Davis
FACS Diva V6.1.1	BD Biosciences
FV10-ASW Viewer	Olympus
FlowJo® V8.7.3	Tree star, Inc.
GenSys V1.5.4.0	Syngene
UCSC genome browser	Kent <i>et al.</i> [122]
GraphPad Prism7	GraphPad Software, Inc.
javaGSEA desktop application V3.0	BROAD Institute, MIT
L ^A T _E X	Leslie Lamport
Light Cycler® 480 Software V1.5.1.62	Roche
Maggelan V7.1 SP	Tecan
Microsoft Office for Mac 2011	Microsoft Corporation
NanoDrop 2000/2000C V1.4.2	Thermo Fisher Scientific
Odyssey® Sa Application Software V1.1	LI-COR® Bioscience
Outknocker.org V1.31	Jonathan L. Schmid-Burgk [215]
R V3.3.3	R foundation, R Development
RStudio V1.0.153	RStudio, Inc.
TexShop V3.84	Richard Koch
ZEN light microscopy software	Zeiss

5.1.3 Consumables and plasticware

Table 5.3: Consumables and plasticware

Article	Company
Blotting paper	VWR
Cell culture flasks (T25, T75)	Sarstedt
Cell culture dishes (10 cm, 15 cm)	Sarstedt
Centrifuge tubes (5 ml)	Eppendorf

Table 5.3: Consumables and plasticware

Centrifuge tubes (15 ml, 50 ml)	Sarstedt
Falcon™ Cell strainers (70 µm)	Thermo Fisher Scientific
Flow cytometry tubes	Sarstedt
Micropipette tips	Starlab
Micropipette tips, with filter	Starlab
Multidispenser tips (5 ml, 12.5 ml)	VWR
Nitrocellulose membrane (0.45 µm)	GE Healthcare
Parafilm® M	Brand
Pasteur glas pipettes	VWR
PCR adhesive seals	Sarstedt
PCR plates (96well)	Sarstedt
PCR stripes and lids (8well)	Axygen
Petri dishes	Sarstedt
qPCR adhesive seals	Biozym Scientific GmbH
qPCR plates	Biozym Scientific GmbH
Reagent reservoirs	Labomedic
Round bottom test plates (96well)	Geiner Bio-One
Serological pipettes (5 ml, 10 ml, 25 ml)	Corning
Spin columns for DNA preparation	Centric Biotec
Spin columns for RNA preparation	Zymo Research Group
Syringes (5 ml, 10 ml, 20 ml)	B. Braun Melsungen AG
Syringe pore filters (0.2 µm, 0.45 µm)	VWR
Tissue culture test plates (6well, 12well, 24well, 96well)	Techno Plastic Products AG

5.1.4 Chemicals

Table 5.4: Chemicals

Substance	Company
Acetic acid (C ₂ H ₄ O ₂)	Carl Roth GmbH
Agar Agar, Kobe I	Carl Roth GmbH
Agarose Powder	Invitrogen, Thermo Fisher Scientific
Ampicillin	Carl Roth GmbH
Ampuwa® ultrapure water	Fresenius Kabi GmbH
Ammonium persulfat ((NH ₄) ₂ S ₂ O ₈)	Carl Roth GmbH
Bovine Serum Albumine (BSA)	Carl Roth GmbH
Albumin Fraction V	
Bromphenolblue (C ₁₉ H ₁₀ Br ₄ O ₅ S)	Carl Roth GmbH
Calcium chloride (CaCl ₂)	Carl Roth GmbH
Dimethylsulfoxide (DMSO) (C ₂ H ₆ OS)	Carl Roth GmbH
Disodium phosphate (Na ₂ HPO ₄)	Carl Roth GmbH

Table 5.4: Chemicals

Dithiothreitol (DTT) ($C_4H_{10}O_2S_2$)	Carl Roth GmbH
Doxycycline monohydrate ($C_{22}H_{24}H_2O_8 \cdot H_2O$)	Sigma-Aldrich
Ethanol, absolute (C_2H_6O)	Carl Roth GmbH
Ethanol, 70%, denatured	Otto Fischar GmbH & Co. KG
Ethidium bromide (EtBr) ($C_{21}H_{20}BrN_3$)	Carl Roth GmbH
Ethylenediaminetetraacetic acid (EDTA) ($C_{10}H_{16}H_2O_8$)	Carl Roth GmbH
D-Glucose ($C_6H_{12}O_6$)	Carl Roth GmbH
Glycerol ($C_3H_8O_3$)	Carl Roth GmbH
Glycogen	Carl Roth GmbH
Guanidinium chloride (CH_6ClH_3)	Carl Roth GmbH
HEPES ($C_8H_{18}N_2O_4S$)	Carl Roth GmbH
Hydrochloric acid (HCl) 32%	Carl Roth GmbH
Hydrochloric acid (HCl) 37%	Carl Roth GmbH
Isopropanol (C_3H_8O)	Carl Roth GmbH
LB medium powder Lennox	Carl Roth GmbH
Magnesium choride ($MgCl_2$)	Merck Millipore
Magnesium sulfate ($MgSO_4$)	Carl Roth GmbH
Methanol (CH_4O)	Carl Roth GmbH
Monopotassium phosphate (KH_2PO_4)	Carl Roth GmbH
Potassium acetate (CH_3CO_2K)	Carl Roth GmbH
Potassium chloride (KCl)	Carl Roth GmbH
Rotiphorese Gel30, 30% solution of Acrylamide (C_3H_5NO)/ Bisacrylamide ($C_7H_{10}N_2O_2$) (37.5:1)	Carl Roth GmbH
Sodium acetate ($C_2H_3NaO_2$)	Carl Roth GmbH
Sodium azide (NaN_3)	AppliChem
Sodium chloride (NaCl)	Carl Roth GmbH
Sodium dodecyl sulfate (SDS) pellets ($NaC_{12}H_{25}SO_4$)	Carl Roth GmbH
Sodium hydroxide (NaOH)	Carl Roth GmbH
Tetramethylethylenediamine (TEMED)	Carl Roth GmbH
Tris-HCl	Carl Roth GmbH
Triton X-100	Sigma-Aldrich
Tween 20	Carl Roth GmbH

5.1.5 Cell culture substances

Table 5.5: Cell culture substances

Substance	Company
Blasticidine S hydrochloride	Sigma-Aldrich
Dulbecco's modified eagles medium (DMEM)	Gibco Life Tech, Thermo Scientific
Dulbecco's phosphate buffered saline (DPBS)	Gibco Life Tech, Thermo Scientific
Fetal Bovine Serum (FBS)	Gibco Life Tech, Thermo Scientific
GlutaMAX™	Gibco Life Tech, Thermo Scientific
L-Glutamine (200 mM)	Invitrogen, Thermo Scientific
Opti-MEM™	Gibco Life Tech, Thermo Scientific
Penicillin/Streptomycin (100x)	Invitrogen, Thermo Scientific
Puromycine dihydrochloride	Sigma-Aldrich
RPMI 1640 medium	Gibco Life Tech, Thermo Scientific
Sodium pyruvate (100 mM)	Gibco Life Tech, Thermo Scientific
Trypsin-EDTA (0.05 %)	Gibco Life Tech, Thermo Scientific

5.1.6 Recombinant proteins and peptidases

Table 5.6: Recombinant proteins and peptidases

Name	Diluent	Stock conc.	Working conc.	Company
HGF	Ampuwa®	100 µg/ml	50 ng/ml	Peprtech
TNF α	Ampuwa®	1000 U/µl	1000 U/ml	Peprtech

5.1.7 Cell culture stimulants and inhibitors

Table 5.7: Cell culture stimulants and inhibitors

Name	Diluent	Stock conc.	Working conc.	Company
Aphidicolin	DMSO	10 mg/ml	1 µg/ml	Sigma Aldrich
5-Azacytidine	DMSO	10 mM	1-10 µM	Sigma Aldrich
BEZ235	DMSO	14.9 mM	1 µM	SelleckChem
MK2206	DMSO	20 mM	1 µM	SelleckChem
Phorbol-12-	DMSO	1 mg/ml	100 ng/ml	Sigma Aldrich

Table 5.7: Cell culture stimulants and inhibitors

myristat- 13-acetat (PMA)					
SCH772984	DMSO	10 mM	1 μ M	SelleckChem	
Sotrastaurin	DMSO	10 mM	1 μ M	SelleckChem	
SP600125	DMSO	10 mM	20 μ M	SelleckChem	
Trametinib	DMSO	1 mM	50 nM	SelleckChem	

5.1.8 Commercially available kits, reagents and enzymes

Table 5.8: Commercially available kits, reagents and enzymes

Reagent	Company
All-in-One cDNA Synthesis SuperMix	Bioutil
BbsI (5,000 U/ml)	NEB
Broad range protein marker sc-2361	Santa Cruz
cOmplete™ protease inhibitor cocktail	Roche
Desoxynucleotide(dNTPs) solution mix, 10 mM	Thermo Scientific
DreamTaq™ DNA polymerase	Thermo Scientific
Evagreen® qPCR-Mix II (ROX)	Biobudget
EZ DNA Methylation-Direct kit	Zymo Research
FACSFlow™	BD Biosciences
FastDigest™ AvrII	Thermo Scientific
FastDigest™ BamHI	Thermo Scientific
FastDigest™ NheI	Thermo Scientific
Fugene® HD transfection reagent	Promega
GeneRuler™ 1 kb DNA ladder	Thermo Scientific
GFP-Trap® MA	ChromoTek GmbH
InnuPREP gel extraction kit	Analytik Jena
InnuPREP PCRpure kit	Analytik Jena
MluI (10,000 U/ml)	NEB
Propidium iodide solution (50 μ /ml) # 556463	BD Bioscience
Proteinase K (800 U/ml)	NEB
PureLink™ HiPure Plasmid MidiPrep kit	Thermo Scientific
PureLink™ RNase A (20 mg/ml)	Thermo Scientific
Phusion® High-Fidelity DNA polymerase	NEB
Sall-HF (20,000 U/ml)	NEB
SimpleChIP® enzymatic chromatin IP kit	CellSignaling
RLT lysis buffer	Qiagen

Table 5.8: Commercially available kits, reagents and enzymes

RW1 RNA wash buffer	Qiagen
T4 DNA Ligase (40,000 U/ml)	NEB
Zymo RNA wash buffer	Zymo Research

5.1.9 Primary antibodies for immunoblot

Table 5.9: Primary antibodies for immunoblot

Directed against	Produced in	Dilution	Clone	Company	Catalog number
AKT	mouse	1:2000	40D4	CellSignaling	CS#2920
β Actin	mouse	1:500	C-4	Santa Cruz	SC-47778
CD73	rabbit	1:1000	D7F9A	CellSignaling	CS#13160
C-FOS	rabbit	1:1000	9F6	CellSignaling	CS#2250
JUN	rabbit	1:1000	60A8	CellSignaling	CS#9165
ERK1/2	rabbit	1:1000	polyclonal	CellSignaling	CS#9102
FOSL1	rabbit	1:200	R-20	Santa Cruz	SC-604
GFP	mouse	1:200	B-2	Santa Cruz	SC-9996
I κ B α	rabbit	1:1000	L35A5	CellSignaling	CS#4814
JUNB	mouse	1:200	C-11	Santa Cruz	SC-8051
MITF	rabbit	1:250	polyclonal	Atlas Antibodies	HPA 003259
pAKT (Ser473)	rabbit	1:2000	D7E	CellSignaling	CS#4060
pMET (Tyr1234/1235)	rabbit	1:1000	D26	CellSignaling	CS#3077
pERK (Tyr204)	mouse	1:200	E-4	Santa Cruz	SC-7383
p38	rabbit	1:1000	D13E1	CellSignaling	CS#8690
pp38 (Thr180/Tyr182)	rabbit	1:1000	D3F9	CellSignaling	CS#4511

5.1.10 Secondary antibodies for immunoblot

Table 5.10: Secondary antibodies for immunoblot

Dye	Directed against	Produced in	Dilution	Company
IRDye680LT	mouse	donkey	1:15,000	LI-COR

Table 5.10: Secondary Antibodies for Immunoblot

IRDye680LT	rabbit	donkey	1:15,000	LI-COR
IRDye800CW	mouse	donkey	1:15,000	LI-COR
IRDye800CW	rabbit	donkey	1:15,000	LI-COR

5.1.11 Antibodies for flow cytometry

Table 5.11: Antibodies for flow cytometry

Dye	Directed against	Produced in	Dilution	Clone	Company
Brilliant Violet 421™	CD73	mouse	1:100	AD2	Biolegend

5.1.12 Molecular biology - buffers, media and agar

10x phosphate buffered saline (PBS):

80 g NaCl
 11.6 g Na₂HPO₄
 2 g KH₂PO₄
 2 g KCL
 add up to 1 l with ddH₂O

1x PBS:

100 ml 10x PBS
 add up to 1 l with ddH₂O

1x TAE:

dissolve in ddH₂O
 40 mM Tris-HCl
 20 mM acetic acid
 1 mM EDTA

6x loading dye:

dissolve in ddH₂O
 10 mM Tris HCl pH 7.6
 0.03% (w/v) Bromophenol Blue
 60% (v/v) Glycerol

EtBr agarose gels:

Table 5.12: Preparation of EtBr agarose gels

	1% gel	1.5% gel	2% gel
Agarose powder	1.5 g	2.25 g	1.3 g
1x TAE	150 ml	150 ml	150 ml
Boil until dissolved			
EtBr	5 µl	5 µl	5 µl

Annealing buffer:

dissolve in Ampuwa[®] H₂O
 100 nM NaCl
 50 mM HEPES
 NaOH to adjust pH to 7.4

Lysogeny Broth (LB) medium:

20 g LB medium powder Lennox
 5 g NaCl
 30g Agar Agar Kobe I
 add up to 1 l ddH₂O
 autoclave for 15min at 121°C
 cool down to room temperature (RT)
 100 mg/l Ampicillin

Agar bacterial plates:

20 g LB medium powder Lennox
 5 g NaCl
 add up to 1 l ddH₂O
 autoclave for 15min at 121°C
 cool down to RT
 100 mg/l Ampicillin
 pour 8ml per petri dish

Resuspension buffer P1:

dissolve in Ampuwa[®] H₂O
 50 mM Tris-HCl pH 8.0
 10 mM EDTA
 100 µg/ml RNaseA
 store at 4°C

Neutralisation buffer N3:

dissolve in Ampuwa[®] H₂O
4.2 M Guanidinium chloride
0.9 M Potassium acetate
32% HCl to adjust pH to 4.8

Wash buffer PE:

dissolve in Ampuwa[®] H₂O:
10 mM Tris-HCl pH 7.5
80% (v/v) ethanol

5.1.13 Cell culture media and buffers

Complete RPMI:

Gibco[®] RPMI 1640
10% (v/v) heat-inactivated (60 min, 56°C) FCS
1% (v/v) Penicillin/Streptomycin
1% (v/v) L-Glutamine
store at 4°C

THP1 medium:

Gibco[®] RPMI 1640
10% (v/v) heat-inactivated (60 min, 56°C) FCS
1% (v/v) Penicillin/Streptomycin
1% (v/v) Sodium pyruvate
store at 4°C

Complete DMEM:

Gibco[®] DMEM
10% (v/v) heat-inactivated (60 min, 56°C) FCS
1% (v/v) Penicillin/Streptomycin
1% (v/v) L-Glutamine
store at 4°C

2x freezing medium:

Gibco[®] DMEM
40% (v/v) medium of respective cell line to be frozen
50% (v/v) FBS

20% (v/v) DMSO
store at 4°C

2x HBS:

dissolve in Ampuwa® H₂O:
274 mM NaCl
10 mM KCl
1.4 mM Na₂HPO₄
42 mM HEPES
15 mM D-Glucose
NaOH adjust pH to 7.05

Fluorescence-activated cell sorting (FACS) buffer:

dissolve in DPBS
2% (v/v) FBS
0.1% (w/v) Sodium azide
store at 4°C

5.1.14 Lysis buffers

Direct Lysis Buffer (DLB):

dissolve in Ampuwa® H₂O:
10 mM Tris-HCl
1 mM CaCl₂
1 mM MgCl₂
1 mM EDTA
1% (v/v) Triton X 100
32% HCl to adjust pH to 7.5
store at 4°C
prior use freshly add 100 µg/ml Proteinase K

Lysis buffer for gDNA isolation:

dissolve in Ampuwa® H₂O:
100 mM Tris-HCl pH 8.0
5 mM EDTA pH 8.0
200 mM NaCl
0.2% (w/v) SDS
prior use freshly add 100 µg/ml Proteinase K

Lysis buffer P2:

dissolve in Ampuwa[®] H₂O: 100 mM Tris-HCl pH 8.0
200 mM NaOH
1% (w/v) SDS
prior use freshly add 100 µg/ml Proteinase K

1x Lämmli buffer:

dissolve in Ampuwa[®] H₂O:
120mM Tris-HCl pH 6.8
4% (w/v) SDS
20% (v/v) Glycerol
0.02% (w/v) Bromophenolblue
20 mM DTT

5.1.15 Immunoblot buffers and preparation of SDS PAGE gels

1 M Tris pH 6.8:

121.1 g Tris-HCl
stir and warm until dissolved
32% HCL to adjust to pH 6.8
add up to 1 l with ddH₂O

1 M Tris pH 8.8:

121.1 g Tris-HCl
stir and warm until dissolved
32% HCL to adjust to pH 8.8
add up to 1 l with ddH₂O

10x SDS running buffer:

29 g Tris-HCl
144 g Glycine
10 g SDS
stir and warm until dissolved
add up to 1 l with ddH₂O

10x Tris-Glycine buffer:

29 g Tris-HCl
 144 g Glycine
 add up to 1 l with ddH₂O

1x Transfer buffer:

100 ml 10x Tris-Glycine buffer
 200 ml Methanol
 add up to 1 l with ddH₂O

10x TBS:

80 g NaCl
 30 g Tris-HCl
 37% HCl to adjust to pH 7.6
 add up to 1 l with ddH₂O

1x TBS:

100 ml 10x TBS
 add up to 1 l with ddH₂O

1x TBS-T:

100 ml 10x TBS
 500 µl Tween-20
 add up to 1 l with ddH₂O

SDS PAGE gels:

Table 5.13: Preparation of SDS PAGE gels

	6% gel	10% gel	12% gel
ddH ₂ O	4.00 ml	2.71 ml	2.04 ml
Rotiphorese [®] Gel30	2.00 ml	3.33 ml	4.00 ml
1M Tris-HCl (pH 8.8)	3.75 ml	3.75 ml	3.75 ml
10% SDS	0.1 ml	0.1 ml	0.1 ml
10% APS	0.1 ml	0.1 ml	0.1 ml
TEMED	8 µl	8 µl	8 µl

SDS polyacrylamide gelelectrophoresis (PAGE) 3% stacking gel:

- 2.26 ml ddH₂O
- 0.3 ml Rotiphorese[®] Gel30
- 0.38 ml 1M Tris-HCl (pH 6.8)
- 30 µl 10% SDS
- 30 µl 10% APS
- 3 µl TEMED

5.1.16 Cell lines and bacteria

Table 5.14: Cell lines and bacteria

Cell line/ bacteria	Obtained from
HEK293T cells	ATCC [®] CRL-3216 [™] purchased from ATCC, Mannassas, VA, USA
<i>Escherichia coli</i> (<i>e. coli</i>) DH10 β	V. Hornung, Bonn, Germany
MaMel human melanoma cell lines	D. Schadendorf, Essen, Germany. Generation described by Ugurel <i>et al</i> [259].
MZ7 melanoma cells	T. Wölfel, Mainz, Germany
SK.Mel28 melanoma cells	T. Wölfel, Mainz, Germany
THP1 monocyte cells	V. Hornung, Bonn, Germany

5.1.17 Primer sequences

All primers were purchased from Microsynth AG (Balgach, Switzerland).

Primers for cloning:

Table 5.15: Primers for cloning

Primer name	Primer sequence (5'-3')	Application
Seq-pLV-tetO-fwd	TGATAGAGAACGTATGTCGAGG	Sequencing
Seq-pLV-tetO-rev	GCAGCGTATCCACATAGCGTAAA	Sequencing
Seq-pRp-fwd	GGAGACGCCATCCACGCTG	Sequencing
Seq-pRp-rev	CTGACCTTGATCTGAACTTCTC	Sequencing
pRpCitrine-Mlul-fwd	TGCATGACGCGTATGGTGAGCAAGGGCGAGGAGCT	PCR
pRpCitrine-Sall-rev	ACTTCAGTCGACCTACTTGTACAGCTCGTCCATGCCG	PCR

Table 5.15: Primers for cloning

pRpcJUN- MluI-fwd	TGCATGACGCGTATGACTGCAAAGATGGAAACGAC	PCR
Px330- gRNA-rev1	TCTAGAGCCATTTGTCTGCAG	PCR
Px330-U6-start	GAGGGCCTATTTCCCATGATTC	PCR/ Sequencing

Primers for analyzing mRNA expression in quantitative polymerase chain reaction (qPCR):

Table 5.16: Primers for analyzing mRNA expression in qPCR

Primer name	Sequence of forward (fwd)-primer (5'-3')	Sequence of reverse (rev)-primer (5'-3')
MITF	AGGAGTTGCTGATGGTGAGG	GAAATCTTGGGCTTGATGGA
MLANA	TTCTTGTGGGCATCTTCTTG	GTCATCGGCTGTTGGTATT
NT5E	GAGTGGCTCGATCAGTCCTT	GGCACTATCTGGTTCACCGT
TYR	CTTCTTGAAGAGGACGGTGC	TGTCCAGGTACAGGGATCT
UBC	CAGGGTACGACCATCTTCCAG	GGAGCCGAGTGACACCATTG

Primers for quantitative PCR of Chromatin Immunoprecipitation (ChIP):

Table 5.17: Primers for ChIP qPCR

Primer name	Sequence of fwd-primer (5'-3')	Sequence of rev-primer (5'-3')
AP1-1	TGTTACTCTTTCCCTCTCTGCTGG	GCCACATACAACCAGGGAGTCA
AP1-2	GCTGGCAGTGCTTCAGGAAATC	GTGACTCAGCTTCATTGCCCAT
AP1-3	CTGCATCATGCATCCTACACTGC	GGAAACTAGAGGGATGAGGCAGTA
AP1-4	CCTGTAAATGAATGCTGCCGTTGG	CCTCCATCCTGGTTCCTGTGTTA
AP1-5	AGAGGAAACTGCGGTTCTGAGATG	CCTCCAGCCTCATTCCCTGACA
AP1-6	CCCAGTTAGGAGGCTGTGGTAG	GTCAATAAAGCCAGAAGCCCTGG
AP1-7	ATGGGTTATGACCAGTAGTAGGGC	CCTGGGGCTGTTCTTGACATCTTA
AP1-8	CCCATGTGCCTTTGATGAGTCAG	CCCTTCCTTTCTCTCGTGTCTT
Ctrl-1	ACCAAAGTCCAGGAAAGGAGGG	CGGAGCTTTCATGCCCTACCT
Ctrl-2	TGCTCGCGGGATGTTACTCTG	GCAGAGAGCCTGGCATGTAGTA
Ctrl-3	TTCAGGTGCCCTCAGTTCCAG	GCTGATACACCAGAGACAGACGT
Ctrl-4	AGAGTCACAAGCTAGGATGCAGG	CTGCTGTTCTGTGACTGTGGC
Ctrl-5	CCTGTGGTTTGTGTCCATCAGTG	GGGAACAAAGGACAGGCTACAGA
Neg-Ctrl	ATGGTTGCCACTGGGGATCT	TGCCAAAGCCTAGGGGAAGA

sgRNA oligonucleotide sequences targeting *NT5E* in intronic c-JUN/AP1-sites and ctrl sites and *NF1* in exon 4 and exon 27 for annealing and cloning in px330:

Table 5.18: sgRNA oligonucleotide sequences

Oligo name	Top strand (TS) oligonucleotide sequence (5'-3')	Bottom strand (BS) oligonucleotide sequence (5'-3')
AP1-1	CACCTATGAGTGAATCACATCCTC	AAACGAGGATGTGATTCACCTCATA
AP1-2	CACCGGGGGCGGTGAGTCAAGC	AAACGCTTGACTCACCGCCCCC
AP1-3	CACCGAGTCACAGTATAATCTGAG	AAACCTCAGATTATACTGTGACTC
AP1-5	CACCGGCAAGTGCTGACTCAATAC	AAACGTATTGAGTCAGCACTTGCC
AP1-6	CACCGCCAAGACAGTGAGTCAC	AAACGTGACTCACTGTCTTGGC
Ctrl	CACCGTGACACCAGGTGAGCTC	AAACGAGCTCACCTGGTGTAC

Primers for first level PCRs evaluating CpG methylation of bisulfite converted DNA, clustered regularly interspaced short palindromic repeats (CRISPR)/CRISPR-associated protein 9(Cas9) *NT5E* intronic AP1-site targeting by deep sequencing:

Table 5.19: Primers for first level MiSeq PCR

Primer name	Primer sequence (5'-3')
AP1-1-NGS-fwd	ACACTCTTTCCCTACACGACGctcttccgatct- CACATACAACCAGGGAGTCAGCT
AP1-1-NGS-rev	TGACTGGAGTTCAGACGTGTGctcttccgatct- CTCCAGTTGCAGCCCCTAAAACA
AP1-2a-NGS-fwd	ACACTCTTTCCCTACACGACGctcttccgatct- AATGAAAATCCTGCCTCCGTCTG
AP1-2a-NGS-rev	TGACTGGAGTTCAGACGTGTGctcttccgatct- GTCTTGTTGCTCACACAAAGCCT
AP1-2b-NGS-fwd	ACACTCTTTCCCTACACGACGctcttccgatct- AGCCCTTCAGCTAGGTTTGCAGT
AP1-2b-NGS-rev	TGACTGGAGTTCAGACGTGTGctcttccgatct- CAGTGCTTCAGGAAATCGGGTGT
AP1-5-NGS-fwd	ACACTCTTTCCCTACACGACGctcttccgatct- GAGTGCAGTAAGAGTACCACCCT
AP1-5-NGS-rev	TGACTGGAGTTCAGACGTGTGctcttccgatct- CACCCATAAAGTGTGAGGAAAC
AP1-6-NGS-fwd	ACACTCTTTCCCTACACGACGctcttccgatct- CCTGACGTCTAGATCTGTATGTC
AP1-6-NGS-rev	TGACTGGAGTTCAGACGTGTGctcttccgatct-

Table 5.19: Primers for first level MiSeq PCR

	CACTAAGGCAGCAACAATAGGTG
Bisulf-NGS-CD73-fwd	ACACTCTTCCCTACACGACGctcttccgatct- GTATTAGGGTATTATTTGGTTTAT
Bisulf-NGS-CD73-rev	TGACTGGAGTTCAGACGTGTGctcttccgatct- CTTACCACACTCTACCATCC
Ctrl1-NGS-fwd	ACACTCTTCCCTACACGACGctcttccgatct- GGTTCACGCACCAAATCATACCA
Ctrl1-NGS-rev	TGACTGGAGTTCAGACGTGTGctcttccgatct- AGGTGTGACATCTTTGAGGTCTC
Ctrl2-NGS-fwd	ACACTCTTCCCTACACGACGctcttccgatct- TGCTTGCCATGCTGGTGTCTCT
Ctrl2-NGS-rev	TGACTGGAGTTCAGACGTGTGctcttccgatct- TTGTTGGGGACTAGGGATGAGAG

Barcoding primers for second level PCRs for deep sequencing:

Table 5.20: Barcoding fwd-primers for second level MiSeq PCRs

Primer name	Fwd primer sequence (5'-3')
D501-long	AATGATACGGCGACCACCGAGATCTACACTATAGCCTACA- CTCTTCCCTACACGACgct
D502-long	AATGATACGGCGACCACCGAGATCTACACATAGAGGCACA- CTCTTCCCTACACGACgct
D503-long	AATGATACGGCGACCACCGAGATCTACACCCTATCCTACA- CTCTTCCCTACACGACgct
D504-long	AATGATACGGCGACCACCGAGATCTACACGGCTCTGAACA- CTCTTCCCTACACGACgct
D505-long	AATGATACGGCGACCACCGAGATCTACACAGGCGAAGACA- CTCTTCCCTACACGACgct
D506-long	AATGATACGGCGACCACCGAGATCTACACTAATCTTAACA- CTCTTCCCTACACGACgct
D507-long	AATGATACGGCGACCACCGAGATCTACACCAGGACGTACA- CTCTTCCCTACACGACgct
D508-long	AATGATACGGCGACCACCGAGATCTACACGTAAGTACACA- CTCTTCCCTACACGACgct

Table 5.21: Barcoding rev-primers for second level MiSeq PCRs

Primer name	Rev primer sequence (5'-3')
D701-long	CAAGCAGAAGACGGCATAACGAGAT- CGAGTAATGTGACTGGAGTTCAGACGTGTgct

Table 5.21: Barcoding rev-primers for second level MiSeq PCRs

D702-long	CAAGCAGAAGACGGCATAACGAGAT- TCTCCGGAGTGACTGGAGTTCAGACGTGTgct
D703-long	CAAGCAGAAGACGGCATAACGAGAT- AATGAGCGGTGACTGGAGTTCAGACGTGTgct
D704-long	CAAGCAGAAGACGGCATAACGAGAT- GGAATCTCGTGACTGGAGTTCAGACGTGTgct
D705-long	CAAGCAGAAGACGGCATAACGAGAT- TTCTGAATGTGACTGGAGTTCAGACGTGTgct
D706-long	CAAGCAGAAGACGGCATAACGAGAT- ACGAATTCGTGACTGGAGTTCAGACGTGTgct
D707-long	CAAGCAGAAGACGGCATAACGAGAT- AGCTTCAGGTGACTGGAGTTCAGACGTGTgct
D708-long	CAAGCAGAAGACGGCATAACGAGAT- GCGCATTAGTGACTGGAGTTCAGACGTGTgct
D709-long	CAAGCAGAAGACGGCATAACGAGAT- CATAGCCGGTGACTGGAGTTCAGACGTGTgct
D710-long	CAAGCAGAAGACGGCATAACGAGAT- TTCGCGGAGTGACTGGAGTTCAGACGTGTgct
D711-long	CAAGCAGAAGACGGCATAACGAGAT- GCGCGAGAGTGACTGGAGTTCAGACGTGTgct
D712-long	CAAGCAGAAGACGGCATAACGAGAT- CTATCGCTGTGACTGGAGTTCAGACGTGTgct

5.2 Experimental procedures

5.2.1 Generation of expression vectors

Cloning of constitutive JUN-Citrine and conditional Citrine/JUN-Citrine expression constructs

For constitutive expression constructs JUN open reading frames (ORF) was derived from the Precision LentiORF Collection pLOC plasmids (Dharmacon, kindly provided by E. Latz, Institute of Innate Immunity, Bonn, Germany). JUN (DQ896432) was cut from pLOC using BamHI/NheI restriction enzymes, pRp235 (kindly provided by E. Latz, Institute of Innate Immunity, Bonn, Germany) was cut by BamHI/AvrII. Fragments were gelpurified, ligated and transformed into *e. coli*. Sequence of ready constructs was validated using primers Seq-pRp-fwd and Seq-pRp-rev. Tetracycline inducible lentiviral plasmid pLV-tetO and transactivator construct pRp rtTA (obtained from J. Uttikal, DKFZ, Heidelberg, Germany) were used for conditional expression of JUN. JUN-Citrine cDNA was amplified from pRp235 JUN. Fragments were gelpurified, digested, PCR-column purified and cloned into pLV-tetO using Sall/MluI restriction sites. Sequence of ready constructs was validated in Sanger sequencing using primers Seq-pLV-tetO-fwd and Seq-pLV-tetO-rev.

PCR reaction:

- 5 µl Phusion® High-Fidelity buffer
- 0.5 µl dNTPs (10 mM stock)
- 1.25 µl pRpCitrine-MluI-fwd/ pRpJUN-MluI-fwd (10 µM stock)
- 1.25 µl pRpCitrine-Sall-rev (10 µM stock)
- 0.5 µl Phusion® polymerase
- 20 ng pRp235 JUN template DNA

PCR protocol:

- 98°C 3 min
- 98°C 20 s
- 60°C 20 s
- 72°C 45 s
- repeat 30x (98°C 20 s, 60°C 20 s, 72°C 45 s)
- 72°C 3 min

Restriction enzyme-based cloning of sgRNAs for CRISPR/Cas9-based genome editing

Single guide RNAs (sgRNAs) for targeting potential AP1 binding sites and control sites in the *NT5E* first intronic enhancer were chosen according to ENCODE ChIP-seq anno-

tated JUN binding sites in *NT5E* and localization of AP1 consensus binding site motifs within and nearby *NT5E*. *NF1* targeting sgRNAs for KO generation were directed to exon 4 and exon 27 in order to cover all splice variants and control for off target effects. For design of sgRNAs rules described at <http://www.genome-engineering.org> were obeyed and targeting sequences were cloned into px330-U6-Chimeric-BB-CBh-hSpCas9 (px330, Addgene #42230) expressing Cas9. BbsI restriction digest was used to generate custom-built overhangs in px330. Targeting sequences were purchased as complementary oligonucleotides with predefined px330 cut BbsI matching overhangs and dissolved at 3 mg/ml. For oligo-annealing 1 μ l of each TS and BS oligonucleotide was mixed in 48 μ l annealing buffer and incubated at 95°C 4 min, 70°C 10 min, 70°C 1 min 30 s, decreasing 1°C per cycle for total 60 cycles. Annealed oligonucleotides were ligated to BbsI digested and gelpurified px330 and transformed into *e. coli*. Sequence of ready constructs was validated using primer px330-U6-start in Sanger sequencing.

Restriction digest

5 μ g of vector backbones was digested in 30 μ l volume with 1.5 μ l of each enzyme for 3 h at 37°C. In case of separate double-digestion, 3 μ l of single enzymes were used. Gelpurified PCR fragments were digested in a volume of 15 μ l with 0.5 μ l of each enzyme for 3 h at 37°C. Reactions involving FastDigest™ enzymes AvrII, BamHI and NheI were performed in FastDigest™ buffer. Digestion by MluI/SalI and BbsI was done in NEB3.1 buffer and NEB2.1 buffer, respectively.

Gel electrophoresis

Digested vector backbones and PCR reactions were mixed with 6x gel loading buffer and separated on agarose gels in 1xTAE buffer at 140 V for 20 min. Addition of 5 μ l ethidium bromide (EtBr) per 150 ml gel solution enabled visualization of DNA fragments at an InGenius3 Gel Documentation System. Fragment size was indicated by GeneRuler 1 kb DNA ladder. 1%, 1.5% and 2% (w/v) agarose gel were used for DNA fragment sizes of >1000 bp, 250-1000 bp and <250 bp, respectively.

Gelpurification of fragments

Following gel electrophoresis gel-pieces of fragments of interest were cut under visualization at a UV transilluminator and purified using the InnuPREP Gel Extraction kit according to the manufacturer's instructions. DNA was eluted in 10 μ l Ampuwa® H₂O.

PCR column cleanup of fragments

For cleanup of digested PCR fragments the InnuPREP PCRpure kit was used according to the manufacturer's instructions. DNA was eluted in 10 μ l Ampuwa[®] H₂O.

Ligation of fragments

For ligation of digested and purified fragments vector backbone and insert DNA were mixed in Ampuwa[®] H₂O in a 3:1 molar ratio in 8 μ l volume plus 1 μ l 10x T4 DNA Ligase buffer. 1 μ l T4 DNA Ligase was added and ligation performed over night (O/N) at 16°C. A control reaction without an insert was performed in parallel for every ligation.

Transformation of ligated constructs into *e. coli* D10H β bacteria

Bacterial agar plates were pre-warmed at 37°C to allow easy absorbance of transformed bacteria suspension. Transformation competent *e. coli* D10H β bacteria were thawed on ice. For re-transformations of ready plasmids 0.5 ng of plasmid DNA, for transformation of ligated constructs 5 μ l of the ligation reaction was pipetted to 50 μ l of competent bacteria on ice, mixed by snipping and incubated for 15min. Heat shock was performed at 42°C for 45 s, followed by immediate incubation on ice for 2 min. Re-transformed bacteria were spread equally on pre-warmed bacterial agar plates and incubated upside down at 37°C for 16 h. For transformations of ligated constructs heat shocked bacteria suspension was transferred to 500 μ l of LB medium without antibiotics and shaken at 1000 rpm for 1 h at 37°C. Bacterial pre-culture was then pelleted at 6000 g for 10 min and 450 μ l of supernatant was aspirated. Bacterial pellet was resuspended, spread equally on pre-warmed bacterial agar plates and incubated upside down at 37°C O/N.

Minipreparation

For small scale DNA preparation single colonies were picked from agar bacterial plates and inoculated into 1.8 ml LB-medium containing 100 μ g/ml Ampicillin. Culture was shaken in a ThermoMixer[®] R at 1000 rpm, 37°C for O/N. Bacteria were pelleted by centrifugation at 6000 g for 10 min and pellet was resuspended in 250 μ l P1 resuspension buffer containing 100 μ g/ml RNase A. For lysis 250 μ l of buffer P2 was added and mixed by inversion. For neutralization 350 μ l of buffer N3 was added and mixture inverted. Precipitate was spun down at 20,000 g for 10 min and supernatant was transferred to spin columns for DNA preparation. DNA was bound to column by centrifugation at 10,000 g for 60 s and washed twice by 750 μ l PE wash buffer. After an additional spin at 20,000 g to remove remaining wash buffer, DNA was eluted in 35 μ l Ampuwa[®] H₂O and concentration was determined at a Nanodrop[™] 2000 instrument using Ampuwa[®] H₂O as a blank.

Midipreparation

For large scale DNA preparation single colonies were picked from agar plates or small samples of bacterial glycerol stocks were transferred to Erlenmeyer flasks into 150 ml LB medium containing 100 µg/ml Ampicilin and shaken at 180 rpm O/N. Bacteria suspension was transferred to 50 ml centrifugation tubes and pelleted at 4500 g for 1 h. DNA was isolated from bacteria pellet using the PureLink™ HiPure Plasmid MidiPrep kit according to the manufacturer's instructions.

Preparation of glycerol stocks

500 µl of bacteria solution was removed immediately before Mini- or Midipreparation, mixed in a screw cap cryovial with 500 µl of 60% v/v glycerol diluted in Ampuwa H₂O and directly frozen at -80°C for long term storage.

Sanger sequencing of ready constructs

Sanger sequencing was performed by Microsynth AG, samples were prepared in Ampuwa® H₂O according to the companies instructions and sent in a total volume of 15 µl with 700 ng plasmid DNA and 3 µl of 10 µM sequencing primer.

5.2.2 Cell culture and generation of cell lines

Cultivation of cell lines

All cell lines were kept in a humidified incubator at 37°C, 5% CO₂ and were passaged up to 3 months, then replaced by cryopreservations of younger passages. Adherent MaMel cell lines were growth in complete RPMI medium. HEK293T cells were grown in DMEM medium. For suspension culture of THP1 cells RPMI 1640-based THP1 medium was used. MaMel cell lines and HEK293T cells were passaged upon 80% confluence according to the ratios indicated in table 5.22. First cells were washed once with 5 ml of DPBS, then dislodged using 0.5 ml, 1 ml and 1.5 ml of 0.05% Trypsin-EDTA for T25 culture flasks, 10 cm culture dishes and T75 culture flasks, respectively and incubated for 5 min at 37°C, 5% CO₂. Trypsin reaction was stopped by adding appropriate amount of FBS-containing culture medium and splitted by removing the respective volume of cell suspension. Then the equal amount of pre-warmed complete RPMI medium was added to remaining cells in culture. THP1 suspension cells were passaged twice a week by removing 3/4 of total cell suspension and readjusting volume by addition of THP1 medium.

Table 5.22: Passaging ratios and schemes for the individual cell lines

Cell line	Splitting ratio	Splitting frequency
HEK293T	1:10	2x/week
MaMel.04	1:3	1x/week
MaMel.15	1:4	2x/week
MaMel.27	1:2	1x/ 2 nd week
MaMel.37a	1:3	2x/week
MaMel.48a	1:4	2x/week
MaMel.54a	1:10	2x/week
MaMel.65	1:10	2x/week
MaMel.67a	1:3	2x/week
MaMel.71	1:3	2x/week
MaMel.79b-e/-l	1:3	2x/week
MaMel.85	1:10	2x/week
MaMel.102	1:5	2x/week
MZ7	1:5	2x/week
SK.Mel28	1:10	2x/week
THP1	1:5	2x/week

Freezing and thawing of cell lines

Aliquots of about 5×10^6 cells were frozen in 1 ml volume. First, cell suspension was harvested and pelleted at RT using 300 g for 5 min. Medium was aspirated, cell pellet was resuspended in remaining 500 μ l of culture medium and transferred to a cryovial. After cooling down cell suspension for at least 5 min on ice, 500 μ l cold 2x freezing medium was added and briefly resuspended. Then, cryovials were immediately transferred to a MrFrosty™ freezing container and kept closed at -80°C for at least 8 h to allow standardized cooling of $-1^\circ\text{C}/\text{min}$. Frozen cells were placed to storage boxes, for long-term storage cells were transferred to -150°C . For thawing frozen cryovial from -80°C was incubated directly at 37°C in a waterbath until only small pieces of ice remained in vial. Cell suspension was eventually homogenized by pipetting up and down and added dropwise to 9 ml of pre-warmed culture medium in a centrifugation tube. Cells were spun at 300 g for 5 min at RT, remaining freezing medium was aspirated and cells resuspended and transferred to culture flask in an appropriate amount of culture medium.

Retroviral and lentiviral transduction of cell lines

HEK293T cells were plated in complete DMEM medium at a density of 1.2×10^6 per 6 well in the morning and were allowed to attach for at least 8 h. Packaging plasmids and plasmids encoding the gene of interest were transfected the same day in the evening by

the Calciumphosphate method: A transfection mixture containing plasmids in 1x HBS was prepared and mixed by brief vortexing. Then, 2.5 M CaCl₂ was added quickly and mixture immediately virtuously vortexed. After an incubation of 15 min at RT mixture was added drop-wise to adherent HEK293T cells. For pRp-based expression plasmids retroviral packaging constructs (gag-pol and pCMV VSV-G), for pLV-based expression plasmids 3rd generation lentiviral packaging system consisting of pCMVdelta8.91 and pCMV VSV-G were used. For every viral transduction a positive control transduction was included consisting of pRpGFP for production of retroviral particles and kH1GFP for production of lentivirus.

Transfection mixtures were prepared as follows:

Retroviral particles:

- 200 µl 1 x HBS
- 2 µg retroviral expression construct
- 2 µg gag-pol
- 220 ng pCMV VSV-G
- 10 µl 2.5 M CaCl₂

Lentiviral particles:

- 200 µl 1 x HBS
- 2 µg lentiviral expression construct
- 1.5 µg pCMVdelta8.91
- 600 ng pCMV VSV-G
- 10 µl 2.5 M CaCl₂

16 h after transfection medium on HEK293T cells was carefully replaced to pre-warmed complete DMEM harvest medium and target cells were seeded into 6 well plates to reach about 80 % of confluence at the time of infection. For infection harvest medium was collected from virus-producing HEK293T cells 40 h after transfection and filtered trough a 0.45 µm syringe filter unit. Medium of target cells was replaced by 2 ml of undiluted virus supernatant per well and incubated for 24 h at 37°C, 5 % CO₂. In the meantime new complete DMEM harvest medium was added to virus-producing HEK293T cells and a second round of infection was performed after 24 h for another 24 h. Finally viral supernatant was removed and complete RPMI medium added. Selection was started 48 h after the last infection with either Puromycin (for all pRp-based plasmids) at a concentration of 2 µg/ml or Blastidicine (for all pLV-based plasmids) at a concentration of 10 µg/ml for at least 5 days. A negative control of non-infected target cells was included for selection and selection was carried out until all cells in the negative control wells were dead. Cells were frozen and experiments were started not before transduced cells had been splitted three times and could be considered security level 1(S1) organisms. For generation of MaMel.79b_{late} lines with tetracycline inducible expression of cJUN-Citrine and Citrine (named: MaMel.79b_{late} inducible cJUN-Citrine

and MaMel.79b_{late} inducible Citrine), infection with pRp rtTA followed by Puromycin selection was done prior to infection with pLV-tetO-cJUN-Citrine or pLV-tetO-Citrine and consecutive Blasticidine selection.

Generation of polyclonal CD73 intronic enhancer CRISPR/Cas9 targeted cell lines

24 h prior to transfection target cells were seeded at a density of 5000 cells per 96well. For AP1-site/ Control site targeting in the CD73 enhancer region of MaMel.79b_{late}JUN-CitrineDOX 150 ng of px330 containing the respective AP1-site/ Ctrl-site targeting sgRNA (AP1-1 , AP1-2a, AP1-2b, AP-5, AP1-6 , Ctrl) was mixed with 50 ng of pRp mTomato in 10 μ l OptiMEM™ medium. For targeting MaMel.54a, MaMel.65, MaMel.85 and SK.Mel28 a reduced set of AP1-site/ Ctrl-site targeting sgRNAs (AP1-2a, AP1-5 and Ctrl) was used along with pRp GFP instead of pRp mTomato. 0.6 μ l of Fugene® HD transfection reagent was added per DNA-OptiMEM™ mixture, briefly vortexed and incubated at RT for 15 min, then mixture was added to the cells. 48 h post transfection cells were FACS sorted to enrich for successfully transfected cells by either sorting on mTomato or GFP depending on the transfection mixture setup and then further expanded in culture.

5.2.3 Stimulation and manipulation of cells

For seeding of cells cell number was determined using a TC10™ automated cell counter. Cell solution was pre-diluted to fit a range of 5×10^4 – 1×10^7 5×10^4 – 1×10^7 cells/ml and 10 μ l of cell suspension applied per counting chamber. Singlet cells were ensured by visual examination of the counting image.

For analysis on cell surface and total protein at baseline or treatment for up to 48 h 200,000 cells were seeded per well into 12 well plates 24 h prior analysis and handled according to immunoblotting and flow cytometric procedures described in the respective section below. For analysis on cell surface and total protein cells were seeded 24 h prior analysis or further treatment and handled according to immunoblotting and flow cytometry procedures described in the respective section below. For baseline expression analysis and treatment for up to 48 h 200,000 cells were seeded per well into 12 well plates. For 4 day or 5 day inhibitor treatment using DMSO, SP600125, Sotrastaurin and MK2206 70,000 cells were seeded per 12 well. Interfering with MAPK cascade signaling by Trametinib and SCH772984 as well as PI3K blockade by BEZ235 strongly inhibited melanoma cell growth, therefore for 4 day or 5 day inhibition 200,000 cells were seeded into 6 well plates. Inhibitors and cytokine/ growth factor stimuli were applied according to the concentrations indicated in tables 5.7 and 5.6, respectively. In case of long term cytokine/ growth factor stimulation treatment was renewed at day 3 for analysis on day 5.

For long term Trametinib inhibition for a total of 18 days, 200,000 cells were seeded

to 3 and 6 additional 6 wells for analysis on day 10 and day 18, respectively. Inhibitor solution was renewed every 5th day. For Trametinib withdrawal experiments cells were washed two times with PBS following 4 days culture in Trametinib and culture medium renewed after 5 days for analysis on day 12 post withdrawal. Again, separate 6 wells for each time point of analysis was seeded.

THP1 SN was generated as described below and aliquots rapidly thawed in a waterbath. For stimulation culture medium was supplemented with 50% v/v of either THP1 SN or THP1 medium for analysis at day 5 on CD73 induction or within 24h for time line experiments of TF accumulation and protein phosphorylation.

5-Azacytidine was dissolved in DMSO and stored at -80°C and used up to six months. As specified for individual experiments, 1-10 µM 5-Azacytidine was used for 6 days to achieve global demethylation and treatment renewed daily. Subsequently, the medium was supplemented for 3 day stimulation with 1000 U/ml TNF α and 50 ng/ml HGF.

Generation of THP1 supernatant

For differentiation of THP1 cells 12×10^6 of suspension cells were seeded per 10 cm dish in 100 ng/ml PMA for 48 h, which was generating a 70% confluent adherent culture. For harvest of supernatant cells were washed twice with PBS, detached with 1 ml 0.05% Trypsin-EDTA for 5 min and re-plated on new 10 cm dishes in 10 ml THP1 cell medium. After 48 h medium was collected, remaining cells removed by 0.45 µm syringe filtering and aliquots quick frozen in a dry ice/ isopropanol bath and stored at -80°C until used for experiments.

5.2.4 RNA isolation, cDNA synthesis and qPCR

RNA isolation

Cells seeded in 12 wells at a confluence ranging from 30-100% (1×10^5 - 10^6 cells depending on experimental set up) were lysed with 350 µl RLT lysis buffer and frozen at -80°C for at least 5 minutes. RNA clean up protocol was adapted from Zymo RNA Clean and Qiagen RNeasy kit protocols. All centrifugation steps were performed at RT. Briefly, thawed lysates were mixed with 70% ethanol in Ampuwa[®] H₂O, volume was applied on a Zymo-Spin[™] II column, following spin at 10,000 g for 60 s. Column was washed first by 500 µl RW1 buffer, centrifuged 10000 g for 60 s, then by 500 µl Zymo wash buffer, centrifuged 10,000 g for 60 s, remaining buffer was completely removed with an additional spin at 20,000 g for 2 min. 20-40 µl of H₂O was added directly on column, incubated for 5 min at RT and RNA eluted at 10,000 g for 1 min. RNA concentration was measured at a Nanodrop 2000 instrument and RNA was stored at -80°C until further analysis.

cDNA synthesis

300-1000 ng of total RNA was transcribed into cDNA in a 10 µl reaction using the All-in-One cDNA synthesis SuperMix (contains a mix of oligo(dT) and random hexamer primers) according to the manufacturer's instructions. For cDNA synthesis the extended protocol guaranteeing higher quality of cDNA was chosen with incubations steps of 10 min at 25°C, followed by 30 min at 42°C and finally 5 min at 85°C. cDNA was stored at -20°C until further analysis.

Quantitative Real-Time-PCR (qPCR)

cDNA was diluted 1:5 with Ampuwa[®] H₂O and technical duplicates of diluted cDNA probe were included in the qPCR run in a 96 well qPCR plate.

Per well a reaction mixture was set up as follows:

- 1 µl of diluted sample cDNA
- 2 µl EvaGreen[®] qPCR Mix II
- 0.6 µl fwd and rev qPCR primer mix of the transcript of interest (10 µM)
- 6.4 µl Ampuwa[®] H₂O.

On a routine bases a standard curve of mixed cDNA from every experiment and primer was included in every sample run to test on amplification efficiency. Primer specificity was tested by melting curve analysis. Analysis of Ubiquitin expression was included for every cDNA sample for normalization and relative mRNA expression. In case of inhibitor treatment or stimulation relative gene expression are shown as referenced to a control condition if not indicated otherwise. For relative quantification analysis the Efficiency Method provided by the Light Cycler[®] 480 Software was applied with CP analysis based on the Second Derivative Maximum method. mRNA expression was expressed as normalized ratio of the relative concentrations (conc.) calculated for the individual samples according to the formula:

$$\text{Normalized Ratio} = \left(\frac{\text{conc. target}}{\text{conc. reference}} \right)_{\text{treated sample}} : \left(\frac{\text{conc. target}}{\text{conc. reference}} \right)_{\text{control treated}}$$

5.2.5 ChIP qPCR

For chromatin immunoprecipitation (ChIP) MaMel.79b_{late}JUN-CitrineDOX and MaMel.79b_{late}CitrineDOX were cultured at a confluency of 80% on three 15 cm dishes each. After 24 h treatment with 25 ng/ml Doxycycline Citrine and JUN-Citrine induction was at peak. Using SimpleChIP[®] Enzymatic Chromatin IP Kit according to the manufacturer's instructions chromatin was crosslinked, purified and digested using optimized protocol of 3 µl of micrococcal nuclease per pooled sample. DNA fragmentation into dinucleosomes was achieved by sonification with three times 20 pulses, each 20 s at 20% output and 20% duty cycle at a Branson Analog Sonifier 250. Proteinase K digestion of a small test aliquot allowed quality control of DNA fragmentation by

visualization on a 1% (w/v) agarose gel. DNA concentration of chromatin preparation was measured at a Nanodrop 2000 spectrometer.

For immunoprecipitation 10 μg of chromatin was diluted into 500 μl 1x ChIP buffer derived from the SimpleChIP[®] Enzymatic Chromatin IP Kit and a 2% Input sample retained for qPCR allowing normalization and calculation of sample site occupancy. Obeying the SimpleChIP[®] protocol 5 μl of IgG and 10 μl of anti-HistonH3 antibodies were set up per ChIP as negative and positive control, respectively. For ChIP against Citrine and JUN-Citrine 25 μl GFP-Trap[®] -MA beads (ChromoTek) were added. According to the GFP-Trap[®] -MA protocol GFP-Trap[®] -MA beads were incubated for 4 h at 4°C, control antibodies were incubated O/N at 4°C as indicated. Magnetic bead separation, sample elution, reverse crosslinking, DNA column purification and elution of final DNA in 50 μl elution reagent C was performed as suggested. Samples were run in technical duplicates in qPCR with each 1 μl of sample input as described above. A standard dilution of the input samples was included to adjust for amplification efficiencies.

% Input was calculated as follows:

$$\text{Input normalized } IP \text{ value: } (\Delta C_t) = (C_t[IP] - (C_t[input] - \log_2 DF))$$

$$\text{with } DF[2\% \text{ input fraction}] = 50$$

$$\% \text{ input} = (2^{-\Delta C_t}) \times 100$$

DF = dilution factor

C_t = cycle threshold

IP = Immunoprecipitation

5.2.6 Immunoblotting

In order not to interfere with phosphorylation states of signal transduction proteins cells were lysed directly from culture dish in 1x Lämmli buffer (20,000 cells / 10 μl Lämmli buffer) and proteins denatured at 95°C for 5 min. 15 μl of sample were run per lane on a SDS PAGE gel. First gels were run at 100 V for 10 min, and then voltage was increased to 140 V until loading front run out of gel. 6%, 10% and 12% SDS PAGE gels were used for protein sizes of >100 kDa, 40-100 kDa and <40 kDa, respectively. A wet blotting system and 20% (v/v) methanol containing transfer buffer were used and protein transfer onto a 0.45 μm pore size nitrocellulose membrane was accomplished at 450 mA for 1.5 h (for large protein transfer from 6% gels 200 mA O/N). Membranes were then blocked in 5% (w/v) BSA in TBS-T for 1h at RT before primary antibodies were added in 5% (w/v) BSA and 0.02% (w/v) sodium acid (for antibody dilution see table 5.9). All antibodies were incubated O/N at 4°C, except antibody directed against Actin that was incubated for 1 h at RT. Following primary antibody incubation

membrane was washed 3 times in TBS-T for 10 min and incubated with fluorescently labeled secondary antibodies (1:15,000) in TBS-T containing 5% (w/v) BSA for 1 h at RT in the dark. Membranes were washed twice in TBS-T and once in TBS for 10 min each and scanned on an Odyssey[®] Sa Imaging System from LI-COR[®]. In case of harvesting cells from experiments involving differential cell growth or when combining lysates from different cell lines an actin loading blot from 10 μ l of lysate was run first and loading was adjusted according to the actin signal strength. Therefore, actin signal was quantified using the Odyssey[®] Sa Application Software.

5.2.7 Flow cytometry based methods

Flow cytometric analysis

For stimulation experiments cells were harvested from 12 wells by 150 μ l of 0.05% Trypsin-EDTA for 5 min at 37°C, 5% CO₂, resuspended in 500 μ l culture medium and 200,000 cells were seeded per round bottom 96 well test plate. An unstained control was included for every single stimulation and inhibition condition and cell line. Cells were pelleted at 420 g, 3 min, washed once with 200 μ l FACS buffer and stained 30 min on ice in 50 μ l FACS buffer with Brilliant Violet 421[™] anti-CD73mAb 1:100 (clone AD2, Biolegend). Antibody was removed by three times washing with 200 μ l FACS buffer, 420 g, 3 min. For 5-Azacytidine treated cells propidium iodide staining (5 μ l per test, BD Bioscience) was included immediately prior FACS analysis. 20,000 cells in the P1 live gate were recorded on a FACS Canto II flow cytometer (BD Bioscience) and analyzed using FloJo[®] software (TreeStar, V7.8 for Mac).

FACS sorting on successfully transfected cells by CRISPR/Cas9 sgRNA constructs

48h post CRISPR/CAS9 construct transfection, cells in 96 wells were washed once with PBS and detached with a centered drop of 0.05% Trypsin-EDTA for 5 min at 37°C. 100 μ l of growth medium were added and cell solution resuspended. pRp mTomato and pRpGFP positive cell fractions for MaMel.79b_{late}JUN-CitrineDOX and MaMel.54a/ MaMel.65/ MaMel.85 respectively were sorted on a FACS ARIA III cell sorter under sterile conditions and replated in a 96 well format for expansion.

FACS sorting of polyclonal CD73 intronic enhancer CRISPR/Cas9 targeted cell lines

In MaMel.79b_{late}JUN-CitrineDOX CRISPR/Cas9 engineered cell lines CD73 expression was induced by 25 ng/ml Doxycycline for 5 days. MaMel54a/ MaMel.65 and MaMel.85 CRISPR/Cas9 engineered cell lines were harvested directly for accession of baseline CD73 levels. For FACS sorting 8 \times 10⁶ individual cell lines were harvested and stained according to the protocol described above, adjusted in volume to 2ml FACS buffer per

staining. FACS sorter machines were operated by Andreas Dolf and Peter Wurst in the FACS core facility of the University Hospital, Bonn. Using a FACS INFLUX cell sorter 100,000 cells of each 10% most dim, 10% brightest and total CD73 positive fraction were sorted in triplicates into FACS buffer, pelleted at 300 g for 5 min and resuspended in 20 μ l of DLB buffer containing 100 μ g/ml Proteinase K and digested at 65°C for 1h, followed by inactivation at 95°C for 15 min. Lysate was further used as template for dual barcoding PCRs for deep sequencing. Simultaneously, samples were read in at FACS Canto II flow cytometer for recording of total cell population CD73 expression levels.

5.2.8 Bisulfite conversion based methylation analysis by deep sequencing

Bisulfite conversion spares methylated cytosine residues from conversion, but all native cytosine residues in DNA are converted to uracil, enabling the detection of methylation status a CpG island by subsequent sequencing procedures. Commonly, subcloning of converted DNA and Sanger sequencing of several clones is used. However, here we use deep sequencing for methylation quantification enabling considerable increase in depth.

Isolation of genomic DNA (gDNA) for bisulfite conversion

5×10^6 were resuspended in 500 μ l lysis buffer for gDNA extraction, Proteinase K added at a final concentration of 100 μ g/ml and incubated at 56°C, 900 rpm O/N. 166.7 μ l of 5 M NaCl was mixed to the lysate and gDNA was precipitated by addition of 2 volumes of ethanol and heavily vortexed. gDNA was captured with a pipet tip, transferred to a new reaction tube and washed in 70% ethanol. gDNA was pelleted at 20,000 g for 5 min at RT, supernatant removed completely, air-dried for 30 min and dissolved in 50 μ l Ampuwa[®] H₂O. DNA concentration was measured at a NanoDrop 2000 system.

Bisulfite conversion assay

For conversion 500 ng of gDNA was included in the conversion reaction using the EZ DNA-Methylation direct kit and the protocol was executed according to the manufacturer's instructions. Bisulfite converted gDNA was eluted in a volume of 10 μ l Ampuwa[®] H₂O and frozen at -80°C until further analysis.

5.2.9 Sample preparation and running deep sequencing

Generation of whole cell lysates as template for DNA amplification

For deep sequencing analysis of CRISPR/Cas9-based targeting in a polyclonal cell population 100,000 cells of the population of interest were lysed in 20 μ l of DLB buffer containing 100 μ g/ml Proteinase K and incubated at 65°C for 1h, followed by 95°C for 15 min. Lysates were directly used for PCR or stored at -20°C until use.

PCR amplification of CRISPR/Cas9-targeted regions from genomic DNA of whole cell lysates and bisulfite converted DNA for deep sequencing analysis

Two consecutive PCRs were set up. In a first step amplification of the region of interest was performed with target region specific primers creating an amplicon of 200-250 bp length and containing an adapter sequence for binding of second level barcoding primers. For CRISPR/Cas9-targeted regions 19 cycles with an annealing temperature of 60°C, for bisulfite converted DNA 34 cycles with an annealing temperature of 54°C were run in first PCR. In a second level PCR an index for deep sequencing was introduced by amplification with a barcoding primer pair binding to the adapter regions of the first level PCR. For quality control 5 μ l of second level PCR products were subjected to gel electrophoresis on a 2% agarose gel. Remaining volume was then pooled for deep sequencing proportionally to the individual PCR signal strengths on gel. If all samples exhibited similar PCR signal strengths 4 μ l of all PCR reactions were pooled for deep sequencing.

Reaction mix for first level PCR:

- 5 μ l Phusion[®] HF 5x buffer
- 0.5 μ l dNTPs (10 mM stock)
- 1.25 μ l target region specific fwd primer (10 μ M stock)
- 1.25 μ l target region specific rev primer (10 μ M stock)
- 0.25 μ l Phusion[®] polymerase
- 4 μ l DLB cell lysate /1 μ l bisulfite converted genomic DNA
- add 25 μ l H₂O

Reaction mix for second level PCR:

- 2.5 μ l Phusion[®] HF 5x buffer
- 0.25 μ l dNTPs (10 mM stock)
- 1.25 μ l barcoding fwd primer (5 μ M stock)
- 1.25 μ l barcoding region specific rev primer (5 μ M stock)
- 0.25 μ l Phusion[®] polymerase
- 2 μ l first level PCR
- 5 μ l H₂O

PCR protocol (first and second level PCR):

98°C 1 min
98°C 20 s
60°C 20 s
72°C 30 s
repeat 19x (95°C 20 s, 60°C 20 s, 72°C 30 s)
72°C 3 min

Sample pool clean up for deep sequencing analysis

For sample pool clean up of experiments aiming at analysis of monoclonal targeting events separate sample pools were mixed in a single tube proportionally to the number of clones. For experiments aiming at sequencing of polyclonal targeting sample pool clean up was performed separately for each experiment. Preparation of sample DNA was done in collaboration with Dr. Jonathan Schmid-Burgk and Dr. Tobias Schmidt in the group of Prof. Dr. Veit Hornung, Bonn. Sample pools were run on a 1% (w/v) agarose gel and PCR product bands from 300-400 bp length were purified by column-based gelpurification. DNA was eluted in 200 µl H₂O each sample. For precipitation 1 µl glycogen, 20 µl 3 M sodium acetate pH 5.2, 220 µl isopropanol was added, virtuously mixed and incubated on ice for 20 min. DNA was pelleted at 20,000 g at 4°C for 5 min, supernatant was removed and pellet washed with 70% (v/v) ethanol. After centrifugation at 20,000 g at 4°C for 5 min, liquid was completely removed and DNA was air-dried. For recovery of DNA pellets were resuspended in 35 µl Ampuwa[®] H₂O and dissolved at 37°C, 900 rpm for 5 min in a ThermoMixer[®]. Finally, remaining non-dissolvable remnants were pellet at 20,000 g for 5 min and 25 µl of supernatant transferred to a new reaction tube. DNA concentration was measured twice on a Nanodrop 2000 spectrometer instrument.

Deep sequencing at Illumina MiSeq

The MiSeq sample cassette was thawed in a waterbath and stored on ice until use. DNA samples were mixed in Illumina hyb buffer according to the desired amount of reads for the respective individual samples (500 and 10,000 reads per clone in monoclonal and polyclonal samples) in a total volume of 350 µl. For calculation, 32 ng of sample DNA were expected to yield 10⁶ reads. 10 µl of sample mixture was denatured by 10 µl 0.2 N NaOH for 5 min. Thereafter 980 µl Illumina hyb buffer was added on ice. For dilution 180 µl of denatured sample was mixed with 420 µl Illumina hyb buffer and total volume applied to the Illumina cassette. Illumina MiSeq was started and run according to the manufacturer's instructions using the single read protocol generating data in FASTQ format for further analysis. MiSeq sequencing runs were conducted by Dr. Jonathan Schmid-Burgk and Dr. Tobias Schmidt in the group of Prof. Veit Hornung, Bonn or forwarded to the deep sequencing core facility of the University Hospital Bonn.

5.2.10 Bioinformatic analyses

Evaluation of deep sequencing data from CRISPR/Cas9-based FACSorting enhancer screening

Deep sequencing data on CRISPR/Cas9-based FACSorting enhancer screening were either analyzed on enrichment/ depletion of successful targeting for a predefined target site using the javascript web-based software outknocker.org [215] or by positional mutation analysis for screening single basepair position-wise enrichment/ depletion of targeting by an algorithm developed in the R programming environment that uses positional mutation tables text-files obtained from outknocker.org as input files.

For validation, technical triplicates of total cell pools of individual CRISPR/Cas9 targeted cultures were sequenced 14 days post transfection and individual sgRNA genome editing frequencies controlled on homogeneity across sgRNAs. Furthermore complexity of the polyclonal cell pool was assured by checking on high diversity of genome editing within individual samples. From here consistency for subsequent was controlled. Sample preparation and sequencing depth was adjusted to stably cover 10,000 cells in input DNA by sequencing, affirming reliability of the fractional sorting and sequencing procedure.

For outknocker.org based analysis AP1 consensus binding motifs targeted by the respective JUN/ AP1 site sgRNAs were set as nuclease target site. Specification of the nuclease target site to AP1 motif sequence coerced InDel frequency analysis to premise InDels overlapping with the canonical AP1 binding motif. For control targeting total guide sequence was used as recommended in the software's instructions. For analysis, percent mutated at target site was determined from the quotient of reads counted with InDels at target site to total reference sequence aligned reads. Next normalization of mutation frequency of CD73^{high} and CD73^{low} sorted samples to mutation frequency in the CD73 total sorted sample was done in order to compensate for intra-experimental differences in editing efficiency due to differential active sgRNAs.

Positional mutation analysis is based on data tables containing the counts of mutated reads for every position across the reference sequence amplicon. Positional mutation frequency was calculated by dividing counts of mutated reads for every single base position by the number of total deletion reads. In order to compensate for differences in deletion lengths affecting the above introduced ratio, we integrated area under curve (AUC) normalization by position-wise dividing positional mutation frequencies by the sum of positional mutation frequencies across the total reference sequence. Biological independent triplicates were then combined and position wise deviation illustrated by error bars of SD.

R based positional mutation analysis enables automated calculation and ggplot based visualization of positional mutation frequencies for a sequence window of CRISPR/Cas9 predicted cutting site +/- 20 bp.

Quantification of CpG island methylation in Bisulfite deep sequencing approach

For quantification of CpG island methylation a specified, custom designed version of the javascript-based Outknocker.org software was written and provided by Dr. Jonathan Schmid-Burgk (BisulfiteSeq quant Table 1.0): Reference amplicon sequence is pasted into the program and converted for all cytosine residues except CpG islands by the program for alignment analysis. Next, deep sequencing raw reads are imported in FASTQ format and aligned to the adjusted reference sequence while ignoring all CpG islands. Positional counts of base frequencies were aggregated from successfully aligned reads and displayed in an output table across the reference sequence. For generation of sequence logos first 100 aligned amplicon sequences are provided by the software. Percent of methylation was then calculated by the ratio of cytosine to thymidine residues at the individual CpG islands and illustrated in pie charts.

UCSC genome browser and ENCODE regulatory tracks TF binding analysis

The UCSC Genome Browser human GRCh37/hg19 assembly from February 2009 was accessed at <http://www.genome.ucsc.edu/>. Genomic sequence surrounding *NT5E* Ref-Seq transcript was loaded and analyzed for chr6:86,108,517 to chr6:86,211,362. ENCODE regulation tracks used comprised layered H3K27Ac, H3K4Me3 and H3K4Me1 layered from 7 cell lines. DNaseI hypersensitivity clusters in 125 cell types and TF ChIPseq from 161 TFs with Factorbook motifs in 91 cell types.

R based melanoma plasticity analyses

For bioinformatic analyses R programming (R version 3.3.3) was used within R Studio (version 1.0.143). Visualization was based on ggplot, ggrepel and ggpubr packages. For data processing packages useful, dplyr, reshape2 and tidyr were loaded.

Microarray datasets GSE51221 ($n = 17$) [13] processed for variance stabilization and normalization by vsn package (bioconductor), GSE4843 ($n = 45$) [107] and GSE7127 ($n = 63$) [118] were acquired from NCBI's Gene Expression Omnibus (GEO) database and loaded into R using the GEOquery package. For annotation hgu133a2.db and AnnotationDbi packages were applied. RMA-normalized data of the BROAD melanoma cell line panel ($n = 88$) as published by Lin *et al* [142] was downloaded from the Melanoma Genomics Portal (<http://portals.broadinstitute.org/IGP/home>) and imported into R.

Data was log₂ transformed and probelIDs of individual genes aggregated on mean expression based on gene symbols for further analysis. Verfaillie *invasive* signature genes were published by Verfaillie *et al* [262], Hoek *invasive* and *proliferative* signature genes were obtained from Hoek *et al* [107] and TNF response signature we had generated previously in our lab by Riesenber *et al* [201] and consists of 237 individual genes with more than 2 fold change in expression by 72h TNF α in 8 of 17 melanoma cell lines of

the GSE51221 cohort [13].

In order to determine individual gene signatures, first, subsetting on probeIDs of genes belonging the respective gene expression signature was performed. Then gene signatures in individual samples were calculated by aggregating on mean expression of probeIDs of the respective signature genes and averaging expression of all signature genes in a next step.

Moving average (movAVG) calculation was adapted from Riesenber *et al* [201] and an improved version of the movAVG algorithm written. In brief, expression data of a given panel is ranked according to marker gene or signature expression that is *invasive* signature expression in the data presented in this study. Mean centered movAVG describes averaged gene expression of a gene of interest across this ranked data panel. Importantly, averaged gene expression is calculated from a sample window with centered mean stepwise moving across the data panel. Sample window is fixed to odd numbers in the algorithm presented and a sample window of $n = 13$ had been used in this study covering a panel size of $n = 88$.

For classifying the BROAD melanoma cell line panel into $MITF^{high}$ *proliferative* and $MITF^{low}$ *invasive* phenotypes cell lines were ranked according to *invasive* gene expression ranked and compartmentalized at inflection point of *MITF* expression. $MITF^{high}$ *proliferative* cell lines were further divided based on *NT5E* expression upon nascent invasiveness into $MITF^{high}$ $CD73^{low}$ *proliferative* cell lines and $MITF^{high}$ $CD73^{high}$ *nascent invasive* cell lines and grouping reproduced by K-means clustering based on *MITF* and *NT5E* expression as described below.

K-means clustering was conducted based on *MITF* and *NT5E* expression as collapsed from individual gene probe IDs within the R environment using implemented default Hartigan and Wong algorithm. Based on plasticity analyses by invasiveness ranking and movAVG implementation three phenotypes were expected and clusters were set to $k = 3$. Algorithm was run with $randomseed = 20$ and $nstart = 0$. For visualization normal confidence ellipses were drawn at a confidence level of 0.95.

Gene set enrichment analysis (GSEA)

Gene set enrichment analyses (GSEA) were run on the GSEA javascript based software (v3.0) [240] downloaded from the BROAD institute website (<http://software.broad-institute.org/gsea/index.jsp>). For analysis probeIDs of the BROAD melanoma cell line panel expression dataset were collapsed to gene symbols as described above. Phenotype labels were generated on fly to cover cell lines of the $MITF^{high}$ *nascent invasive* and $MITF^{high}$ *proliferative* phenotype that had been assigned by cell state interrogation. Analysis on the C2 collection of curated gene sets ($n = 2235$) derived from the BROAD Molecular Signature Database v.6.1 (MSigDB) (<http://software.broadinstitute.org/gsea/msigdb/index.jsp>) was performed with permutation type set to gene sets and keeping the default of 1000 permutations to calculate enrichment scores for $MITF^{high}$ *nascent invasive* phenotype versus $MITF^{high}$ *proliferative* phenotype. Impact of gene sets was

determined by ranking according to normalized enrichment score (NES) and false discovery rate (FDR) corrected p-values.

5.2.11 Statistics

If not indicated otherwise FACS and immunoblot data show representative experiments of three replicates. qPCR, ChIP and enhancer screening data are depicted as means of $n=3$ with error bars indicating SD.

Statistical tests performed are indicated in figure legends of the individual experiments. If not indicated otherwise two-sided paired and un-paired Student's T test were performed in Excel. Boxplots comparing gene expression across melanoma phenotypes were calculated and plotted within the R environment and evaluated by ggplot builtin statistics in two-sided unpaired Student's T-Tests with multiple comparison correction according to Benjamini and Hochberg via FDR. For stimulation and inhibitor panels comparing more than two groups ANOVA was run within the GraphPad Prism software and Bonferroni post-hoc test used for multiple comparison correction comparing individual treatment conditions to the respective DMSO control sample. For correlation analysis Pearson correlation with 0.95 confidence level and two-sided testing on significance was used. Significance levels are indicated as follows: *, $P<0.05$; **, $P<0.01$; ***, $P<0.001$; n.s.=none significant.

6 Results

6.1 CD73 is a marker for melanoma cell plasticity

6.1.1 Bioinformatic analysis on a large panel of melanoma cell lines reveals CD73 as a marker expressed upon *nascent invasiveness*

The current concept of melanoma cell plasticity defines two opposing cell states: The MITF^{high} *proliferative* cell state is formed by a highly differentiated population of melanoma cells and is opposed by a MITF^{low} *invasive* cell state [34, 107]. During phenotype switching melanoma cells undergo dedifferentiation and acquire an *invasive* gene expression signature. It has been shown that inflammation is a key trigger in that process [136, 280]. In more detail, we were able to show that a MITF / JUN antagonism is involved in orchestrating phenotype switching on a mechanistic level [201]. However, the detailed mechanisms of plasticity remain largely unknown. Paradigms have recently shifted from polarization into predefined phenotypes to understanding plasticity as a continuum of cell polarization [226]. We speculated that melanoma cell plasticity likely integrates into those paradigms and additional transition cell states such as a *nascent invasive* phenotype should be found during melanoma phenotype switching. The description of any transition cell state would yield fundamental insights into the mechanisms of melanoma cell plasticity.

In order to identify marker genes and mechanisms for such a *nascent invasive* melanoma cell state we made use of mRNA expression data of the well-characterized BROAD panel of melanoma cell lines ($n = 88$) [142] and ranked them according to their invasiveness, as calculated by expression of an EMT-like *invasive* gene signature published by Verfaillie *et al.* [262] (Figure 6.1 A). As expected, integration of *MITF* mRNA expression data showed significant anti-correlation with melanoma cell invasiveness and clearly separated MITF^{high} *invasive*^{low} from MITF^{low} *invasive*^{high} cell lines into the hitherto described melanoma phenotypes MITF^{high} *proliferative* and MITF^{low} *invasive* (Figure 6.1 , A, left diagram). As a control, cell line classification was confirmed by applying the widely accepted *invasive* and *proliferative* gene signatures published by Hoek *et al.* [107] (Figure 6.1 , A, right diagram).

For identification of an early plasticity marker we were especially interested in highly variably expressed genes within the MITF^{high} *proliferative* cell lines. Based on our previous

findings on inflammation priming melanoma cells for dedifferentiation and phenotype switching [136] we hypothesized that inflammatory marker genes are suitable candidates for indicating intrinsic inflammatory pathway activation and as such a *nascent invasive* cell state. Confirmative, expression of the $\text{TNF}\alpha$ response gene signature highly correlated with both established *invasive* gene signatures in the analyzed cell line panel (Figure 6.1, B). In the following, we filtered $\text{TNF}\alpha$ regulated genes that showed high variability in gene expression in the $\text{MITF}^{\text{high}}$ cell line fraction ($n = 57$) (Figure 6.1, C). Ranking according to variance in gene expression identified a small set of candidate plasticity markers (Figure 6.1, D). Among them we were especially interested in *NT5E* which encodes the 5'ectonucleotidase CD73 and constitutes a novel target in cancer immunotherapy [98]. CD73 converts AMP to immunosuppressive adenosine and is thereby shaping an anti-inflammatory tumor microenvironment [9]. Interestingly, CD73 is also an accepted marker for mesenchymal stem cells [58]. As a GPI-anchored plasma membrane protein it constitutes a well accessible marker for detection and isolation of cells.

In order to validate CD73 as a *nascent invasive* cell state marker we next analyzed *NT5E* mRNA expression in our panel ranked by *invasive* signature (Figure 6.1, E). Assuringly, we found CD73 to be diminished from $\text{MITF}^{\text{high}}$ *proliferative* cell lines with low *invasive* signature. *NT5E* expression starts in a subpopulation of $\text{MITF}^{\text{high}}$ *proliferative* cell lines upon *nascent invasiveness* and is further up-regulated in cell lines of the MITF^{low} *invasive* phenotype exhibiting strong increase in *invasive* signature gene expression. (Figure 6.1, E and F). Thereby, CD73 splits the $\text{MITF}^{\text{high}}$ *proliferative* phenotype into two distinct phenotypes, a $\text{MITF}^{\text{high}}$ CD73^{low} *proliferative* phenotype that is non-invasive and a $\text{MITF}^{\text{high}}$ $\text{CD73}^{\text{high}}$ *nascent invasive* phenotype, which we in the following classified as the $\text{MITF}^{\text{high}}$ *proliferative* and $\text{MITF}^{\text{high}}$ *nascent invasive* phenotype, respectively.

Affirmatively, the three subsets of melanoma phenotypes were also found when applying K-means clustering based on *MITF* and *NT5E* mRNA expression and defining three cluster centers as depicted in Figure 6.1, G. Multiple comparison analyses between the subsets showed that *NT5E* was robustly up-regulated already in the *nascent invasive* cell state while *MITF* and *proliferative* signature genes were still expressed. Inflammatory and *invasive* gene expression signatures were significantly up-regulated upon to the *nascent invasive* cell state (Figure 6.1, H). In contrast, other candidates of highly variably expressed $\text{TNF}\alpha$ response genes did not validate as *nascent invasive* phenotype marker but varied in gene expression within the $\text{MITF}^{\text{high}}$ *proliferative* cell lines independent from their *nascent invasiveness* (data not shown).

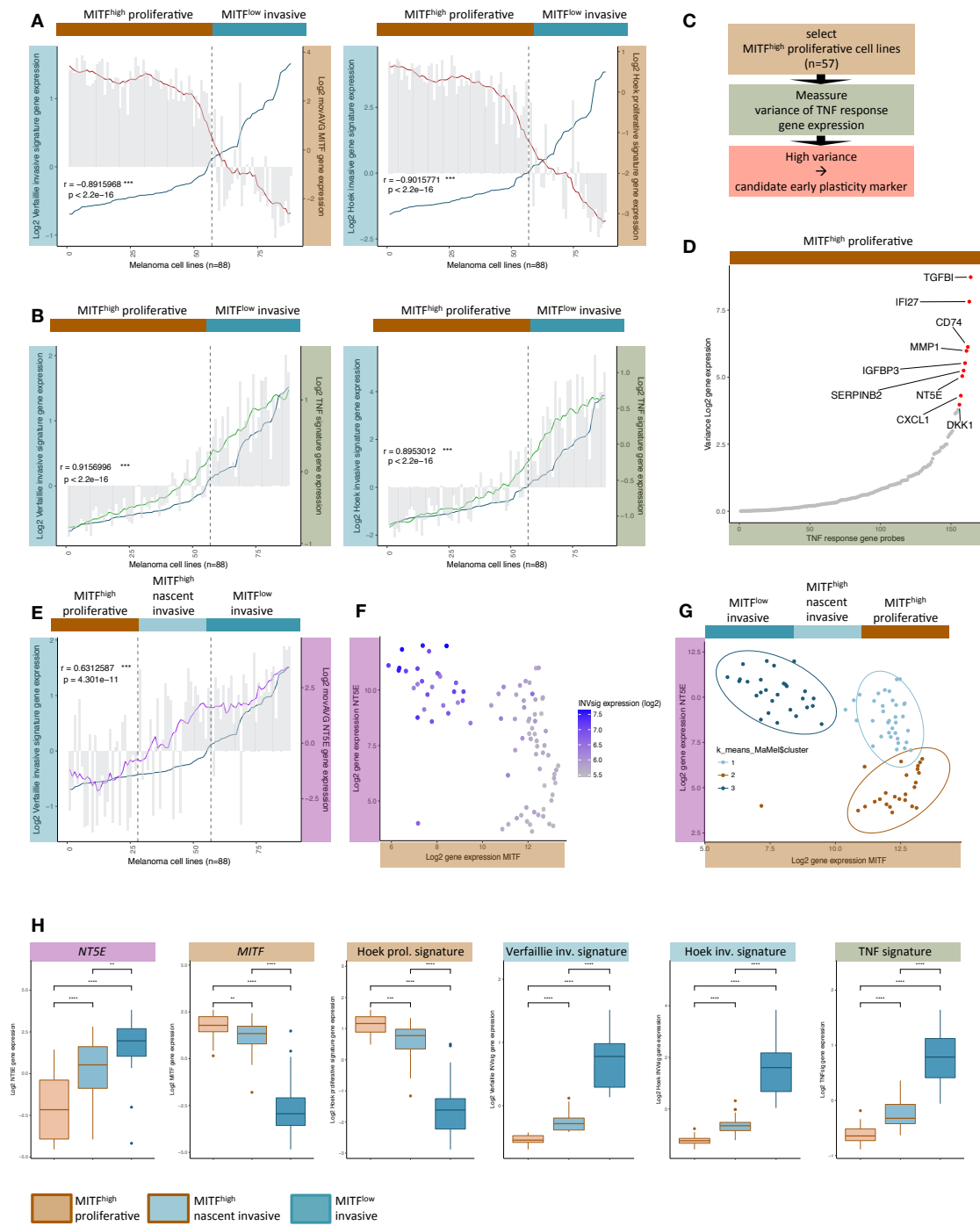


Figure 6.1: **CD73** marks a *nascent invasive* phenotype in melanoma: Continued caption see next page.

Figure 6.1: **CD73 marks a nascent invasive phenotype in melanoma (A)**: BROAD melanoma cell line panel ($n = 88$) ranked by Verfaillie (left diagram) and Hoek (right diagram) *invasive* signature gene expression. *MITF* expression as movAVG, bar charts indicating expression in individual samples. Dashed lines separate *MITF*^{high} *invasive*^{low} ($n = 57$) and *MITF*^{low} *invasive* ($n = 31$) cell lines. Pearson correlation with two-sided significance testing. **(B)**: Same as **(A)** but implementing expression of the TNF response gene signature [201]). **(C)**: Schematic overview on the experimental strategy for identification of nascent plasticity markers. **(D)**: Variance of TNF response genes by individual gene probes in *MITF*^{high} *proliferative* cell lines ($n = 57$) and plasticity marker candidates with variance > 4.0 highlighted. **(E)**: Same as **(A)** but implementing *NT5E* expression. Dashed line at left shows median separation of *MITF*^{high} *proliferative* ($n = 28$) and *MITF*^{high} *nascent invasive* cell lines ($n = 29$). **(F)**: Dot plots of *MITF* and *NT5E* expression for the BROAD melanoma cell line panel ($n = 88$). *Invasive* signature gene expression (INVsig) as blue color gradient. **(G)**: same as **(F)** but applying K-means clustering with $k=3$. Ellipses at 0.95 confidence level. **(H)**: *NT5E*, *MITF* and signature gene expression for the BROAD melanoma cell line panel ($n = 88$) clustered by phenotype as shown in **(G)** (inv. = invasive, prol. = proliferative). Two-sided, un-paired Student's T-Tests with multiple comparison correction according to Benjamini & Hochberg (aka FDR). movAVG group size=13. Expression data log₂ transformed. *, $P < 0.05$; **, $P < 0.01$; ***, $P < 0.001$; ****, $P < 0.00001$.

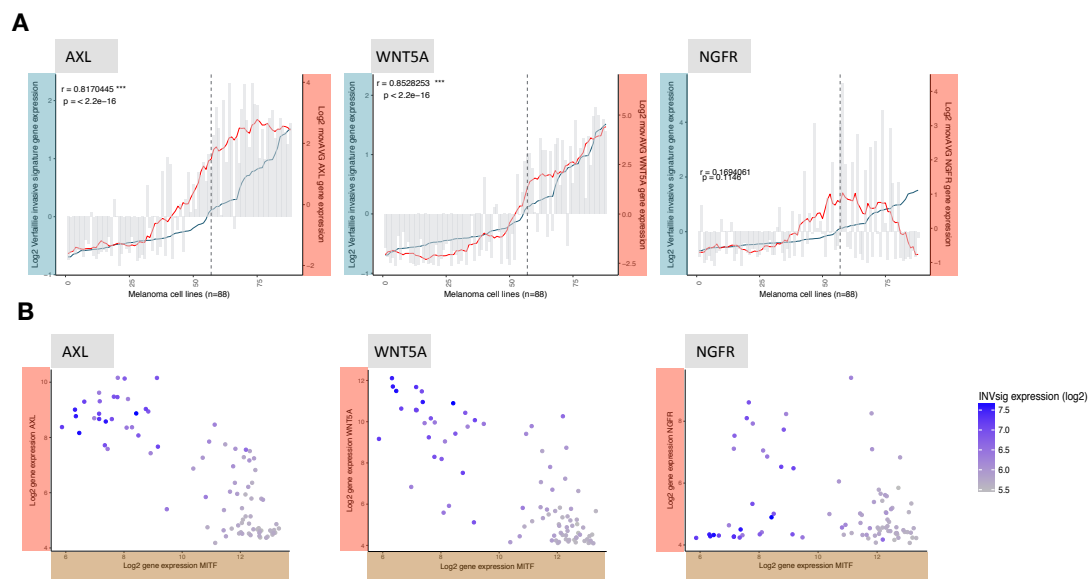


Figure 6.2: **Common *invasive* phenotype markers fail to indicate early phenotype switching. (A)**: BROAD melanoma cell line panel ($n = 88$) ranked by Verfaillie *invasive* signature and expression of *invasive* phenotype markers implemented as indicated by movAVG and bars for individual cell lines' marker expression. Dashed lines separate *MITF*^{high} *proliferative* ($n = 57$) and *MITF*^{low} *invasive* cell lines ($n = 31$). Pearson correlation with two-sided significance testing. **(B)**: Dot plots of plasticity marker gene expression as indicated in figure and *MITF* expression with *invasive* signature expression (INVsig) as blue color gradient shown for the BROAD melanoma cell line panel ($n = 88$). movAVG group size=13. Expression data log₂ transformed. ****, $P < 0.00001$.

6.1.2 Established *invasive* phenotype markers in melanoma are not suitable for describing a *nascent invasive* phenotype

AXL, WNT5A and NGFR constitute common markers for describing melanoma cell *invasive* phenotype switching. In a next approach we analyzed those *invasive* phenotype markers on their capability in discriminating between a MITF^{high} *proliferative* and MITF^{low} *invasive* cell state in our panel of melanoma cell lines. We found strong correlation of *invasive* marker expression with melanoma cell invasiveness for all except NGFR, which was highly variably expressed throughout all melanoma phenotypes (Figure 6.2, A and B). NGFR expression was even reduced in the fraction of most dedifferentiated melanoma cell lines. When checking on elevated marker expression upon *nascent invasiveness*, we found up-regulated expression of AXL in some cell lines, however less consistent than NT5E upregulation seen in the *nascent invasive* cell state (Figure 6.2, A and Figure 6.1, E).

6.1.3 A *nascent invasive* phenotype is primed to phenotype switching

Based on the above delineated concept, we next asked whether a *nascent invasive* phenotype is primed for inflammation-induced dedifferentiation and phenotype switching. For addressing that issue, we referred to the GSE51221 mRNA microarray of melanoma cell lines ($n = 17$). This dataset was generated in our lab by 72 h TNF α stimulation in order to analyze intrinsic inflammatory pathway activation in melanoma [13]. According to expression of MITF and NT5E, cells were grouped into MITF^{high} *proliferative*, MITF^{high} *nascent invasive* and MITF^{low} *invasive* phenotypes as introduced earlier (Figure 6.3, A). In agreement with our previous observations, we observed a significant increase of NT5E expression in the group of MITF^{high} *nascent invasive* cell lines when compared to cell lines of the MITF^{high} *proliferative* group (Figure 6.3, B). NT5E expression further increased in the MITF^{low} *invasive* phenotype and MITF expression simultaneously decreased. Along, we found considerable, yet not significant increase in inflammatory and *invasive* gene expression signatures in the MITF^{high} *nascent invasive* compared to the MITF^{high} *proliferative* phenotype. Both signatures are further up-regulated in cell lines of the MITF^{low} *invasive* phenotype.

Intriguingly, matching to the above introduced hypothesis, cell lines belonging to the *nascent invasive* phenotype indeed show stronger dedifferentiation in response to TNF α stimulation as monitored in decrease in MITF expression (Figure 6.3, B). In addition, inflammatory TNF α signature genes are more prominently induced in MITF^{high} *nascent invasive* when compared to MITF^{high} *proliferative* cell lines in response to TNF α stimulation. As expected, NT5E expression is up-regulated by inflammatory TNF α stimulation across all groups of cell lines (Figure 6.3, B).

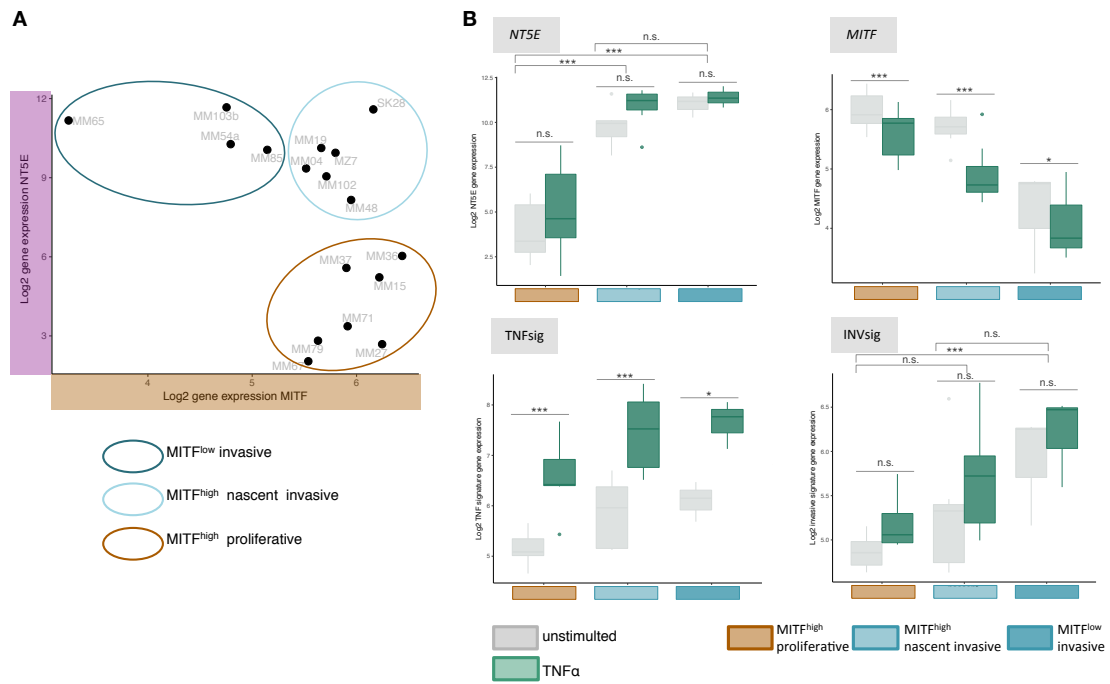


Figure 6.3: **A nascent invasive phenotype is primed to phenotype switching.** **(A):** Subset of unstimulated cell lines of GSE51221 ($n = 17$) plotted for *NT5E* and *MITF* expression. **(B):** Boxplots showing *NT5E*, *MITF*, TNF response signature (TNFsig) and Verfaillie *invasive* signature (INVsig) expression in cell lines grouped as indicated by clusters in **(A)** +/- 72 h 1000 U/ml TNF α . Gene expression log₂ transformed. For statistics two-way ANOVA with Bonferroni multiple comparison correction. *, $P < 0.05$; ***, $P < 0.001$; n.s.=none significant.

In summary, our data propose a novel *nascent invasive* phenotype in melanoma plasticity which can be defined by the concurrent expression of CD73 and MITF. Furthermore, our experiments suggest priming of *nascent invasiveness* in melanoma cells for inflammation-triggered phenotype switching.

6.1.4 CD73 expression in *nascent invasive* melanoma cells is associated with mitogenic and inflammatory signaling pathways

Next, we wanted to explore pathways that are correlated with MITF^{high} CD73^{high} *nascent invasive* phenotype in order to gain further insights into the regulation of CD73 expression in melanoma. In order to retrieve gene sets and pathways positively correlating with CD73 expression in melanoma, we performed GSEA on MITF^{high} *nascent invasive* cell lines ($n = 28$) by comparing to MITF^{high} *proliferative* cell lines ($n = 28$) of the BROAD panel of melanoma cell lines ($n = 88$) using the C2 collection of curated gene sets from the Molecular Signature Database v.6.1 (MSigDB) (Figure 6.4, A). All

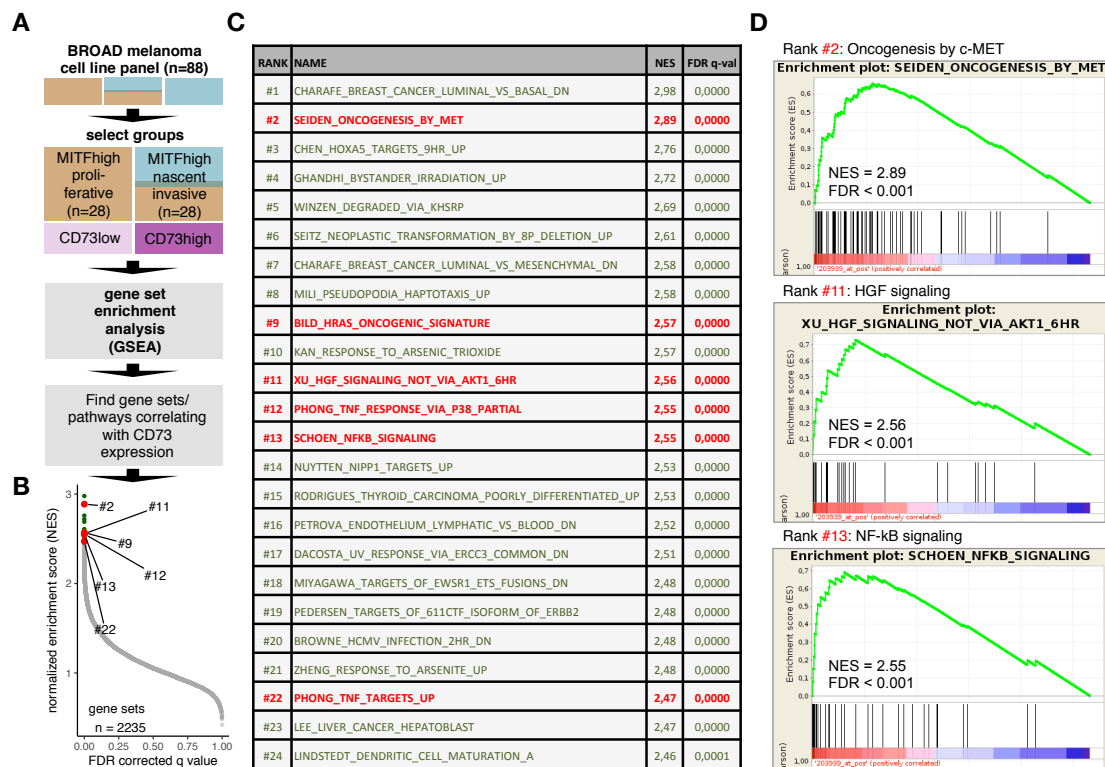


Figure 6.4: **GSEA identifies mitogenic and inflammatory pathways in the regulation of melanoma CD73 expression.** (A): Overview of the bioinformatic analyses for pathways enrichment in melanoma *nascent invasive* phenotype.

(B): Ranking of C2 collection of curated gene sets from MSigBD v.6.1 ($n = 2235$) according to FDR corrected q-values and NES after GSEA on MITF^{high} *nascent invasive* phenotype against MITF^{high} *proliferative* phenotype based on the BROAD melanoma cell line panel ($n = 88$). (C): List of top rank 24 gene sets of analysis from (A). (D): Enrichment plots of mitogenic and inflammatory gene sets of analysis from (A).

gene sets analyzed ($n = 2235$) were ranked according to NES and by increasing FDR corrected p-values (Figure 6.4, B). In accordance with previous filtering on TNF α regulated genes for identification of CD73, we found an enrichment of NF- κ B signaling (rank #13) and TNF α targets (rank #12 and rank #22) in CD73 expressing MITF^{high} *nascent invasive* cell lines (Figure 6.4, C and D). However surprisingly, among the top ranking gene expression signatures we also found mitogenic signaling gene sets, such as HGF signaling on rank #12 and HRAS signaling on rank #9 and in especially gene sets of oncogenic MET signaling (rank #2) to be highly enriched upon CD73 expression in the MITF^{high} *nascent invasive* phenotype.

In conclusion, our analysis show mitogenic signaling together with inflammatory pathway activation to coincide with CD73 expression within a *nascent invasive* phenotype.

6.2 Mitogenic inflammatory signaling drives CD73 expression in melanoma through the MAPK pathway

6.2.1 A melanoma cell line panel as a model to study CD73 regulation *in vitro*

In the following we aimed to test this hypothesis by consecutive functional studies on basis of a melanoma cell line panel available for cell culture *in vitro* analysis that would represent the above delineated concept of melanoma phenotypic plasticity. For that, we referred to the GSE51221 cohort of melanoma cell lines ($n = 17$) [13] and integrated known MAPK signaling related driver mutation status, described by Hoek *et al.* [107]. When we FACS analyzed a subset ($n = 14$) of cell lines for CD73 expression, we could confirm highly variable cell surface expression of CD73 (Figure 6.5, A) that well corresponded to the phenotypes classified previously (Figure 6.3, A). We recapitulated that CD73 was co-expressed along with MITF in a subgroup of melanoma cell lines, and highly expressed in melanoma cell lines negative for MITF (Figure 6.5, B).

Three cell lines of the MITF^{high} *proliferative* phenotype showed complete absence of CD73 expression: MaMel.27, MaMel.67a and MaMel.79b_{early} (MaMel.79b-e) (Figure 6.5, A and B). Based on reports describing epigenetic regulation of *NT5E* [267, 171], we questioned if promoter silencing is present for the CD73^{low} phenotype in that fraction of melanoma cell lines. Bisulfite conversion assay followed by deep sequencing of the CpG island within the 5' regulatory sequence at the end of *NT5E* exon 1 yielded detailed information about the methylation status of the individual cell lines. It confirmed high CpG island methylation exactly for those cell lines that were negative for CD73 expression (Figure 6.5, A). Interestingly, we were able to establish a subculture of one of those cell lines, MaMel.79b_{early}, that showed phenotype switching and CD73 upregulation under prolonged passaging (termed MaMel.79b_{late}, MaMel79b-l). Bisulfite sequencing of that culture confirms remodeling at the *NT5E* genomic locus by continuous decrease of CpG island methylation (Figure 6.5, A).

Two cell lines, MaMel.15 and MaMel.71, did not show epigenetic silencing at the *NT5E* locus, but still had low CD73 expression. These two cell lines were the only ones that did not harbor any activating mutations in the MAPK signaling pathway (Figure 6.5, A). In consequence, they exhibit low ERK phosphorylation levels when compared to melanoma cell lines with positive MAPK driver mutation status (Figure 6.5, B). We speculated that lack of CD73 expression in MaMel.15 and MaMel.71 might be the result of insufficient MAPK signaling and hypothesized that both cell lines represent a suitable model system for testing cooperative induction of CD73 by mitogenic and inflammatory stimuli.

In conclusion, mitogenic stimulation induces melanoma CD73 expression in differentiated melanoma cells which exhibit insufficient MAPK signaling and CD73 induction is strongly amplified in the combination with inflammatory triggers.

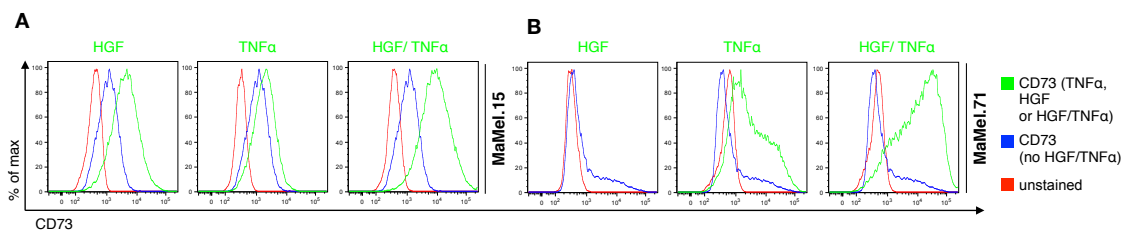


Figure 6.6: **Cooperative CD73 induction by mitogenic and inflammatory stimuli.** (A): Representative CD73 FACS histograms in MaMel.15 (A) and MaMel.71 (B) after 5 days of 1000 U/ml $\text{TNF}\alpha$, 50 ng/ml HGF or combinatorial treatment.

6.2.3 Epigenetic remodeling at the *NT5E* locus is required for induction of CD73

We next speculated whether epigenetic silencing of *NT5E* can be overcome by the co-stimulation procedure and stimulated the CpG island methylated cell lines MaMel.27, MaMel.67a and MaMel.79b_{early} according to the above introduced stimulation protocol. However, we found no upregulation of CD73 by neither of the stimulation conditions (Figure 6.7, A). These observations prompted us hypothesize that epigenetic remodeling at the *NT5E* locus is required to allow induction of CD73 expression by inflammatory and mitogenic signaling. Using 5-Azacytidine, we globally demethylated MaMel.79b_{early} and MaMel.67a and simultaneously subjected the cultures to our co-stimulation approach. Deep sequencing-based bisulfite sequencing confirmed sufficient demethylation by 5-Azacytidine of the *NT5E* CpG island in both cell lines. Demethylation was stronger in MaMel.79b_{early} with a further increase upon co-stimulation (Figure 6.7, B). By FACS analysis we indeed observed induction of CD73 upon global demethylation in a 5-Azacytidine concentration dependent manner for both cell lines tested (Figure 6.7, C). In accordance with the degree of demethylation, we saw stronger upregulation of CD73 in MaMel.79b_{early}, than in MaMel.67a. HGF / $\text{TNF}\alpha$ co-stimulation further amplified CD73 expression in both cell lines, again with more pronounced induction observed for the cell line showing more advanced demethylation under stimulation, MaMel.79b_{early} (Figure 6.7, C).

In summary, we show epigenetic silencing at the 5' regulatory CpG island in *NT5E* in some of the $\text{MITF}^{\text{high}}$ *proliferative* cell lines accounts for the absence of CD73 and the resistance to up-regulate CD73 in response to mitogenic / inflammatory stimulation.

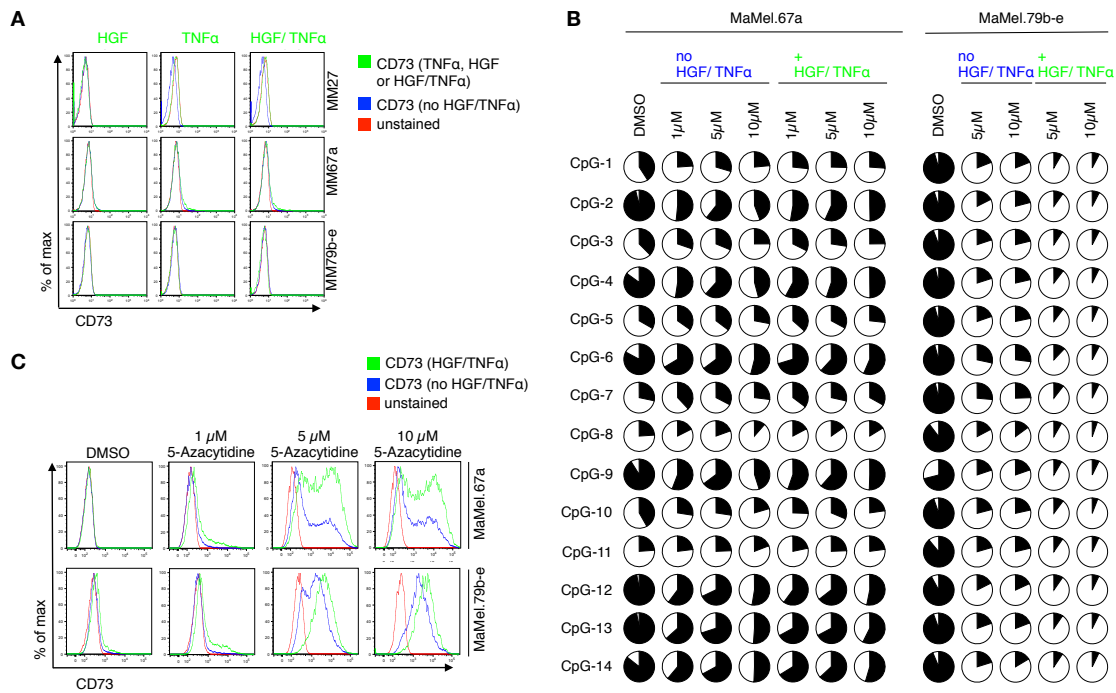


Figure 6.7: **Epigenetic remodeling induces CD73 expression and susceptibility to mitogenic inflammatory stimulation.** **(A):** Representative CD73 FACS histograms for the cell lines indicated, after 5 days of 1000 U/ml TNF α , 50 ng/ml HGF or combinatorial treatment. **(B):** Pie charts of deep sequencing based bisulfite sequencing analysis covering the *NT5E* CpG island within in MaMel.67a (left) and MaMel.79b_{early} (right). Cells treated 6 days, daily with DMSO or 5-Azacytidine and 3 more days by 1000 U/ml TNF α and 50 ng/ml HGF or mock. **(C):** Representative CD73 FACS histograms for MaMel.67a and MaMel.79b_{early} for the experimental procedure as described in **(B)**. MaMel.79b_{early} = MaMel.79b-e.

6.2.4 CD73 induction in melanoma by both mitogenic and inflammatory stimuli depends on MAPK signaling cascade activation

In a next step, we wondered whether which mitogenic signaling pathway is driving the observed induction of CD73. In MaMel.15 and MaMel.71 we interfered with both most relevant growth factor receptor ligation activated pathways, either MAPK signaling by MEK inhibition (MEKi) or AKT-PI3K-signaling by PI3Ki in conjunction with the co-stimulation procedure. Most surprisingly both, the separate inflammatory and the mitogenic induction of CD73 expression were completely dependent on MAPK signaling, while PI3Ki had no effect. (Figure 6.8, A). In addition, cooperative CD73 induction under co-stimulation was completely abrogated in the presence of MEK. The findings were reproducible on a total protein level in immunoblot analyses confirming abolished ERK phosphorylation und MEKi despite stimulation and on a mRNA level in qPCR analysis (Figure 6.8, B and C).

MEKi was also able to block $TNF\alpha$ dependent induction of CD73 in cell lines with positive MAPK mutation status as tested for the NRAS mutant cell line MaMel.79b_{late} (Figure 6.8, D). Of note, MaMel.79b_{late} was able to induce CD73 expression in response to inflammatory $TNF\alpha$ stimulation whereas parental MaMel.79b_{early} harboring *NT5E* CpG island methylation was not. This finding nicely appends to previous investigation on the impact of epigenetic remodeling on inducibility of CD73 in melanoma.

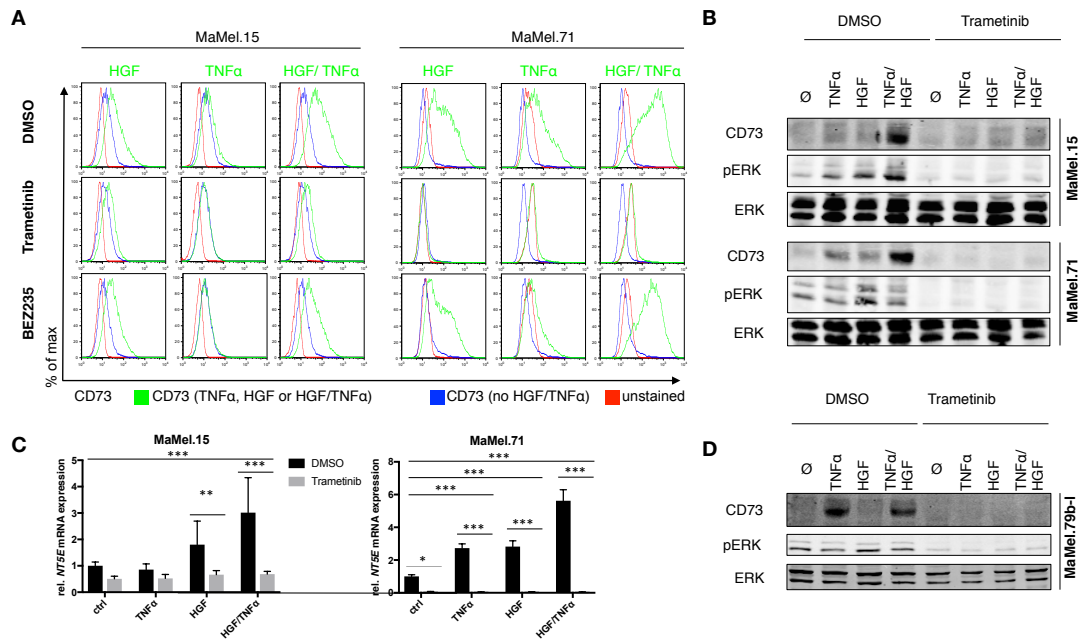


Figure 6.8: **MAPK cascade signaling orchestrates mitogenic inflammatory CD73 induction in melanoma.** **(A):** Representative CD73 FACS histograms of MaMel.15 (left) and MaMel.71 (right) treated 5 days by 1000 U/ml $TNF\alpha$, 50 ng/ml HGF or by combination together with 50 nM Trametinib, 1 μ M BEZ235 or DMSO. **(B):** Representative immunoblot analysis of the experimental procedure as described in **(A)** including DMSO and 50 nM Trametinib treatment. MaMel.15 and MaMel.71 in upper and lower blots, respectively. **(C):** qPCR analysis of the experimental procedure from **(A)** on MaMel.71 and MaMel.15 (upper and lower panels, respectively). Relative (rel.) *NT5E* mRNA with values relative to *UBC* and referenced to unstimulated DMSO control (ctrl) shown as mean of $n = 3$ with error bars as SD. Two-way ANOVA analysis. Post-hoc testing by Bonferroni's multiple comparisons test was either conducted to compare means across inhibitor treatment conditions or to validate various stimuli in DMSO or Trametinib conditions against ctrl. *, $P < 0.05$; **, $P < 0.01$; ***, $P < 0.001$. **(D):** Immunoblots of MaMel.79b_{late} (MaMel.79-l) with same experimental procedures as in **(A)** but only 50 nM Trametinib.

6.2.5 Inflammatory macrophage supernatant constitutes a source for melanoma cell CD73 induction

Next, we aimed to investigate on potential sources for mitogenic / inflammatory signals in the tumor environment. We focused on inflammatory macrophages as a major source for $TNF\alpha$ in the inflamed tumor tissue and during remodeling processes leading to cancer progression and metastasis [190].

We translated this in our *in vitro* setting to stimulation of melanoma cells by inflammatory macrophage supernatant. We used PMA in order to differentiate THP1 suspension monocytes into adherent macrophages and harvested inflammatory THP1 cell supernatant for melanoma cell stimulation according to the protocol shown in Figure 6.9, A. In short term timeline stimulation experiments of MaMel.15 and MaMel.71 we found robust activation of the MAPK cascade as visualized in high increase of ERK phosphorylation but also some impact on p38 and AKT signaling pathway (Figure 6.9, B). THP1 SN promoted melanoma cell dedifferentiation resulting in reduction of *MITF*, *MLANA* and *TYR* expression levels in qPCR analysis (Figure 6.9, C). Remarkably, treatment of MaMel.15 and MaMel.71 with THP1 SN resulted in a robust and very strong increase of CD73 expression in both cell lines (Figure 6.9, D) and the induction could again be blocked by Trametinib.

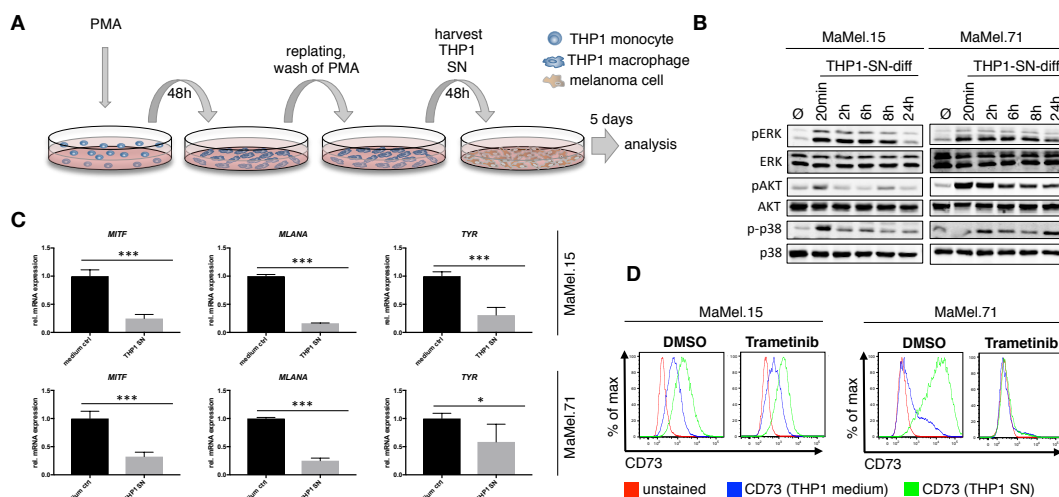


Figure 6.9: **THP1 macrophage secretome induces melanoma cell CD73 expression.** (A): Outline of the THP1 cell differentiation protocol for generating inflammatory supernatant. (B): Immunoblots from MaMel.15 (left) and MaMel.71 (right) upon stimulation with pure THP1 SN for indicated periods of time. (C): qPCR analysis on indicated differentiation genes in MaMel.15 (upper blots) and MaMel.71 (lower blots) treated by 50% v/v THP1 SN and THP1 medium for 5 days. Expression normalized to *UBC*. Means of biological triplicates with error bars showing SD. Two-tailed, un-paired Student's T-Tests. *, $P < 0.05$; ***, $P < 0.001$. (D): CD73 FACS histogram analysis of a representative experiment of MaMel.15 (left) and MaMel.71 (right) treated by THP1 SN as described in (B) and co-inhibited by 50 nM Trametinib.

6.2.6 Baseline CD73 expression depends on MAPK signaling in melanoma

So far we investigated the molecular pathways that account for CD73 *de novo* induction in melanoma cells that do not or only marginally express CD73 on a baseline level. We have consistently observed inflammatory/ mitogenic stimuli to converge on MAPK cascade activation. This prompted us to downregulation of CD73 baseline expression in cell lines of the *nascent invasive* or *invasive* cell state by blocking MAPK signaling.

In this intention we treated CD73 positive melanoma cell lines from our panel with the MEK inhibitor Trametinib and recorded CD73 expression by FACS analysis. We observed a consistent and robust decrease of surface CD73 levels upon MAPK cascade blockade for all cell lines except MaMel.54a with most effective downregulation observed in SK.Mel28 (Figure 6.10, A). Immunoblot analysis confirmed inhibition of downstream ERK phosphorylation in response to MEKi and proved reduction of CD73 on a total protein level (Figure 6.10, B). Interestingly, partial reactivation of ERK signaling occurred in those cell lines with a more dedifferentiated phenotype, i.e. MaMel.85 and MaMel.65. This fits to reports stating a dedifferentiated phenotype to be prone to primary targeted therapy resistance [167].

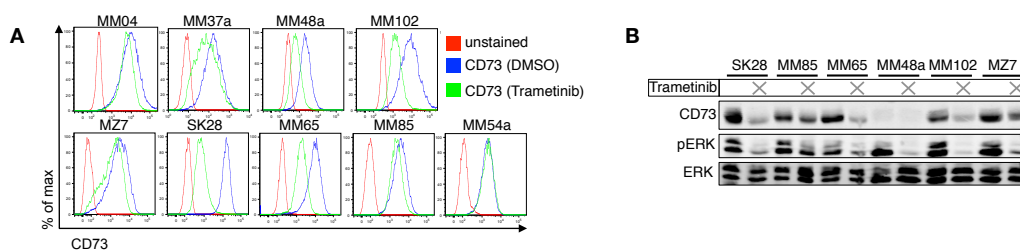


Figure 6.10: **Baseline CD73 expression is decreased by MAPK inhibition.** (A): Representative CD73 FACS analysis at baseline and after 4 days 50 nM Trametinib in a panel of CD73 positive melanoma cell lines. (B): Representative immunoblot analysis on CD73 positive melanoma cell lines after 96h of 50 nM Trametinib or DMSO (MaMel. = MM, SK.Mel28 = SK28).

MAPK signaling is a key signaling pathway for melanoma growth and survival [50]. In order to exclude that reduction of CD73 expression is a secondary effect of therapy induced cell cycle arrest we treated cells with the fungal antibiotic Aphidicolin that is inhibiting eukaryotic replication, likewise similarly effecting cell growth than when applying MAPK signaling blockade. We found that Aphidicolin did not reduce, but rather increase CD73 expression (Figure 6.11, A), excluding growth arrest related changes to account for the downregulation of CD73 expression in melanoma. Interestingly, on mRNA level Aphidicolin treatment slightly reduced *NT5E* expression, but still to a lower extent when compared *NT5E* reduction mediated by MAPK blockade (Figure 6.11, B).

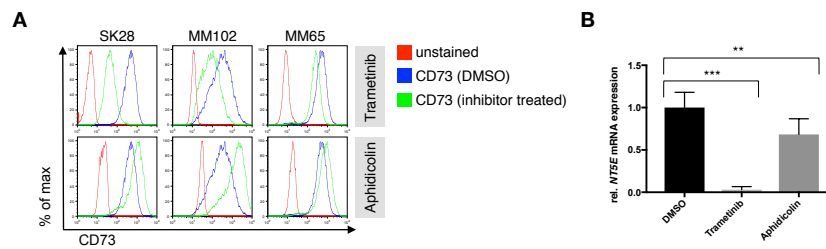


Figure 6.11: **Cell cycle arrest does not account for the reduction of CD73 expression (A):** Representative CD73 FACS analysis in SK.Mel28, MaMel.102 and MaMel.65 at baseline and after 4 days either 50 nM Trametinib or 1 μ /ml Aphidicolin (MaMel. = MM, SK.Mel28 = SK28). **(B):** *NT5E* mRNA as mean of biological triplicates from diverse melanoma cell lines. Expression normalized to *UBC* and DMSO control set as reference. Error bars show SD. Statistics by one-way ANOVA and post-hoc testing by Bonferroni's multiple comparisons test. **, $P < 0.01$; ***, $P < 0.001$.

We wondered whether prolonged inhibition of the MAPK pathway further reduced CD73. Indeed, we observed progressive loss of CD73 from day 4, day 10 to day 18 of MEKi (Figure 6.12, A). Vice versa, we next sought to address whether restoring ERK phosphorylation and MAPK signaling in a setting of previous MEKi would then also restore CD73 expression on melanoma cells. For that, we withdrew MEKi after 4 days and monitored CD73 expression over time. In SK.Mel28 and MZ7, CD73 expression was fully restored after 12 days, MaMel.37a and MaMel.48a recovered most of CD73 surface protein (Figure 6.12, B). Only MaMel.102 showed progressive loss of CD73 surface protein even after removal of Trametinib treatment, which was consistent with the strong ablation of CD73 under long-term inhibition.

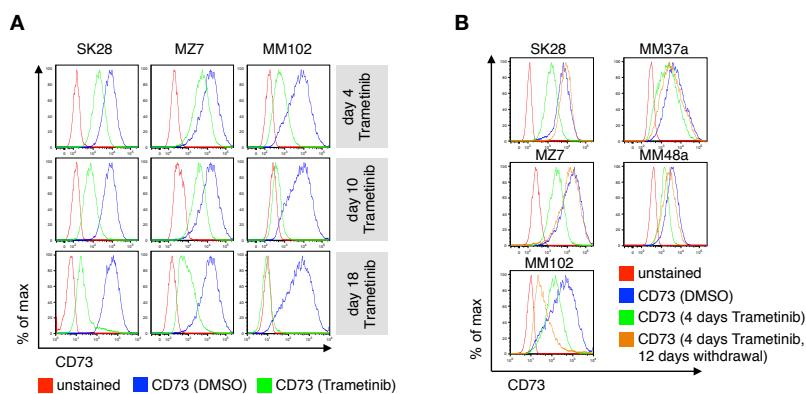


Figure 6.12: **Prolonged MAPK blockade further decreases - rehabilitating MAPK activity restores CD73 expression (A):** Representative timeline experiment showing CD73 FACS analysis at day 4, day 10 and day 18 of 50 nM Trametinib in the cell lines SK.Mel28, MZ7 and MaMel.102. **(B):** CD73 FACS analyses after 4 days of 50 nM Trametinib and after additional 12 days upon removal of inhibitor treatment in melanoma cell lines as indicated (MaMel. = MM, SK.Mel28 = SK28).

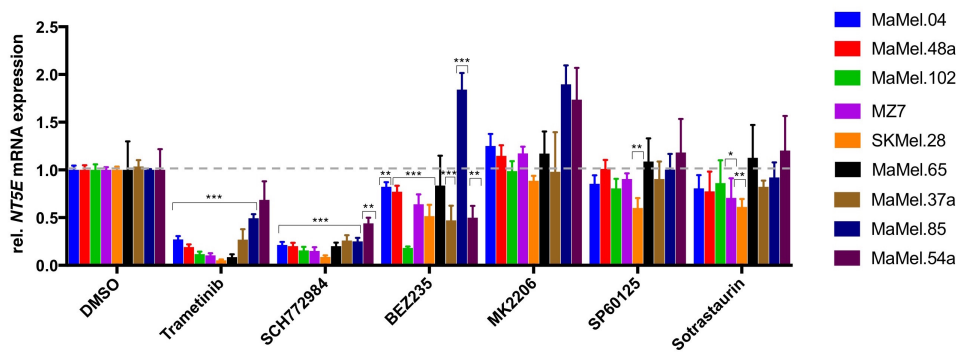


Figure 6.13: **Testing an inhibitor panel for CD73 regulation beyond MAPK signaling** qPCR for *NT5E* expression in melanoma cell line panel (n=9) after 4 days inhibitor treatment as indicated. 50 nM Trametinib (MEKi), 100 nM SCH772984 (ERKi), 1 μ /ml BEZ235 (PI3Ki), 1 μ /ml MK2206 (AKTi), 20 μ /ml SP600125 (JNKi) and 1 μ /ml Sotrastaurin (PKCi). Shown are means plus SD of n=3. Data is normalized to *UBC* expression and DMSO control condition set as reference. For statistical testing cell line wise comparison to DMSO ctrl by un-paired two-sided Student's T-Test with multiple comparison correction according to Benjamini and Hochberg (=FDR). *, P<0.05; **, P<0.01; ***, P<0.001. (MaMel. = MM, SK.Mel28 = SK28).

Finally, we intended to reproduce our findings on CD73 regulation via the MAPK cascade on mRNA expression level and further testing key pathways transmitting signaling in melanoma. We found strong and consistent downregulation of *NT5E* mRNA in our cell line panel upon MEKi (Figure 6.13). Comparable results were achieved by SCH772984, which blocks ERK signaling. Interfering with PI3K/AKT-, JNK- and PKC signaling showed varying effects on *NT5E* mRNA expression, depending on the individual cell lines and method of analysis. Whereas PI3K blockade (BEZ235) was able to decrease *NT5E* mRNA in some cell lines such an effect was not seen for AKT (MK2206) inhibition. JNK (SP600125) and PKC blockade (Sotrastaurin) also did not impact on CD73 expression.

In summary, considering mRNA and FACS expression data across the cell line panel tested, only MAPK signaling was consistently found to control melanoma cell CD73 expression.

6.3 JUN/ AP1 complexes control transcription of *NT5E* in dependence on MAPK activation

6.3.1 The search for transcription factors that correlate with *CD73* expression in melanoma points to JUN

In a next step, we were interested in finding the downstream molecular mechanisms regulating *CD73* expression in melanoma. For this, we made use of previously annotated *NT5E* binding TFs from the ENCODE ChIPseq data of the ENCODE Human Feb. 2009 (GRCh37/hg19) assembly TF ChIPseq (161 TF of 91 cell types as at March 2012 Freeze). Figure 6.14, A visualizes the *NT5E* transcript sequence in the UCSC genome browser together with regulatory tracks, such as H3K27 acetylation and H3K4 monomethylation indicating potential enhancer sites, as well as H3K4 trimethylation for promotor sites and DNase cluster for regions of open chromatin. Due to the active chromatin marks in an intergenic region about 50 kb upstream of the *NT5E* locus we expanded the region of interest to include this locus. In total, we covered a region with 335 potential TF binding sites of 88 individual TFs (Figure 6.14, A). Many TF binding sites accumulated in this potential distant cis-regulatory element, another fraction surrounded the transcriptional start site. Interestingly, we also found TFs binding sites accumulating within an first intronic region of *NT5E* with additional high H3K27 acetylation and H3K4 monomethylation.

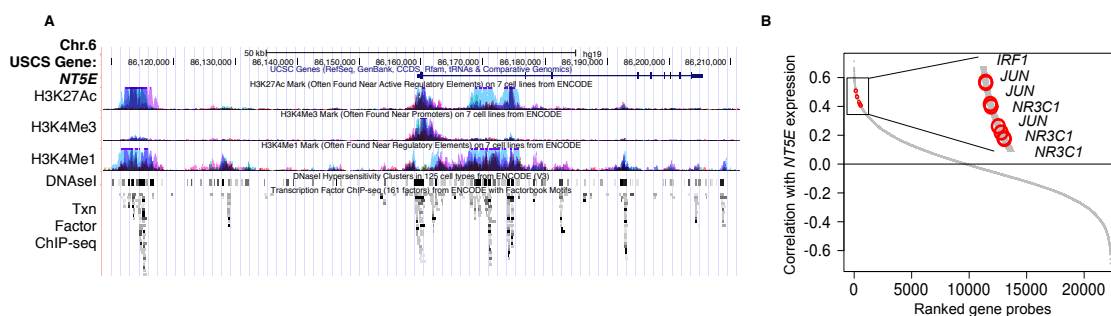


Figure 6.14: **JUN is a transcription factor with ENCODE annotated binding in *NT5E* and highly correlates with melanoma cell *CD73* expression.** (A): UCSC genome browser screenshot of human GRCh37/hg19 assembly for genomic locus at *NT5E*. RefSeq transcript and ENCODE regulation tracks layered H3K27Ac, H3K4Me3 and H3K4Me1. DNaseI hypersensitivity clusters and squish view of ENCODE TF ChIPseq from 161 TFs in 91 cell types. (B): ENCODE *NT5E* binding TFs in ranked order from positive to negative correlation with *NT5E* expression in the BROAD panel of melanoma cell lines ($n = 88$). Correlation analysis performed for individual gene probe IDs against the *NT5E* gene probe ID 203939-at. Probes with Pearson correlation > 0.4 highlighted.

For identification of TFs relevant for the regulation of *CD73* in melanoma, we next correlated mRNA expression of the selected candidate TFs with mRNA expression of *NT5E* for the BROAD panel of melanoma cell lines ($n = 88$). Figure 6.14, B illustrates

TFs with Pearson correlation ≥ 0.4 for this analysis. Among the top hits we found *IRF1*, *NR3C1* and *JUN*.

Finding JUN was highly interesting: We and others have recently described an important function of JUN/ AP1 complexes during stress- and inflammation mediated *invasive* phenotype switching in melanoma, plus it is involved in adaptive therapy resistance [201, 51, 69, 68, 249, 192]. JUN belongs to the heterodimeric AP1 TF family acting downstream of the JNK and ERK-MEK signaling pathways [81, 233]. Dimerization partners of JUN comprise FOSL1 (FRA-1), FOSL1 (FRA-2) and c-FOS [119]. It essentially impacts on melanoma cell proliferation, progression, migration, and invasion [64, 131, 224]. The fact that JUN/ AP1 complexes are capable of integrating both inflammatory and mitogenic triggers, makes it a highly promising candidate for mediating CD73 induction during phenotype switching.

6.3.2 Cooperative upregulation of CD73 is accompanied by the induction of JUN/ AP1 family members

Having found CD73 as an indicator of a *nascent invasive* phenotype and to be inducible by inflammatory regenerative signaling, we speculated on the involvement of JUN in the convergence of the signaling pathways. In accordance with previous findings on JUN/ AP1 in melanoma plasticity, we found that JUN and the AP1 heterodimerization partner FOSL1 were strongest expressed in *invasive* melanoma cell lines, which were positive for CD73 and negative for MITF (Figure 6.15, A). We next wondered whether cooperative induction of CD73 by mitogenic (HGF), together with inflammatory ($\text{TNF}\alpha$) stimulation is accompanied by the cooperative induction of JUN. For this, we performed immunoblot analyses in both of our MAPK cascade associated mutation status naïve model cell lines, MaMel.15 and MaMel.71, in response to prolonged mitogenic/inflammatory co-stimulation. Indeed, we observed cooperative, stable induction of JUN and to a lesser degree stabilization of additional factors of the JUN/ AP1 TF family, such as FOSL1 and JUNB (Figure 6.15, B). Similarly, long term stimulation by supernatant derived from differentiated THP1 cells, but not from undifferentiated THP1 cells, established a $\text{CD73}^{\text{high}}$, JUN^{high} phenotype in both cell line models. Additionally, we found upregulation of JUNB and FOSL1 primarily in MaMel.71 (Figure 6.15, C).

In summary, findings on JUN as ENCODE ChIPseq annotated TF showing enriched binding to the *NT5E* genomic locus and highly correlating with melanoma *NT5E* mRNA expression *in silico* were supported by *in vitro* data on cooperative induction of JUN alongside with elevation of CD73 expression levels by mitogenic together with inflammatory stimulation. Based on those findings, we were prompted to the question whether JUN is mediating CD73 expression in melanoma cells.

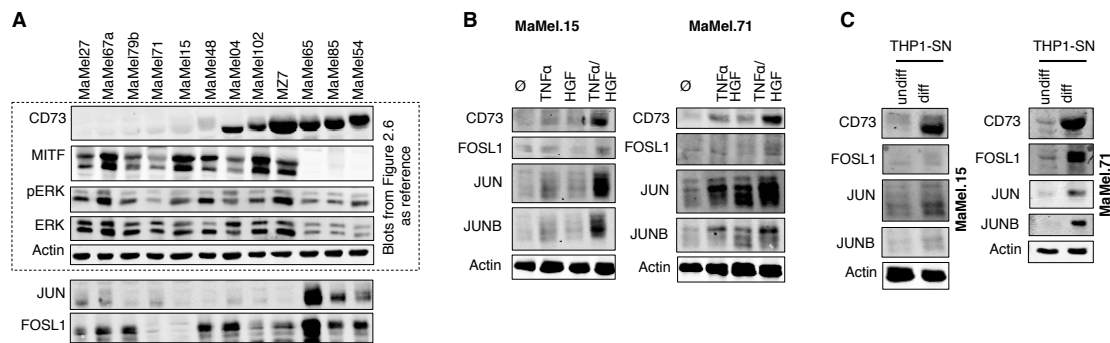


Figure 6.15: **Invasive cell state correlates with CD73 / JUN and induction of CD73 is accompanied by accumulation of JUN/ AP1 factors.** (A): Immunoblot in the melanoma cell line panel as introduced in Figure 6.5, B. (B): Representative immunoblots in MaMel.15 (left) and MaMel.71 (right) with 1000 U/ml TNF α , 50 ng HGF, or combinatorial treatment for 5 days. (C): Immunoblots at 5 days 50% (v/v) SN from differentiated THP1 cells (diff) and 50% (v/v) SN from undifferentiated THP1 cells (undiff) in MaMel.15 (left) and MaMel.71 (right).

6.3.3 JUN strongly induces melanoma cell CD73 in dependence of MAPK activation

In order to evaluate the impact of JUN for CD73 induction, we stably overexpressed JUN by retroviral infection of vector constructs carrying either JUN-citrine or citrine as a control in MaMel.15. Surprisingly, overexpression of JUN under basal conditions was not stable and no induction of CD73 was observed (Figure 6.16, A and B). As shown earlier (Figure 6.6, A), MaMel.15 is negative for oncogenic driver mutations in the MAPK signaling cascade and ectopic JUN stabilized upon mitogenic stimulation by EGF or HGF. It is known that oncogenic MAPK cascade activation leads to post-translational modification as well as transcriptional activation of JUN, thereby, increasing JUN protein stability and transcript abundance [242, 263, 146]. Indeed, upon MAPK activation mediated stabilization, we observed induction of CD73 that was further increased in cooperation with inflammatory TNF α stimulation in a magnitude that was not present by control vector expressing cells (Figure 6.16, A and B). Additionally, CD73 induction correlated with the induction of FOSL1 upon mitogenic stimulation, which is in line with literature, stating in cancer cells by ERK-dependent phosphorylation [263]. It is known that JUN induces *FOSL1* expression by binding to promoter and first intronic elements within the *FOSL1* genomic locus [22, 36]. This is an interesting observation as in the context of EMT transformation and tumor cell plasticity JUN/ FOSL1 heterodimers play an important role [55]. Hence, data presume close connectivity of JUN functionality for melanoma cell CD73 regulation in heterodimers, orchestrated by inflammatory stimulation, and stabilized by mitogenic signaling.

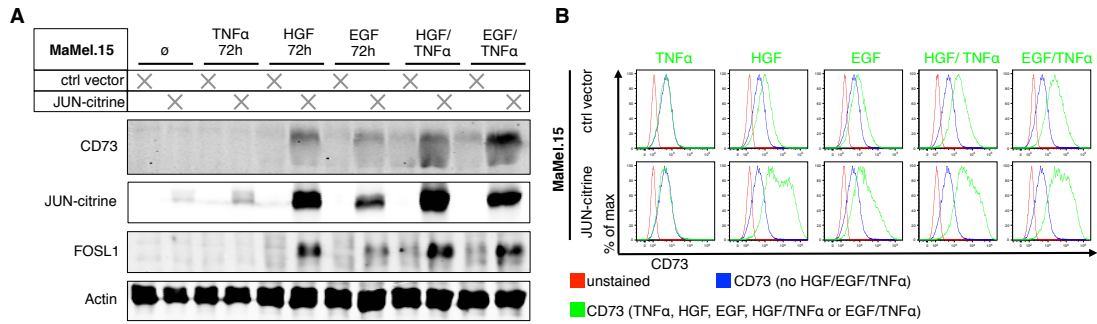


Figure 6.16: **Ectopic JUN induces CD73 in MaMel.15 upon stabilization by mitogenic stimulation.** (A): Immunoblots in MaMel.15 expressing citrine control or JUN-citrine vector after 72h 1000 U/ml TNF α , 100 ng/ml EGF and 100 ng/ml HGF in the indicated combinations. (B): Same as (A) but CD73 FACS analysis at day 5 of stimulation.

Based on the above delineated results, we assumed that JUN overexpression in melanoma cell lines with positive MAPK driver mutation status should lead to immediate induction of CD73. We selected the *nascent invasive* melanoma cell lines MaMel.48a, MaMel.102, MZ7, and MaMel.37a with positive BRAF or NRAS mutation status for JUN stable overexpression. Remarkably, we observed stable expression of ectopic JUN and robust upregulation for both CD73 protein and *NT5E* mRNA expression across all cell lines tested (Figure 6.17, A and B). JUN overexpression led to robust melanoma cell dedifferentiation as visualized by the loss of MITF expression (Figure 6.17, A). Furthermore, we again observed upregulation and stabilization of FOSL1 by ectopic JUN, in line with our previous data.

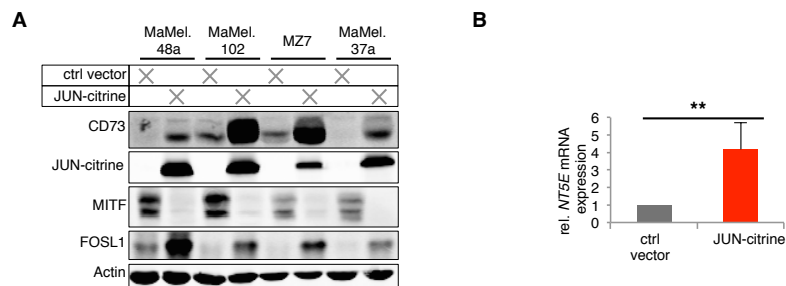


Figure 6.17: **Ectopic JUN boosts CD73 expression in *nascent invasive* melanoma cells** (A): Immunoblots showing MaMel.48a, MaMel.102, MZ7 and MaMel.37a, transduced with citrine control vector or JUN-citrine vector for the indicated proteins. (B): qPCR analysis on mean of *NT5E* expression across all cell lines transduced with JUN-citrine or citrine (n=4), normalized to *UBC*. Expression in citrine vector set as reference. Error bars indicate SD. Two-sided paired Student's T-Test. **, P<0.01.

6.3.4 A conditional expression system to study defined JUN transcriptional activity on the *NT5E* genomic locus

Having found strong induction of CD73 by JUN, we were intrigued whether we can dissect the regulation on a genomic level. As reported earlier, constitutive overexpression of JUN does not only strongly impact and modulate the expression of its AP1 complex heterodimerization partners but also initiates remodeling and cell state transition. Hence, for studying defined JUN transcriptional activity on the *NT5E* genomic locus, we aimed to set up a JUN doxycycline(DOX)-dependent conditional expression system. For that purpose, we selected the NRAS (p.Q61K) mutant cell line MaMel.79b_{late} which shows constitutive MAPK signaling activation enabling stabilization of ectopic JUN while at the same time harboring baseline expression levels of the AP1 heterodimerization partner FOSL1 (Figure 6.15, A). Furthermore, MaMel.79b_{late} exhibits low levels of CD73 and is devoid of JUN (Figure 6.5, A), making it a good model system to study defined effects of JUN on CD73.

As shown in Figure 6.18 A, inflammatory TNF α stimulation of the unmodified cell line MaMel.79b_{late} leads to immediate induction of JUN accompanied by MITF downregulation and furthermore is followed by strong accumulation of FOSL1 protein. Upon prolonged TNF α stimulation, CD73 is robustly induced (Figure 6.8, D). Of note, as a result of pre-activated MAPK signaling, we observed constitutive ERK phosphorylation that was not further increased neither by mitogenic HGF stimulation nor by combinatorial treatment (Figure 6.18 A). Also, no further accumulation of FOSL1 and JUN protein was found in the latter stimulation conditions which is in line with previous findings on absence of CD73 induction by mitogenic stimulation (Figure 6.8, D).

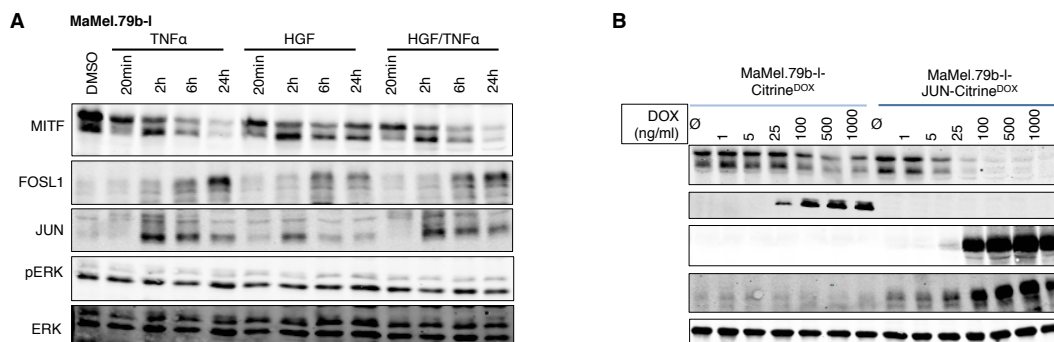


Figure 6.18: **Establishment of a JUN conditional cell line system in MaMel.79b_{late}.** **(A):** Immunoblots showing MaMel79b_{late} stimulated for the indicated periods of time with 1000 U/ml TNF α , 50 ng/ml HGF and combinatorial treatment. **(B):** Immunoblots on DOX titration in indicated concentrations after 24h in MaMel.79b_{late}CitrineDOX (left) and MaMel.79b_{late}JUN-CitrineDOX (right).

Following lenti- and retroviral transduction of the conditional expression constructs into MaMel.79b_{late}, DOX titration showed a concentration dependent increase of JUN-

Citrine and Citrine protein expression in the screening cell line MaMel.79b_{late}JUN-CitrineDOX and the control cell line MaMel.79b_{late}CitrineDOX, respectively (Figure 6.18, B), yielding a minimal effective concentration of 25 ng/ml DOX for future experiments. JUN accumulation was accompanied by a successive increase in FOSL1 protein and decrease in MITF protein (Figure 6.18, B).

6.3.5 Transient JUN induction establishes a MITF^{high} / CD73^{high} phenotype in melanoma

In timeline experiments with a low dose pulse of DOX we observed only transient JUN-citrine expression that was accompanied by transient suppression of MITF at peak of JUN-citrine induction but still resulted in upregulation of CD73 expression (Figure 6.19, A). This generated a *nascent invasive* phenotype bearing CD73 expression along with a positive MITF status in absence of JUN. On the contrary, induction of the Citrine control construct was stable and had no impact on neither CD73 nor MITF expression. We next evaluated the findings in more detail on a transcriptional level and compared the effects of pulse JUN-citrine to durable expression of JUN-citrine (Figure 6.19, B). 48h post pulse DOX treatment *MITF* was depleted, *NT5E* induction was not yet observed. At the same time, citrine induction in control cell population did not effect *MITF* expression. For durable induction of JUN-citrine DOX treatment was renewed for another 48h, whereas for pulse JUN induction medium containing remnants of DOX was replaced.

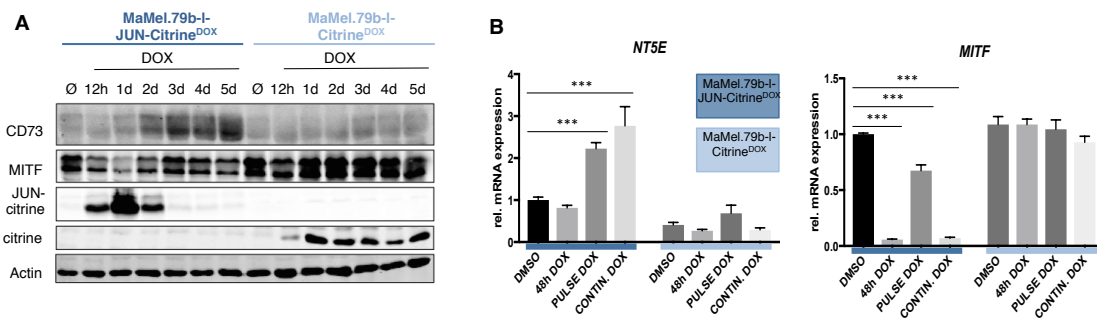


Figure 6.19: **Transient JUN in MaMel.79b_{late}JUN-CitrineDOX establishes a MITF^{high} CD73^{high} phenotype.** (A): Representative immunoblots for 10 ng/ml doxycycline (DOX) treatment in MaMel.79b_{late}JUN-CitrineDOX (left) and MaMel.79b_{late}CitrineDOX (right) at indicated time points. (B): qPCR experiments of n=3 showing cell lines as indicated in (A), but for 96 h with medium replacement after 48 h and DOX at 100 ng/ml. DMSO (48 h medium + 48 h medium), 48 h DOX (48 h medium + 48 h DOX), PULSE DOX (48 h DOX + 48 h medium), CONTIN. DOX (48 h DOX + 48 h DOX). Error bars showing SD. DMSO control set as reference. One-way ANOVA analysis with post-hoc Bonferroni correction for multiple comparisons. ***, P<0.001.

Continuous JUN-Citrine expression led to comparably strong induction of *NT5E* mRNA in the absence of *MITF* expression, as observed for transient JUN-citrine pulse, but here

MITF expression was largely restored (Figure 6.19, B). Again, sole citrine induction did not interfere with *NT5E* levels in any condition.

In summary, the data suggest the side-by-side generation of an *invasive* and a *nascent invasive* phenotype from a *proliferative* cell state, with transient JUN promoting nascent de-differentiation and incipient phenotype switching and stable JUN leading to full phenotype switching. Further mechanistically insights on melanoma plasticity might be gained from RNAseq analysis on the above delineated experimental setting.

6.3.6 ChIP qPCR reveals prominent binding of JUN to AP1 consensus sites located in *NT5E*

Making use of our JUN-inducible melanoma cell line model, we were next interested in finding the detailed binding sites of JUN in *NT5E*. We referred back to the ENCODE ChIPseq dataset and searched for annotated JUN binding sites, plus additional intronic control sites within H3K27Ac^{low} regions of *NT5E* for designing a tiling approach for ChIP qPCR (Figure 6.20, A). After DOX induction of the constructs, we used the citrine tag to purify genomic binding regions for JUN-citrine and citrine only as a control. Amplification on the immunoprecipitated DNA for the candidate JUN binding sites and control sites yielded significant enrichment of JUN-citrine over citrine samples only for two regions within *NT5E* that span the AP1 #1 and AP1 #2 sites, which are located upstream of *NT5E*, and the first intronic AP1 #5 and AP1 #6 sites (Figure 6.20, B). Indeed, binding of JUN in *NT5E* for those two regions coincided with elevated H3K27Ac enhancer marks (Figure 6.20, A). Moreover, canonical AP1 binding motifs are centrally located within the significantly enriched regions regions.

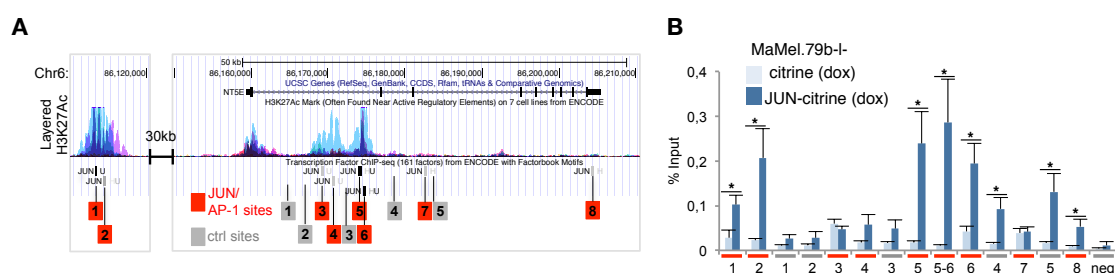


Figure 6.20: **Prominent binding of JUN to *NT5E* intronic enhancer region in ChIP qPCR.** **(A):** Screenshot of human GRCh37/hg19 assembly surrounding *NT5E* in the UCSC genome browser with layered H3K27Ac and TF ChIP seq track for annotated JUN binding sites. JUN/ AP1 sites for ChIP qPCR amplification indicated in red, control amplicon sites indicated in grey. **(B):** Means of % input from biological triplicates of ChIP qPCR analysis performed in MaMel.79b_{late}JUN-citrineDOX after 24 h pulse by 25 ng/ml DOX. MaMel.79b_{late}citrineDOX as a reference. Error bars indicate SEM. Significance tested by one-sided Student's T-Test for enrichment. *, P<0.05.

In summary, our findings substantiate the role of JUN in the direct regulation of *NT5E* expression in melanoma by showing enriched binding of JUN to several ENCODE ChIPseq predicted AP1 binding sites within the *NT5E* genomic locus.

6.4 A CRISPR/Cas9-FACSorting enhancer screening approach for functional validation of AP1 binding sites in *NT5E*

6.4.1 Development of the CRISPR/Cas9-FACSorting enhancer screen

Having shown that JUN is recruited to defined binding sites within *NT5E*, we were next interested if binding of JUN to those sites is of functional relevance for the induction of CD73. For this purpose we designed an enhancer screening approach, that uses CRISPR/Cas9 to disrupt JUN/ AP1 binding motifs of interest and subsequent functional validation of CD73 expression by FACSorting in conjunction with deep sequencing of the AP1 sites targeted in the fractions sorted. We assumed that when destructing an AP1 site that was of functional relevance for the induction of CD73, we should see decreased induction in response to JUN/ AP1 activation. In consequence, relevant AP1 sites with a strong phenotype should be accessible by mere FACS analysis of CD73. Additionally, we postulated that those cells that acquired insertions and deletions (InDels) within a functional relevant AP1 binding motif should become enriched in the CD73^{low} inducible sub-fraction and vice versa depleted from the CD73^{high} inducible sub-fraction. Hence, the combination of FACSorting CD73^{high} and CD73^{low} expressing sub-fractions followed by deep sequencing in an arrayed screening approach should allow to causatively couple a phenotype observed to distinct genomic alterations. The schematic overview in Figure 6.21, A introduces the screening approach and illustrates its main principles.

Selection of the candidate sites throughout *NT5E* for CRISPR/Cas9-based targeting was made based on significant enrichment of JUN binding to genomic DNA fragments in ChIP qPCR analysis and yielded 8 potential sites. Subsequently, these sites were matched to ENCODE annotated TFs binding in *NT5E* with a canonical AP1 binding site, resulting in a final set of 5 candidate AP1 sites plus an extra control targeting site within a H3K27Ac/ H3K4Me3/DNaseI^{low} region of the first intron of *NT5E* (Figure 6.21, B). sgRNAs were designed to cut most nearby the canonical AP1 binding motif (Figure 6.21, C).

We used our model cell line MaMel.79b_{late}JUN-citrineDOX and side-by-side transfected the CRISPR/Cas9 constructs directed against the individual JUN/ AP1 and control sites in *NT5E*. We induced CD73 for 5 days by DOX pulsed transient JUN-citrine expression

and conducted FACS analysis. In parallel, FACS sorting of the 10% lowest CD73 and 10% highest CD73 fractions, as well as the total population of viable cells was performed and AP1 and control site InDel formation quantified by deep sequencing (Figure 6.21, A).

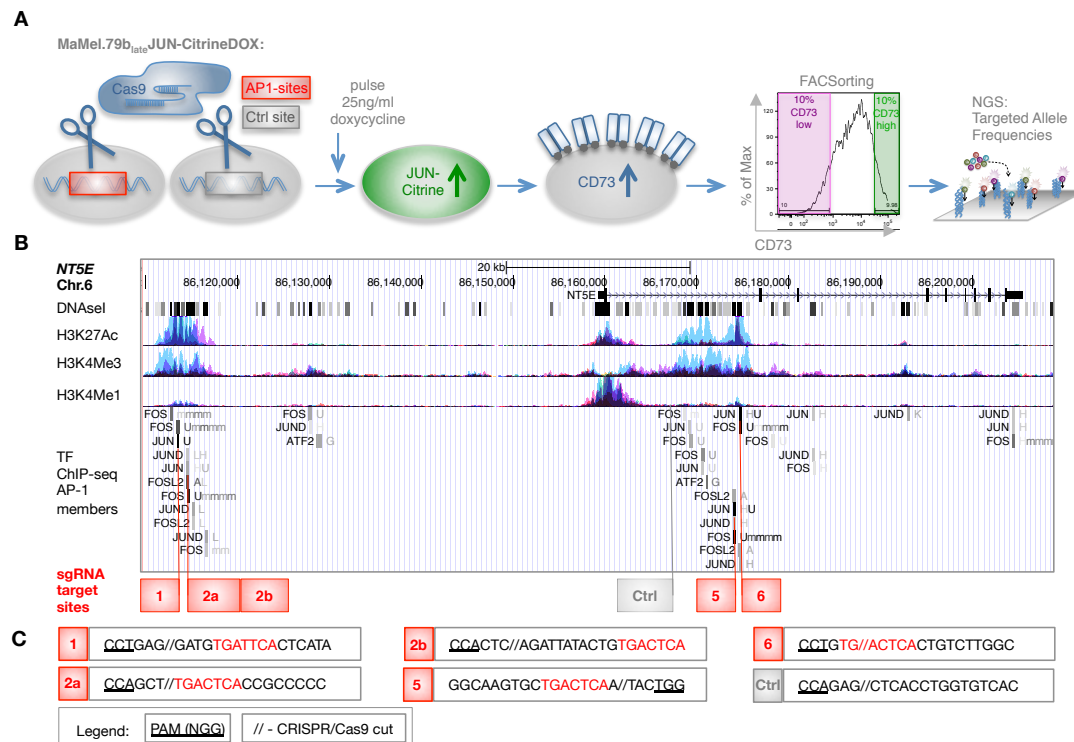


Figure 6.21: **Design of the CRISPR/Cas9-FACS sorting enhancer screening approach.** (A): Schematic outline of the CRISPR/Cas9-based CD73 FACS sorting approach for enhancer screening in MaMel.79b_{late}JUN-citrineDOX to identify JUN binding sites in *NT5E* relevant for CD73 induction. (B): UCSC genome browser screenshot of *NT5E* locus with ENCODE regulatory tracks as indicated. JUN/AP1 sites #1, #2a, #2b, #5, #6 and Control site targeted are mapped. (C): Target site sequences for sgRNAs used. Protospacer adjacent motif (PAM) underlined, CRISPR/Cas9 cutting sites indicated by // and canonical AP1 binding motifs highlighted in red.

6.4.2 JUN induces CD73 by binding to a specific AP1 consensus site in *NT5E*

Figure 6.22, A visualizes the results from biological triplicates of the screening approach, showing targeting efficiencies at individual sites in the CD73 sorted fractions and the unsorted cell pools. Efficient genome editing with some minor individual variance across all sgRNAs used was observed in the unsorted cell pools. Interestingly, AP1 site-specified editing, defined by the disruption of the canonical AP1 binding motif nearby/in the sgRNA target sites, varied substantially in the unsorted cell pools for

individual sgRNAs. This perfectly corresponds to the distance of target site cutting from the respective AP1 motif (Figure 6.21, C). It cannot be avoided due to the limitations given by sgRNA design rules [45, 80]. However, normalization of editing in the sorted fractions to editing in the unsorted cell pool allows to compensate for this effect.

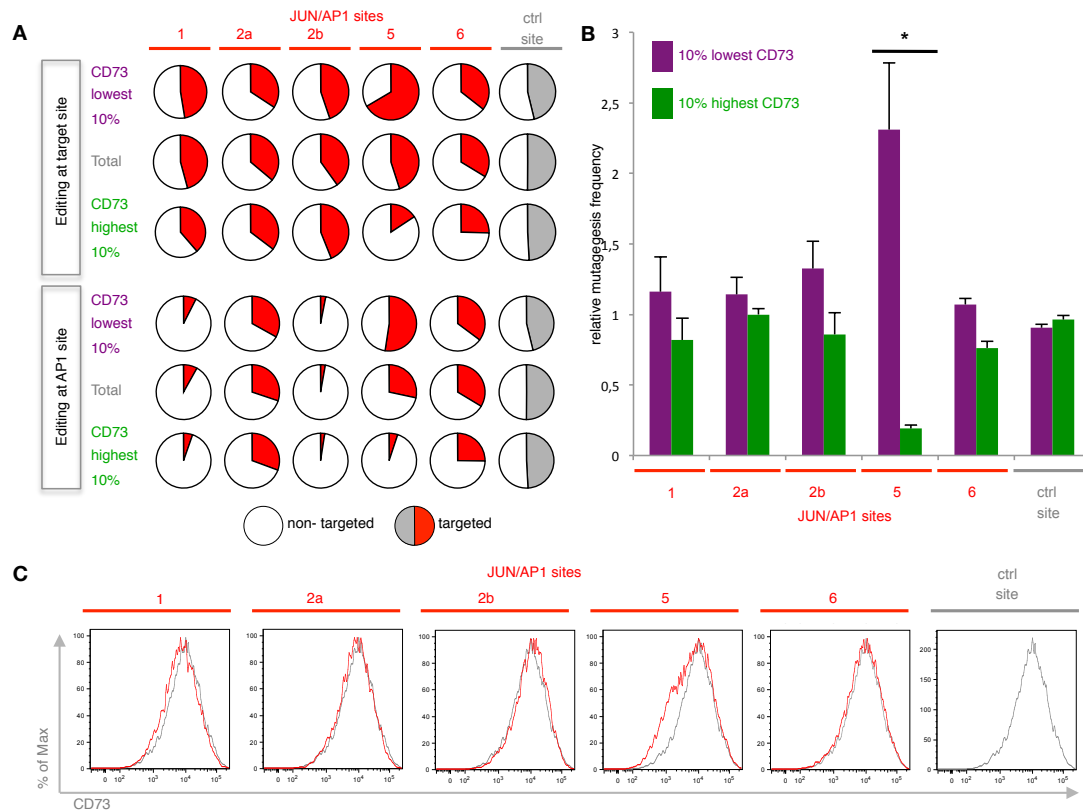


Figure 6.22: CRISPR/Cas9-based FACS sorting approach for enhancer screening identifies AP1 #5 site for CD73 induction by JUN. (A): Pie charts showing successful genome editing by the respective AP1 and control sgRNAs for target site and specified AP1 site editing. Sorting conditions CD73 lowest and highest 10% and unsorted cell pool (Total) are indicated. Mean of biological triplicates consisting of technical triplicates shown. **(B):** Bar charts illustrating results as presented in **(B)** but after normalization of AP1 site editing frequencies on AP1 site editing in the respective total cell populations. Un-paired two-sided Student's T-Test. *, $P < 0.05$. **(C):** Representative CD73 FACS analysis of one biological replicate as shown in **(A)** and **(B)** of CRISPR/Cas9 (AP1/ctrl site) targeted MaMel.79b_{late}JUN-citrineDOX after 25 ng/ml DOX pulse at day 5.

The evaluation of the screening approach revealed one defined AP1 binding motif that showed major functional relevance for the induction of CD73 by JUN: The AP1 #5 site. Quantification of AP1 site targeting prior normalization already demonstrates a strong enrichment of 52% AP1 #5 site targeted mutagenesis in the 10% lowest CD73 sub-fraction (Figure 6.22, A). Vice versa, a strong depletion of AP1 #5 site targeting in the 10% highest CD73 sub-fraction with only 4% AP1 #5 site editing is seen. Following normalization, significant enrichment in of AP1 site disruption in CD73^{low}

versus CD73^{high} sorted cells is again found only for the AP1 #5 site (Figure 6.22, B). Intriguingly, we even observed reduced induction of CD73 in a sub-fraction of cells after targeting the AP1 #5 site, which became apparent as a shoulder of CD73^{low} inducible cells in FACS analysis (Figure 6.22, C).

In summary, the results demonstrate that destructing the AP1 #5 site functionally impairs CD73 induction in our cell line model. JUN/ AP1 complexes require binding to the AP1 #5 site within the first intron of *NT5E* to stimulate its expression in melanoma. Strikingly, the AP1 #5 site aligns perfectly to the region of strongest enrichment of JUN binding to *NT5E* in our ChIP qPCR experiments presented above.

6.4.3 Positional mutation analysis constitutes a method for the identification of previously unknown enhancer elements with single base pair resolution

We used the CRISPR/Cas9-based FACSorting enhancer screening approach in the previous section to address the question whether specific predefined TF binding sites are of functional importance for the expression of CD73. However, quite often, potential enhancer regions and detailed TF binding sites remain elusive. Thus, a screening approach allowing identification of such sites and simultaneously proving their functional relevance in an endogenous context would be highly desirable. We hypothesized that in our approach the combination of FACSorting-based phenotype screening and subsequent genotyping of a polyclonal edited cell pool should qualify for the identification of unknown enhancer elements. CRISPR/Cas9 genome editing by a single sgRNA results in a variety of genomic alterations leading to a polyclonal mutated cell population. Those editing events that destroy the integrity of a functionally important enhancer element will accumulate in low expressing fraction during FACSorting. In case the enhancer element has not been determined before, one can thus tile a potential enhancer region via sgRNAs in an arrayed fashion and analyze for every sgRNA position-wise enrichment of genome editing to retrieve functionally important enhancer motives with resolution down to single basepairs (bp).

To survey this idea in a proof of principle approach, we developed positional mutation analysis, comparing genome editing in CD73^{high} and CD73^{low} sorted cells position-wise after targeting by the individual sgRNAs across the respective amplicons sequenced. Figure 6.23 shows the results for sequences from 20 bp ahead to 20 bp past the CRISPR/Cas9 cutting sites. Affirmative, we found highest editing frequencies at or nearby the CRISPR/Cas9 cutting sites, 3 bps upstream of the protospacer adjacent motif (PAM). We did not see any differences in position-wise deletion frequency for CD73^{high} and CD73^{low} sorted cells targeted by the ctrl site sgRNA thus excluding artifacts from FACSorting procedure to influence the analysis.

Impressively, in line with our preceding analyses, we detected an increase of positional mutation frequency specifically at the canonical binding motif TGA₂CTCA of the AP1

#5 site in CD73^{low} versus CD73^{high} FACSsorted cells. In addition, we observed a compensatory editing enrichment in CD73^{high} FACSsorted cells nearby the CRISPR/Cas9 cutting site but distal of the AP1 #5 site consensus binding motif. To this extent we observed both of the effects only after targeting the AP1 #5 site but not for any other candidate AP1 sites throughout *NT5E*.

In summary, we were able to unbiasedly retrieve the canonical AP1 binding motif TGACTCA of the AP1 #5 site as a sequence motif that is required for the induction of CD73 by JUN in melanoma and thereby, validate our approach for functional enhancer screening to uncover novel regulatory elements.

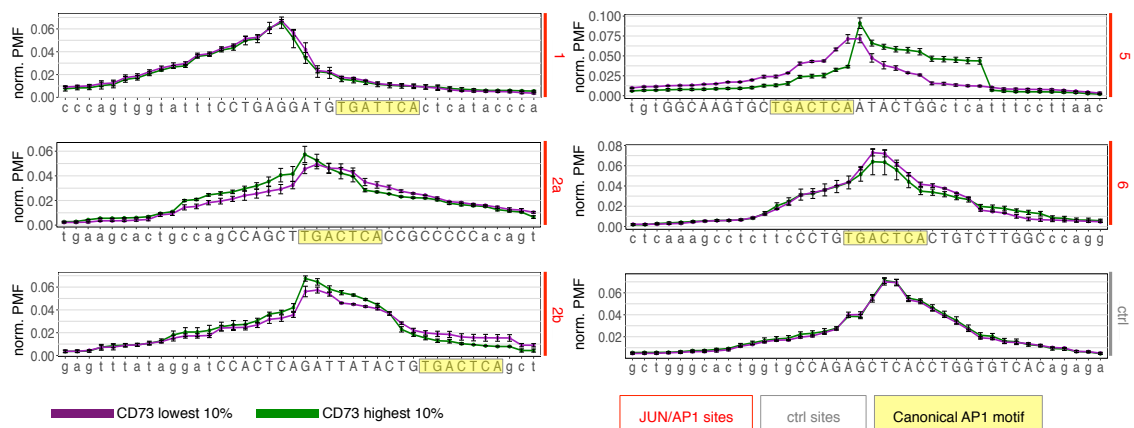


Figure 6.23: **Proof of principle positional mutation analysis identifies the canonical AP1 #5 site motif for CD73 regulation by JUN** Positional mutation analysis in MaMel.79b^{late}JUN-citrineDOX, CRISPR/Cas9 targeted at indicated sites, treated by 25 ng/ml DOX for 5 days, FACS sorted on 10% highest (green lines) and 10% lowest (purple lines) CD73 expressing cells and fractions deep sequenced. Positional mutation frequency (PMF) is normalized (norm.) to area under curve as divided by the sum of all mutation frequencies. Data show means of n=3 with error bars indicating SD.

6.4.4 CD73 baseline expression depends on JUN binding to the first intronic AP1 #5 site in *NT5E*

Having found that one defined AP1 site in *NT5E* significantly accounts for CD73 induction by JUN, we next questioned whether CD73 baseline expression in melanoma is subjected to similar regulation. Using our CRISPR/Cas9-based genome engineering approach, we targeted the AP1 #5 site, the AP1 #2a site and the ctrl site in the CD73 positive melanoma cell lines SK.Mel28, MaMel.65, MaMel.54a and MaMel.85 and continued by FACS sorting and deep sequencing as described above. In this reduced set of targeting sgRNAs we selected the AP1 #2a site as an AP1 site targeting control sgRNA, in order to evaluate the effects of AP1 #5 site editing for baseline CD73 expression. sgRNA #2a had shown most similar editing frequencies compared to sgRNA

#5 and both sgRNAs cut one bp apart from the respective AP1 canonical binding motives.

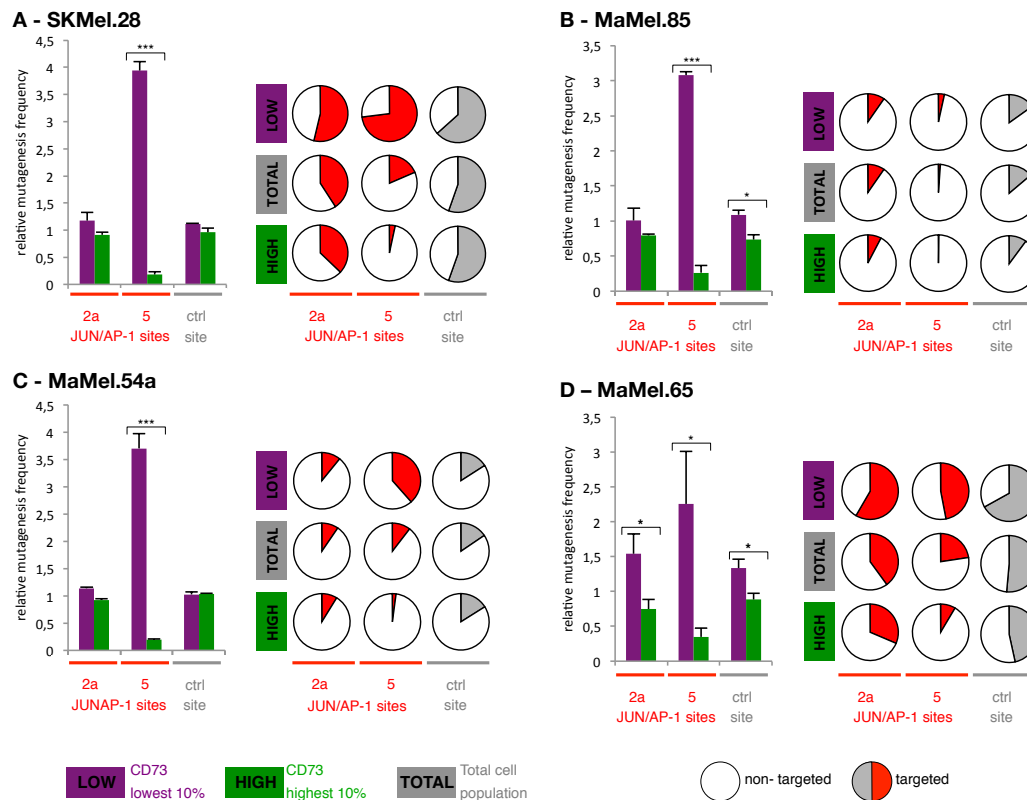


Figure 6.24: **The AP1 #5 site is relevant for CD73 expression in SK.Mel.28, MaMel.85, MaMel.54a and MaMel.65.** (A): SK.Mel.28, (B): MaMel.85, (C): MaMel.54a and (D): MaMel.65 CRISPR/Cas9 targeted at AP1 #2a - , AP1 #5 - and ctrl site. Panels left: Relative mutagenesis frequency at the respective AP1 sites for AP1 site targeting and at target site for ctrl site targeting depicted in CD73^{low} sorted cells (purple bars) and CD73^{high} sorted cells (green bars) as normalized to editing frequencies in total cell population is shown in bar charts as mean of n=3 with error bars indicating SD. Significance tested by two-sided unpaired Student's T-Test. *, P<0.05; ***, P<0.001. Panels right: Pie charts illustrating genome editing frequencies as mean n=3 at the target sites and for conditions as specified above.

Figure 6.24 illustrates AP1 site editing for sgRNAs #2a and #5 and target site editing for ctrl sgRNA in pie charts from 3 independent experiments for the total cell populations as well as for the fractions sorted. Bar charts depict respective AP1 site and ctrl site mutagenesis frequencies following normalization on the total cell population editing efficiency (Figure 6.24). Surprisingly, mutagenesis efficiencies highly varied for the individual cell lines and sgRNAs. Reduced mutagenesis frequency in MaMel.54a and MaMel.85 might be explained by limited transfectability of both cell lines (Figure 6.24, B and C). We were highly intrigued that even though observing such variation and limitation in editing efficiency, we consistently see a predominant and significant enrichment of AP1 site editing in CD73^{low} sorted cells when disrupting

the AP1 #5 site in all cell lines analyzed and independent from CRISPR/Cas9 editing activity.

In accordance with previous observations, the AP1 #5 site was the only relevant target site that consistently impacted on CD73 expression. In SK.Mel28 we detected a 20 fold enrichment of AP1 #5 site editing in the CD73^{low} sorted compared to CD73^{high} sorted fraction (Figure 6.24, A). MaMel.85 that exhibited the most limited mutagenesis frequency of only 1.1% in sgRNA #5 targeted cells, still held an 18 fold enrichment of editing at the AP1 #5 site of CD73^{low} sorted cells (Figure 6.24, A). Similarly, MaMel.54a and MaMel.65 showed a 18 fold and 5.5 fold enrichment for sgRNA #5 targeted CD73^{low} sorted cells, respectively. Destruction of the ctrl site did not majorly change CD73 expression in the cell lines, some minor enrichment was observed for MaMel.85 and MaMel.65 (Figure 6.24, B and D). Likewise, editing by the sgRNA # 2a did not lead to an enrichment of AP1 #2a disruption in CD73^{low} sorted cells in a dimension that was perceivable from AP1 #5 site editing. Some minor enrichment was observable again for MaMel.85 and MaMel.65 CD73^{low} sorted cells, with a 1.5 fold and 1.4 fold increase, respectively.

We next recapitulated positional mutation analysis again in this context as illustrated in Figure 6.25. Position-wise distribution of genome editing for a 40 bp sequence surrounding the CRISPR/Cas9 target sites of sgRNAs #2a, #5 and ctrl has been calculated for CD73^{low} and ^{high} sorted SK.Mel28, MaMel.85, MaMel.54a and MaMel.65. We affirmatively observed enrichment of editing in the CD73^{low} sorted fraction of cells at specifically the AP1 #5 canonical binding motif TGA_{CT}CA for SK.Mel28 and MaMel.54a (Figure 6.25, A and C). In line, those cell lines showed most prominent enrichment of AP1 #5 targeting in the CD73^{low} sorted fraction in previous analyses. Enrichment of editing in an AP1 binding motif other than the AP1 #5 canonical binding site was not found in CD73 depleted cells in any cell line investigated.

As a side note, in this instance genome editing efficiency is impacting on the potency of positional mutation analysis which can be readily observed for MaMel.85 targeted by sgRNA #5 (Figure 6.25, B) and should be considered and sgRNAs optimized for future analysis, in especially when designing screens for the identification of unknown enhancer elements.

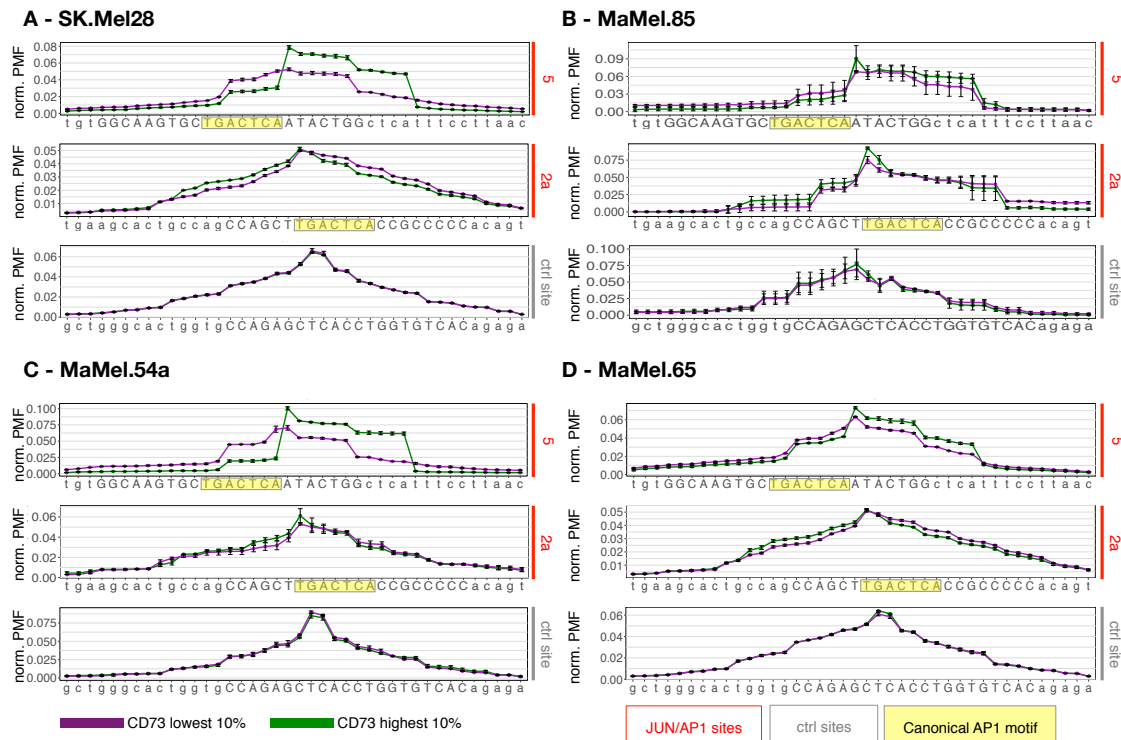


Figure 6.25: **Positional mutation analysis confirms the relevance of AP1 #5 for baseline CD73 expression** Positional mutation analysis for (A): SK.Mel28, (B): MaMel.85, (C): MaMel.54a and (D): MaMel.65, CRISPR/Cas9 targeted at the AP1 #2a -, AP1 #5 - and ctrl site. Green and purple lines show FACSsorted fractions of 10% highest and 10% lowest CD73 expressing cells, respectively, that are deep sequenced for genome editing and analyzed on positional mutation frequency (PMF). PMF is normalized (norm.) to area under curve as divided by the sum of all mutation frequencies. Data show means of $n=3$ with error bars indicating SD.

6.4.5 Disruption of the first intronic AP1 #5 site in *NT5E* leads to long term depletion of CD73

In a final experimental setting, we aimed to check whether CD73^{low} expressing subpopulations that arise in CD73 positive melanoma cell lines after targeting the AP1 #5 site, exhibit persistent downregulation of CD73 surface expression. For that referred to SK.Mel28 as a representative cell line model. We FACSsorted CD73^{high} and CD73^{low} subpopulations of cells targeted by CRISPR/Cas9 at the AP1 #2a, AP1 #5, and ctrl site and tracked CD73 surface expression for up to one week (day 0, day 3, and day 7 after FACSsorting) as illustrated in Figure 6.26, A. As expected, we found stable depletion of CD73 surface expression only for CD73^{low} sorted cells in the AP1 #5 sgRNA targeting condition (Figure 6.26, B). CD73^{low} sorted cell populations targeted by the sgRNA #2a and ctrl sgRNA restore baseline CD73 expression levels already after 3 days. Of note, CD73^{high} sorted cells of the AP1 #5 site targeting condition also restored parental

CD73 surface and total protein expression levels at day 7 post sorting. This finding was corroborated by mRNA and total protein expression analyses (Figure 6.26, C). At 24h post FACS sorting, we found strong depletion of *NT5E* mRNA only when sorting on the CD73^{low} fraction of sgRNA #5 transfected cells which persisted for at least one week after FACS sorting. Interestingly, we already noticed some decrease in *NT5E* mRNA in the unsorted total cell population of AP1 #5 site CRISPR/Cas9 targeted cells (Figure 6.26, B). On a total protein level, the effect of FACS sorting on CD73^{low} and CD73^{high} expressing fractions was well-detectable by a decrease and an increase of total protein after 24h. Only cells targeted at the AP1 #5 site kept the differential expression after 7 days.

In summary, we identify a first intronic enhancer within *NT5E* that critically regulates CD73 baseline expression via JUN binding to a canonical AP1 site motif, here named AP1 #5 site. JUN promotes upregulation of CD73 in CD73^{low} expressing melanoma cell lines via this JUN/ AP1 signaling axis and is also involved in CD73 baseline expression as demonstrated in various melanoma cell lines.

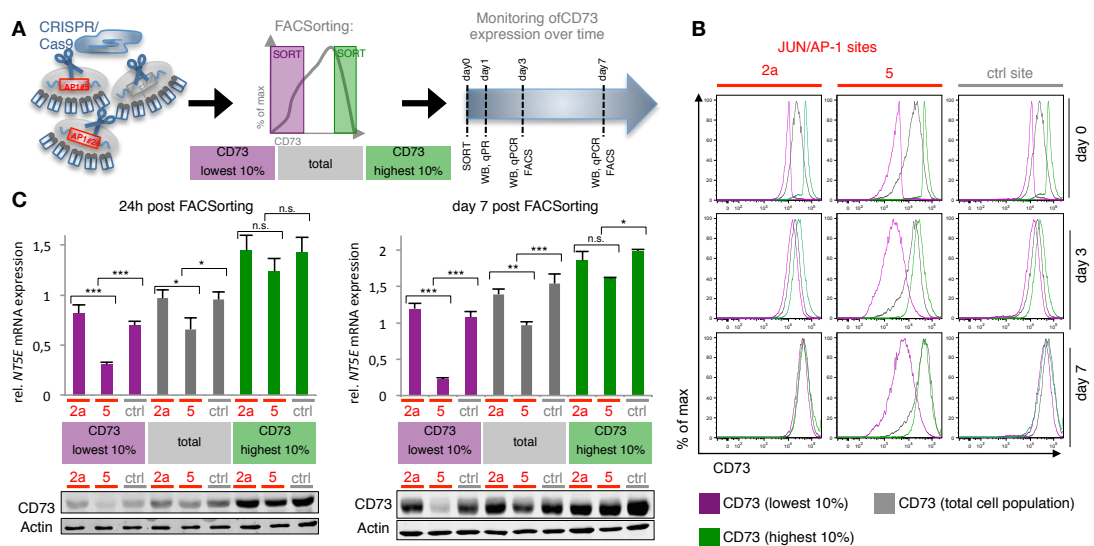


Figure 6.26: **SK.Mel28 show long term depletion of CD73 when enriching on AP1 #5 site disruption by FACS sorting.** (A): Schematic overview on the experimental procedure for long term monitoring of CD73 post FACS sorting in AP1/ Ctrl site CRISPR/Cas9 targeted SK.Mel28. (B): CD73 FACS histograms in SK.Mel28 CRISPR/Cas9 targeted at AP1/ Ctrl sites as indicated and FACS sorted on 10% lowest and 10% highest CD73 expressing cells in re-FACS at day 0, day 3 and day 7 post sorting. CD73^{low} and CD73^{high} sorted cells are depicted in purple and green in the follow-ups, respectively. (C): Same as (B) but showing qPCR analysis at top and immunoblot analysis at bottom at 24 h post sort (left) and at day 7 post sort (right). Relative *NT5E* expression as normalized to *UBC* is shown in mean values from 3 independent experiments with error bars indicating SD. One-way ANOVA and multiple comparison testing within sorted fractions corrected according to Bonferroni. *, P<0.05; ***, P<0.001; n.s.=none significant.

7 Discussion

Phenotypic plasticity of cancer cells has evolved as a novel hallmark of cancer [79]. It is a major cause for melanoma cell aggressiveness and difficulty to sustainably fight melanoma [110]. So far, models of melanoma phenotype switching are based on two alternative cell states, defined by the presence or absence of MITF [34]. In order to increase the understanding and provide further knowledge for future therapeutical targeting of melanoma cell plasticity, we have investigated additional transitional cell states and novel plasticity markers in the present study. We found a *nascent invasive* cell state, which can be described by expression of the 5'ectonucleotidase CD73 in the MITF^{high} fraction of melanoma cells, and which exhibits an early inflammatory, early invasive gene expression signature. Intriguingly, CD73 expression was cooperatively induced by mitogenic and inflammatory signaling and depended on the MAPK signaling cascade. We found the transcription factor JUN being as a main transcriptional regulator, activating CD73 expression via an intronic JUN/ AP1 binding site. CD73 constitutes an upcoming target in checkpoint immune blockade of melanoma [7], hence knowledge about CD73 regulation in melanoma phenotype switching provides essential insights into the reciprocal interactions of therapeutic interventions and melanoma plasticity.

7.1 The trajectory of melanoma cell state transitions

Melanoma phenotype switching has been established as a binary decision between a stem cell like *invasive* and a differentiated *proliferative* phenotype [34, 107]. Mechanistic analyses on melanoma phenotype switching focussed on comparing transcriptional profiles and epigenetic regulations between those two cell states, and concepts were adapted from the well-defined transitions between epithelial and mesenchymal cells, EMT and MET. However, the comparison of phenotypes of maximal dissimilarity hampers a decoding of the process of interconversion. Here, we expand the known two alternative melanoma cell states by the identification of an early intermediate phenotype, and thereby allow novel insights into the mechanisms of cell state interconversions. We term it a *nascent invasive* phenotype, as it can be characterized by a *nascent invasive* and *nascent inflammatory* transcriptional signature and can be identified by the co-expression of CD73 along with MITF (Figure 6.1, E-H).

The identification of an intermediate cell state is in line with reports on partial or incomplete EMT of epithelial cells, that evolve by progressive loss of epithelial features and cooperative gain of mesenchymal traits, resulting in an intermediate transition phenotype, sharing characteristics of both traits [170]. Stable and metastable partial EMT phenotypes play an important role during embryonic development, fibrosis, wound healing, and, most interestingly, have been highlighted for carcinoma progression [170]. As an example, in wound healing keratinocytes undergo partial EMT gaining migratory capacity while retaining epithelial characteristics, such as cell-cell adhesion, and migrate in clusters along the wound edges in order to close the wound [274]. Importantly, partial EMT and collective cell migration is also frequently observed during metastatic dissemination of carcinoma cells [214, 197, 205, 279, 237]. Additionally, the co-existence of epithelial and mesenchymal traits was associated with increased aggressiveness and poor outcome in breast cancer [209].

Already 20 years ago, a negative prognosis has been described for human melanoma, co-expressing epithelial keratin and mesenchymal vimentin [100]. Moreover, partial EMT-like phenotypes and collective cell migration are well accepted features of neural crest cells during the early developmental process of delamination and migration to distant sites [244]. Disseminating melanoma cells with a bi-phenotypic nature have been described during the process of perivascular mimicry. For example, strongly pigmented melanoma cells have been reported to migrate along perivascular routes in response to UV-induced neutrophilic inflammation in a melanoma mouse model [13]. Other studies analyzing perivascular mimicry showed the presence of melanosomes, a feature of the *proliferative* phenotype, to coincide with vasculogenic networks, which is marking *invasive* melanoma cells [152, 101]. Such data are indicative for a role of an intermediate melanoma cell state during metastasis formation. In line, CD73 expression in melanoma, which our data suggest as a maker for *nascent invasiveness*, has been associated with metastasis formation in several melanoma mouse models [275, 235, 268].

The development of therapy resistance constitutes an additional aspect that a partial EMT phenotype has been shown to contribute to. In their study of targeted drug resistance in lung cancer, Sharma *et al.* observed stochastic and, importantly, reversible occurrence of drug-resistant precursors at low frequency within PC9 cells, which persisted therapy and gave rise to a sub-fraction of expanding fully drug-resistant progeny [223]. Intriguingly, the authors observe global transcriptional differences between all three subpopulations: The parental culture, the drug-persistent progenitors, and the drug-resistant cell population, indicating nascent phenotype switching in the early drug-persistent cells. Interestingly, full phenotype switching and expansion of resistant cells was observed to descent from only a fraction of drug-persistent progenitors. The establishment of full drug resistance seems to depend on both the susceptibility of the drug-persistent cancer cell to progress and on the prolonged exposure to therapeutic stress stimulation. On a mechanistic level, Sharma and colleagues identified epigenetic remodeling during phenotype switching, which depends on the histone demethylase JARID1a and begins in drug-persistent progenitor cells. Complementary,

we showed that expression of the *nascent invasive* cell state marker CD73 required global epigenetic remodeling in addition to inflammatory mitogenic stress stimulation in our panel of melanoma cell lines (Figure 6.5, A and Figure 6.7), indicating that chromatin modifications are an early event in the process of melanoma phenotype switching as well.

Based on the broad evidence for a partial EMT phenotype and its role in carcinoma, similar concepts presumably apply for cell state interconversions in melanoma. It is unclear why an intermediate phenotype in melanoma has not been identified earlier by the numerous previously published large scale transcriptome analyses.

The predominance of metastable interstates in a cell type with an intrinsic low threshold for phenotype switching, such as neural crest-origin melanoma cells, might provide a possible explanation. The highly plastic nature of melanoma cells has been demonstrated by metastatic melanoma cells that were transplanted and reprogrammed within the developing chicken embryo to reconstitute a neural crest phenotype migrating along environmental gradients to finally contribute to a plethora of neural crest derived lineages [135]. In support, our data show that inflammatory and *invasive* gene expression signatures are not increasing linearly, but exponentially upon progressive melanoma cell dedifferentiation. Thus we see only moderate induction of inflammatory and *invasive* signature genes in the *nascent invasive* phenotype (Figure 6.1), which can still exhibit a priming effect on further melanoma cell dedifferentiation upon inflammatory stimulation. Indeed, we have shown that *nascent invasive* melanoma cells are more prone to inflammation-induced dedifferentiation and show a stronger inflammatory response than *proliferative* melanoma cells when treated with $TNF\alpha$ (Figure 6.3, B). This is also strongly reminiscent of our previous findings on varying penetrance of $TNF\alpha$ -mediated induction of JUN and *invasive* phenotype switching, resulting in the classification of poor switching and strong switching melanoma cell lines [201].

Another theory relates to the aspect that cell state transitions may not only follow one route along a sequential transition process but may exist in many facets with multiple, and even co-existing intermediate states. In our data such a hypothesis is supported by the finding that individual genes of the *invasive* and inflammatory gene expression signature highly vary across different cell lines belonging to the same phenotype (Figure 6.1, B). Confirmatively, CD73 is steadily expressed upon a *nascent invasive* phenotype but with high individual variance (Figure 6.1, E).

Finally, even though the concept of melanoma cell plasticity is based on EMT, and even though EMT-like processes are common during neural crest development, one has to keep in mind that EMT of epithelial origin is highly complex and shaped by a plethora of tissue specific extracellular signals converging on multiple tissue specific EMT TFs, even exerting tissue specific roles. [169]. As an example, whereas SNAIL promotes EMT and metastasis in breast cancer [252], such an effect has not been observed for pancreatic cancer [283], but here ZEB1 has been described as a main factor for EMT induction [133]. In melanoma, members of the ZEB family even hold antagonistic functions, as ZEB1 and ZEB2 have been involved in tumor promotion and

reduction of aggressiveness, respectively [53, 33]. As a consequence, single mesenchymal markers are often insufficient to characterize EMT processes in cancer and the adaptation of EMT-like plasticity in melanoma to epithelial EMT has to be done with caution.

Currently, the establishment of scRNA-seq technologies are advancing the field of cancer plasticity, allowing novel insights into the variability of single cell phenotypes within a tumor mass. Initial exciting publications are supporting a concept of multi-stage melanoma cell plasticity. At the end of last year, Ennen and colleagues published scRNA-seq data of 472 cells from 5 primary melanomas. In line with the *nascent invasive* phenotype emerging from our bioinformatic analyses, the authors found some MITF^{high} melanoma cells co-expressing *invasive* signature genes. Interestingly, when they validated their results for a selection of candidate co-expressed markers by immunohistochemical stainings they found both intertumoral, as well as intratumoral differences in co-expression of *proliferative* and *invasive* cell state markers [66]. In another recent work, Shaffer and co-workers showed an involvement of an intermediate, slow-cycling melanoma cell state in the development of non-genetic resistance against targeted therapy [221]: Vemurafenib pre-resistant cells majorly differed from the plenum of sensitive melanoma cells with respect to their transcriptome and expression of resistance markers. In a subsequent phase of expansion followed by drug-treatment, resistant melanoma cells underwent additional massive epigenetic rewiring. Interestingly, the final switch for therapy resistance is driven by an activation of JUN/ AP1 signaling fitting to our observations of inflammatory stress signaling via JUN to drive *invasive* phenotype switching in melanoma. However, in contrast to our model of an early inflammatory and invasive gene expression signature marking the *nascent invasive* phenotype in a fraction of differentiated cell lines, the authors found cellular reprogramming to be initiated by down-regulation of SOX10 and associated differentiation programs. In a further study, an interesting R-based tool for cell state identification from scRNA-seq data was published lately [3], emphasizing the rising interest in using single cell transcriptome data for elucidating cellular plasticity. The presented algorithm identifies gene regulatory networks based on integration of cis-regulatory networks in so-called regulons. Cell types or phenotypes are determined by shared binary regulon activity, creating regulatory subnetworks. In line with previous literature, Aibar *et al.* show data on 1200 single cells from 14 melanoma lesions, which cluster according to predefined MITF^{high} *proliferative* and MITF^{low} *invasive* cell states. Shared MITF^{high} regulatory subnetworks with MITF/STAT/IRF constitute central TFs on the one hand and *invasive* regulatory subnetworks harboring high expression of WNT5A/LOXL2/ZEB1 on the other hand. Affirmatively, MITF^{high} regulatory subnetwork activity is completely absent in the *invasive* phenotype (Figure 7.1). Intriguingly, even though the authors are not highlighting it in their paper, their data show activity of *invasive* regulatory subnetworks in a fraction of MITF^{high} cells, which also form a separate population in t-SNE analysis (Figure 7.1), and fits our description of an MITF^{high} *nascent invasive* phenotype.

A very recent publication, which similar to ours, investigated further transition cell

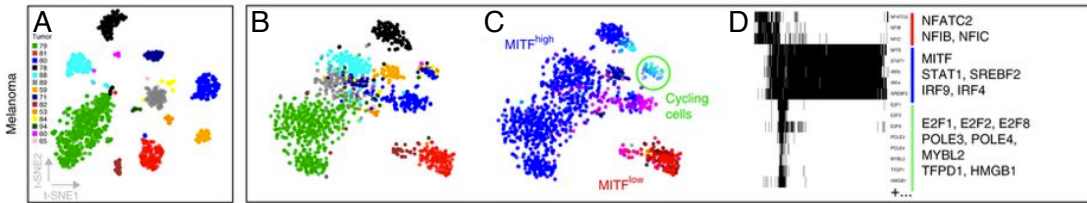


Figure 7.1: ***Nascent invasive phenotype switching becomes apparent in single cell RNAseq data by Aibar et al. for coinciding MITF and invasive regulon activity***. (A): T-SNE plot based on the expression matrices, colored by tumor of origin. (B and C): T-SNE plots based on the binary regulon activity, colored by gene regulatory network activity. (D): Single-cell regulatory network clustering map. Data adopted from Aibar *et al.*, Figure 3 [3].

stages by means of bioinformatic analyses of melanoma expression datasets, suggests a 4 stage phenotype switching model, which is imitating stages of melanocyte development in a reverse route of dedifferentiation, starting from a melanocytic cell state, followed by a transitory cell state and a neural crest-like cell state, resulting in a final undifferentiated cell state [255]. Strikingly, Tsoi *et al.* confirmed the importance of mitogenic signaling along with inflammatory signaling on this route of melanoma cell dedifferentiation, which we pointed out in our study as well. Furthermore, the authors provide an online-tool, allowing visualization of genes of interest within PCA analysis data to annotated melanoma cell phenotypes. As shown in Figure 7.2, visualization of CD73 in sub-phenotypes clearly shows that CD73 expression distinctively overlaps with the proposed transitory cell state, and is increased overall in the neural crest-like and the dedifferentiated phenotype. In contrast, classical *invasive* markers AXL and WNT5a are negative in this early dedifferentiated cell population which is fitting to the analysis presented in Figure 6.2 of this study and hinting on an overlap of the *nascent invasive* phenotype of our work and the transitory phenotype of Tsoi *et al.*

In contrast to the commonly preferred trajectory of cell state transitions with *proliferative* melanoma cells undergoing dedifferentiation into a final neural-crest stem cell-like *invasive* phenotype, Tsoi *et al.* describe a trajectory of melanoma phenotype switching that passes an intermediate neural crest precursor fate and results in a dedifferentiated omnipotent stem cell-like phenotype with more mesenchymal, inflammatory characteristics. In support of this concept, we observed that the sub-population of most dedifferentiated melanoma cells are indeed negative for the neural-crest marker NGFR (Figure 6.2, A). Moreover, based on the fact that CD73 represents a well-established marker for mesenchymal stem cells [32], our observation of elevated CD73 expression starting in *nascent invasive* melanoma cells and increasing to robust CD73 expression in a fully dedifferentiated phenotype reinforces the importance of mesenchymal cell traits in full dedifferentiated melanoma cells. In addition to that, expression of CD73 on melanoma cell lines has been described to correlate with expression of mesenchymal markers before, yet the molecular mechanisms remained unclear [207]. Also, during embryonic

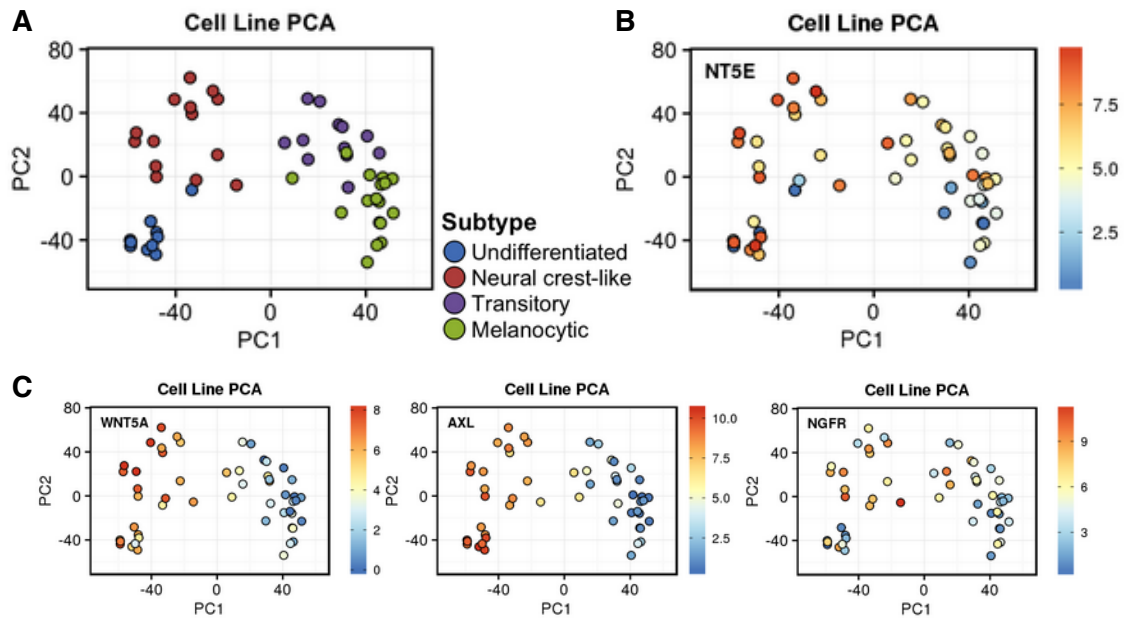


Figure 7.2: ***Nascent invasive phenotype switching in comparison to the plasticity model proposed by Tsoi et al.*** (A): Data adopted from Tsoi *et al.*, Figure 1C [255]. Panel of human melanoma cell lines ($n=53$) shown as PCA, assigned to 4 subtypes by consensus hierarchical clustering. Stages of melanocyte differentiation are specified by comparative analysis to *in vitro* induction of embryonic stem cells into melanocytes. (B): Web tool, provided by Tsoi *et al.* on <http://systems.crump.ucla.edu/dediff/> for visualization of gene of interest superimposed on the analysis as presented in (A), showing expression of *NT5E*. (C): Same as (B), but illustrating *WNT5A*, *AXL* and *NGFR* expression from left to right.

stem cell reprogramming towards a neural crest lineage, the occurrence of mesenchymal features and subpopulations have been repetitively observed [49, 138], hinting on a close cross-talk of those two stem cell types during reprogramming events. Summarizing currently available data, one can postulate, that melanoma stem cells, which have been characterized as a rare fraction of cancer cells expressing neural crest markers, are forming a metastable intermediate cell state, and that therapeutic intervention, stress and inflammation may lead to a shift of balances, promoting switching to a more stable, fully dedifferentiated cell type. Hence, intermediate melanoma cell states, such as above described pre-resistant melanoma cells, might endow melanoma with the capacity of priming for environmental changes, such as development of therapy resistance. In support of this hypothesis, a recent publication on renal cell carcinoma suggested CD73 as a marker for CSCs with increased tumorigenicity and resistance to therapeutic stress [232]. It will be interesting to investigate whether pre-resistant melanoma cells are indeed positive for CD73, implying *nascent invasive* phenotype switching as a resistance mechanism.

7.2 CD73, a melanoma plasticity marker with an important role in tumor immunosuppression

So far, melanoma plasticity markers were identified on the basis of mutual exclusive expression in the *proliferative* or the *invasive* cell state. In the present study we investigated intermediate cell states and retrieved a previously unknown *nascent invasive* phenotype, which can be identified by the co-localisation of MITF, the *bona fide proliferative* cell state marker, and CD73, a novel marker of *invasive* and *nascent invasive* melanoma cells.

Intriguingly, CD73 constitutes a novel target for cancer immunotherapy. Physiologically, CD73 expression can be found on a variety of immune cell subtypes, like T cells, B cells and myeloid cells, but also on mesenchymal stem cells, as well as bone marrow stromal cells, endothelial and epithelial cells in many diverse tissues [44]. The function of CD73 has mostly been attributed to its extracellular enzymatic activity in the cascade of adenosine triphosphate (ATP) breakdown, hydrolyzing adenosine monophosphate (AMP) into adenosine, which is modulating various cellular responses via adenosine receptors. Among other functions, CD73 can regulate vascular integrity and ischemic re-perfusion [284], but it also controls immune responses in a negative feedback loop in order to limit excessive inflammation [44, 177], which has emerged as a key mechanism of tumor immunosuppression [9]. An effective anti-tumor immune response is accompanied by destruction of tumor cells, leading to release of pro-inflammatory ATP. Here, the presence of CD73 in the tumor microenvironment acts as a molecular switch, that turns an ATP-rich anti-tumor immune response into an adenosine-rich broad immunosuppression [9]. Hematopoietic and non-hematopoietic host cells as well as tumor cells can express CD73 to provide sources of adenosine, which interferes locally and suppresses many types of immune cells: Immunosuppressive adenosine receptors are up-regulated upon T cell activation [281] and adenosine ligation impairs both T helper cell and cytotoxic T cell functions [281]. Furthermore, adenosine inhibits NK cell activation [193]. It impairs phagocytosis and at the same time promotes alternative macrophage polarization [48], as well as expansion of myeloid derived suppressor cells (MDSCs) [206]. Additionally, adenosine stimulation causes abnormal dendritic cell maturation into a pro-tumorigenic, pro-angiogenic phenotype, characterized by secretion of vascular endothelial growth factor (VEGF) [172] and supports expansion of regulatory T cells [178]. Another interesting aspect, which has only been appreciated recently, is the impact of chronic adenosine signaling to render tumor endothelial cells *anergic*, which means that the tumor vasculature is not responsive to stimuli up-regulating adhesion molecules and allowing extravasation of lymphocytes, but at the same time myeloid cell infiltration is still supported [243, 268]. As a consequence, adenosine signaling not only impairs immune cell function within the tumor microenvironment but also prevents entrance of anti-tumoral immune cells. Lastly, adenosine signaling in breast cancer cell line models was found to also directly promote cancer cell migration and metastasis formation [162]. The broad spectrum of CD73 expression and adenosinergic signaling

in mediating immunosuppression and promoting tumor progression has put pharmacological inhibition of CD73 and adenosine receptors into the focus to develop novel ways of immune checkpoint blockade [7, 11, 10]. Numerous pre-clinical studies have demonstrated A2A adenosine receptor inhibition to limit tumor growth [282, 8]. Based on the success of pre-clinical A2A adenosine receptor studies, phase I clinical trials involving antibody mediated blockade of CD73 (NCT02503774) and small molecule interference with A2A adenosine receptor (NCT02503774 and NCT02655822) in solid cancer are currently ongoing [98].

Previous studies have revealed mechanisms of how full dedifferentiation of melanoma cells in response to inflammation and therapeutical stress promotes resistance. For example, the attack of anti-tumor T cells can be bypassed by the down-regulation of melanocytic target antigens [136] and a stem cell-like dedifferentiated transcriptional program allows uncoupling of melanoma cell survival and proliferation signaling from oncogene driver activity [129, 167]. Our work provides novel insights into melanoma cell phenotype switching and links it to the acquisition of an immunosuppressive phenotype by expression of CD73. According to our model, full melanoma cell dedifferentiation might not coercively be required for the establishment of an immunosuppressive tumor microenvironment. On the contrary, CD73 expression is present in differentiated melanoma cells upon nascent increase of invasive and inflammatory signature gene expression. For example, inflammatory macrophages, which form a first line of immune defense, provide a source of TNF α for the induction of CD73 in our model system (Figure 6.9). Based on this observation, we assume that melanoma up-regulate CD73 *in vivo* when exposed to acute or chronic stress conditions, which is the case during uncontrolled tumor growth, leading to hypoxia and starvation stress, as well as during therapeutical interventions accompanied by tissue destruction and inflammation [108, 136, 70]. Importantly, only transient activity of AP1/ JUN signaling is required for the induction of CD73 (Figure 6.19), and we postulate that expression of CD73 on tumor cells indicates previous exposure to cellular stress and memorizes preceding inflammation. Following this assumption, a switch to a *nascent invasive* phenotype is primed to counteract further inflammatory triggers by remodeling the tumor microenvironment via the adenosinergic axis, which could be a maladaptive modus exploiting the physiological role of CD73 in shutting down excess inflammation. Hence, resistance to cancer immunotherapy might rather constitute an early event during melanoma phenotype switching. Of note, a cancer stem cell-like phenotype associated with evasion from immune recognition has recently been attributed to tissue resident stem cells [1]. Agudo *et al.* showed that quiescent tissue stem cells of various origin can bypass cytotoxic T cell recognition and destruction by down-regulation of various components of the antigen presentation machinery.

7.3 Survey on the functional relevance of CD73 expression for EMT and inflammatory phenotype switching

Common *invasive* cell state markers, among them AXL and WNT5a, are not only marking, but also participating in progressive dedifferentiation [57, 218]. Having observed CD73 expression to be up-regulated upon *nascent invasive* phenotype switching raises the question, whether CD73 is functionally involved in that process. Indeed, a recent study showed that CD73 plays a role for EMT switching of ovarian carcinoma cells [148]. Lupia and colleagues showed, that in ovarian carcinoma spheroid cultures shRNA mediated knock-down of CD73 or CD73 inhibitor treatment impaired the formation of tumorigenic spheres, led to a down-regulation of key EMT genes, and, most importantly, hampered the acquisition of a stem cell-like phenotype. Inversely, adenosine stimulation further up-regulated those stemness associated TFs. Similarly, in neuroendocrine pancreatic tumors, CD73 was reported to be over-expressed in the fraction of CSCs and to be relevant for sphere formation as well as motility of cancer cells [120]. Endogenous plastic somatic cells constitute another interesting CD73 expressing cell population endowed with a functional role of CD73 for cell plasticity: Pan *et al.* have analyzed this rare and highly plastic population of cells, which is exhibiting omnipotent stem cell capabilities and can be found at very low frequency in adult tissue [182]. Interestingly, the stem cell phenotype was dependent on expression of 4 factors, among them is CD73. CD73 was found to be relevant for adenosine generation and signaling via the A2B adenosine receptor inducing expression of stem cell TFs. The fact that rare adult neural crest stem cells in the skin, adipose tissue and bone marrow express CD73 [46] may hint to a similar role. It remains to be determined whether the same function is involved in melanoma cell plasticity. The fact that melanoma cell lines of the *nascent invasive* phenotype show stable expression of CD73 along with MITF differentiation signature, but otherwise only nascent dedifferentiation marks, suggests that further factors are required for initiation of full dedifferentiation. From another perspective, priming of dedifferentiation and inflammation in melanoma cells upon expression of CD73 in the *nascent invasive* cell state raises the question whether CD73 is causative for this effect. Preliminary transcriptome data of CD73 CRISPR/Cas9 KO and control melanoma cell lines however did not indicate changes of *invasive* phenotype-associated gene expression (data not shown). Further analyses will be needed in order to answer this question.

In recent years, it has become clear that inflammation and chronic regenerative stress signaling are key triggers of melanoma phenotype switching, converging on AP1/ JUN as a central axis promoting dedifferentiation of melanoma cells [201]. A study by Schwitalla and colleagues revealed a direct role of $\text{TNF}\alpha$ mediated $\text{NF}\kappa\text{B}$ activation in intestinal epithelial cells for directed dedifferentiation and tumorigenicity [216]. Wound healing has been assigned the mechanistic counterpart for processes occurring during chronic inflammation in cancer. Indeed, inflammation-induced dedifferentiation repre-

sents a key mechanism for re-establishing tissue integrity after injury and similar growth factors, which we have highlighted for melanoma cell dedifferentiation and induction of melanoma cell phenotype switching in the present study are involved [15]. For example, $\text{TNF}\alpha$ is an important mediator of keratinocyte EMT during the process of wound healing [274]. Keratinocytes of c-Met deficient mice were not able to close skin wounds [41]. Furthermore, key signaling events during keratinocyte EMT and wound healing have been identified to include JUN/ AP1 signaling and the MAPK cascade [196]. Ample literature exist on the influence of metabolic, oxidative and hypoxic stress, as well as inflammation on the induction of EMT in cancer [147, 239]. A plethora of cytokines with EMT inducing properties in carcinoma have been discovered, such as $\text{TNF}\alpha$, $\text{TGF}\beta$, $\text{IL1}\beta$, IL6, IL8, CCL-2/-5/-18/-20/-21, IL23 and IL17 [239]. The modulation of cancer cell states by microenvironmental inflammatory triggers is not a one way route, but rather shaped by reciprocal interactions of cancer cells and cells of the tumor microenvironment. In melanoma we showed that phenotype switching towards an *invasive* cell state is associated with a progressive increase in inflammatory capacity, and inflammatory melanoma cells promote the conversion of an immune response within the tumor towards chronic pro-tumorigenic inflammation. Furthermore, the melanoma inflammatory secretome was revealed to foster an *invasive* cell state in an autocrine manner [256, 272, 231]. In addition, also for CSCs of other cancer entities, the auto-regulation of stemness has been attributed to the inflammatory secretome of tumor cells [250, 87]. With respect to this notion, the induction of CD73 on melanoma cells upon inflammation-induced dedifferentiation might exploit the function of negative feedback regulation towards a pro-tumorigenic regenerative inflammatory environment and thereby might further support *invasive* phenotype switching. Direct impact of CD73 expression on melanoma cells and adenosine signaling on shaping the pro-tumorigenic inflammatory capacity of melanoma cells has to be investigated in future studies.

7.4 Melanoma CD73 expression links to primary and acquired resistance towards cancer immunotherapy

During tumor growth, nutrient deprivation and hypoxia create an environment of chronic inflammation and regenerative mitogenic signaling, which is even enforced under therapy [136, 70, 175, 38]. Hence, the question arises whether melanoma cell CD73 induction in response to therapy-induced stress and inflammation is causally involved in therapy resistance. Pre-clinical mouse models showed non-redundant immunosuppressive mechanisms in the tumor microenvironment playing an important role for primary resistance towards immune checkpoint blockade [174]. To this effect, depletion of tumoral MDSCs or regulatory T cells was shown to improve anti-PD-L1 therapy [102, 261]. Interestingly, gene signatures of chronic inflammation, hypoxia and dedifferentiation

have been associated with a poor response to PD-1 immune checkpoint blockade [113], which might hint to the induction of CD73 in this context and, in the following, its involvement in therapy resistance. Another interesting study reported the recurrence of MDSCs upon acquired resistance to BRAFi, which could not be overcome by CTLA-4 or PD-1 immune checkpoint blockade [236]. With MDSCs expressing CD73 and being a major source of adenosine in the tumor microenvironment, this might hint on a role of CD73-adenosinergic signaling also in this context of resistance to targeted therapy. Pre-clinical studies in a syngeneic transplanted B16F10 melanoma mouse model have demonstrated effective combinatorial treatment by either CTLA-4 or PD-L1 immune checkpoint therapy together with A2A adenosine receptor signaling blockade [163, 114]. PD-1 blockade has been shown to up-regulate A2A adenosine receptors on tumoral CD8 positive T cells. In the presence of CD73 this is limiting effective T cell reactivation, thereby leading to the suggestion of CD73 as a biomarker for impaired responsiveness to PD-1 blockade [18, 19].

An additional implication of adenosine signaling in primary therapy resistance is CD73 immunosuppressive pre-conditioning in conjunction with therapy-induced cell death and obligatory release of excessive ATP. Extracellular ATP is promoting a pro-inflammatory tumor environment and an anti-tumor immune response. On the other hand, high abundance of enzymes breaking down ATP during an initially effective anti-tumor therapy could eventually boost tumor immune escape. In line, regulatory T cells expressing CD39 and CD73 and substantially contributing to purinergic breakdown in the tumor have been shown to provide their own substrate when encountering oxidative stress, undergoing apoptosis and releasing ATP [151].

Direct evidence for acquired resistance of melanoma against immunotherapy due to up-regulation of melanoma cell CD73 expression is still pending. In a mouse model of syngeneic HCMel3 melanoma cell inoculation and PMEL-directed ACT, our lab has previously shown that melanoma initially undergo remission in response to immunotherapy, however they relapse later due to inflammation-induced dedifferentiation [136]. In our recent publication, we examined changes in melanoma phenotypes in this model prior to therapy, early during therapy and during late escape. Indeed, we observed progressive induction of CD73, which was strongly and stably induced upon full dedifferentiation, supporting the *in vivo* relevance of CD73 induction by inflammatory mitogenic stress conditions, and furthermore hinting to an involvement in therapy-induced immune escape [195]. In collaboration with Antony Ribas, we have analyzed expression of CD73 in serial metastatic melanoma biopsies from patients who received an ACT directed against MART-1 together with DC vaccination (NCT00910650). Affirmatively, one patient's metastasis, which lost MART-1 target antigen expression and showed dedifferentiation, revealed emerging CD73 expression under therapy, resulting in high expression upon progression and failure of therapy [195]. A very recent case study published by the group of Antony Ribas on the same patient further substantiated our findings, showing that therapy escape was mediated by inflammation-induced dedifferentiation and can be mimicked by TNF α treatment of patient-derived melanoma cell lines [160]. Future studies will be required to finally decipher the relevance of CD73 up-regulation for

acquired resistance against cancer immunotherapy.

7.5 Prognostic implications of CD73 marker expression on *nascent invasive* melanoma

CD73 was identified as a negative prognostic marker in several types of cancer: In triple-negative breast cancer tumoral CD73 expression correlated with poor prognosis and promoted therapy resistance [144, 29]. In colorectal and ovarian cancer, expression of CD73 was associated with reduced survival [181, 257]. However, the association of melanoma cell CD73 expression and disease progression seems to be less clear.

In our work we found that melanoma cell CD73 expression is highly heterogenous, and regulation of melanoma cell CD73 under anti-PD-1 therapy is highly dynamic, even though we did not observe down-regulation of CD73 in patients after therapy failure [195]. The dynamic regulation of CD73 might reflect its expression in a *nascent invasive* cell state and discloses plastic responses of melanoma during treatment. Interestingly, a soluble enzymatic active form of CD73 (sCD73) can be generated by cleavage from the plasma membrane of predominately lymphocytes and tumor cells under pathologic conditions, making it an interesting potential biomarker for serum diagnostics [4, 130]. Based on this technology, a recent publication provided data in a study cohort of 37 patients suffering from metastatic melanoma, which suggested sCD73 as negative prognostic marker for anti-PD-1 therapy based on decrease of progression free survival from 14.2 to 2.6 months in case sCD73 was detectable in patients' serum prior to therapy [166]. Clearly, data are supporting a role of CD73 expression for acquired therapy resistance, and targeting the CD73-adenosinergic axis has high potential for combinatorial immunotherapies. Still, variable expression of CD73 prior to therapy and dynamic regulation of CD73 under therapy points to a critical assessment of CD73 as a pre-treatment biomarker for therapy success and suggests that combinatorial immunotherapies involving A2A adenosine receptor and CD73 blockade should be considered independently from pre-treatment expression of CD73.

7.6 The relevance of MAPK signaling for CD73 expression on melanoma cells

Another important therapeutically relevant aspect is the MAPK-dependent expression of CD73 in melanoma cells. In the present study we found that CD73-positive melanoma cell lines strongly down-regulate CD73 expression upon interference with MEK/ERK signaling (Figure 6.10). In line, a recent study has provided similar results showing

decreased *NT5E* transcript levels in A375 melanoma cells upon inhibition of MAPK cascade signaling [143].

MAPK dependency of CD73 expression is a favorable point of attack for targeting melanoma cell CD73 expression, as MAPK hyper-activation is a central oncogenic driver of melanoma. BRAFi and MEKi are already successfully used to limit melanoma growth and improve patient outcome [5, 132]. Indeed, in a combined effort together with the group of Mark Smyth, we were able to show that patients with BRAF mutations show decreased expression of CD73 in all cases upon BRAFi and in more than half of all cases upon combinatorial treatment with BRAFi and MEKi [277]. Moreover, re-expression or increase of CD73 expression post BRAFi correlated with rapid disease progression [277].

MAPK blockade has various immune activating activities in melanoma [62, 111, 143, 31]. Showing that MAPKi blocks tumoral CD73 expression and thereby limits adenosine generation by tumor cells provides further insights on how targeted therapy may strengthen anti-tumor immune responses. Combinatorial treatment of CD73 inhibition and A2A adenosine receptor blockade has shown promising results in preclinical trials superior to mono-therapy [276], and it implies potential benefits for combined MAPK blockade together with A2A adenosine receptor inhibition. According to our findings, one might assume synergistic anti-cancer immunity from the increase of tumor immunogenicity by the direct effects of MAPKi, together with dual resolution of the CD73-adenosinergic immunosuppressive axis by decreasing the source of adenosine due to MAPK-dependent down-regulation of CD73, while in parallel inhibiting adenosine receptor signaling. Intriguingly, our studies indeed provided insights into a significantly improved treatment outcome achieved by MAPKi together with A2A adenosine receptor blockade in relation to the respective mono-therapies [277].

Hyper-activation of the MAPK signaling cascade in melanoma is known to have an important role for melanoma *invasive* phenotype switching [33]. Given that melanoma cell CD73 expression upon *nascent invasive* cell state is driven by MAPK signaling, the question arises whether positive MAPK driver mutation status correlates with CD73 expression on melanoma cells. In our collaborative study we only found a non-significant trend of positive BRAF mutation status being associated with high CD73 expression [277]. Our finding of epigenetic silencing leading to absence of CD73 expression in BRAF mutant melanoma cell lines (Figure 6.5, A), which can be resolved upon global demethylation (Figure 6.7), provides a plausible explanation for the missing link between positive MAPK mutation status and CD73 expression in melanoma. In contrast to melanoma, a previous publication supports this concept in other tumor types: Nevedomskaya and coworkers analyzed BRAF and NRAS mutation status as well as expression of CD73 in the NC-60 cell line panel, revealing a significant correlation across all cancer entities tested [168]. Along these lines, rare BRAF-mutant serous ovarian carcinomas were found to express elevated levels of CD73 in comparison to BRAF-WT tumors [273].

7.7 Conclusion

Stress signaling and inflammation guides melanoma phenotype switching in a reciprocal interplay of tumor cells and microenvironmental co-actors. This has detrimental consequences for the treatment of cancer. Efficient treatment schemes have to be specified to target tumor cells in their environment rather than establishing therapies that concentrate on interference with tumor cell specific signaling mechanisms. The failure of MAPK targeted therapies to achieve long term benefits for patients is one example.

In this work, we provide novel link of melanoma phenotype switching in a regenerative inflammatory environment to the upregulation of a key immunosuppressive molecular switch: The 5'ectonucleotidase CD73. Transient mitogenic and inflammatory stimulation converges on JUN/ AP1 central stress signaling nodes to induce *nascent invasive* phenotype switching, marked by the expression of CD73. Continuous stress signaling results in full *invasive* phenotype switching and the expression of classical *invasive* markers along with high levels of CD73 (summarized in Figure 7.3). Importantly, the identification of an intermediate cell state beyond the current classification of opposing *invasive* and *proliferative* cell states will allow a more detailed understanding of cell state transitions in the future. For epithelial cancer, the importance of transitory, partial EMT cell states for the development of therapy resistance and metastatic progression is beginning to be understood. Most likely transitory phenotypes play an even more important role in highly plastic neural crest-derived cancers. Moreover, the up-regulation of CD73 in that context uncloses insights on how phenotype switching and tumor immune evasion are orchestrated in an interplay of tumor cell - immune cell - microenvironment interactions. Finding *invasive* phenotype switching coupled to MAPK-dependent regulation of an upcoming target for cancer immunotherapy fosters approaches of combinatorial therapy targeting the CD73-adenosinergic axis in combination with immune checkpoint blockade. The fact that sCD73 can be measured by serum diagnostic in patients even holds potential for staging patients' responses to immunotherapies.

Still open questions remaining comprise whether there is a functional relevance of CD73 for melanoma cell phenotype switching and, more importantly, whether CD73 up-regulation by inflammation and constitutive stress signaling during therapy contributes to acquired therapy resistance.

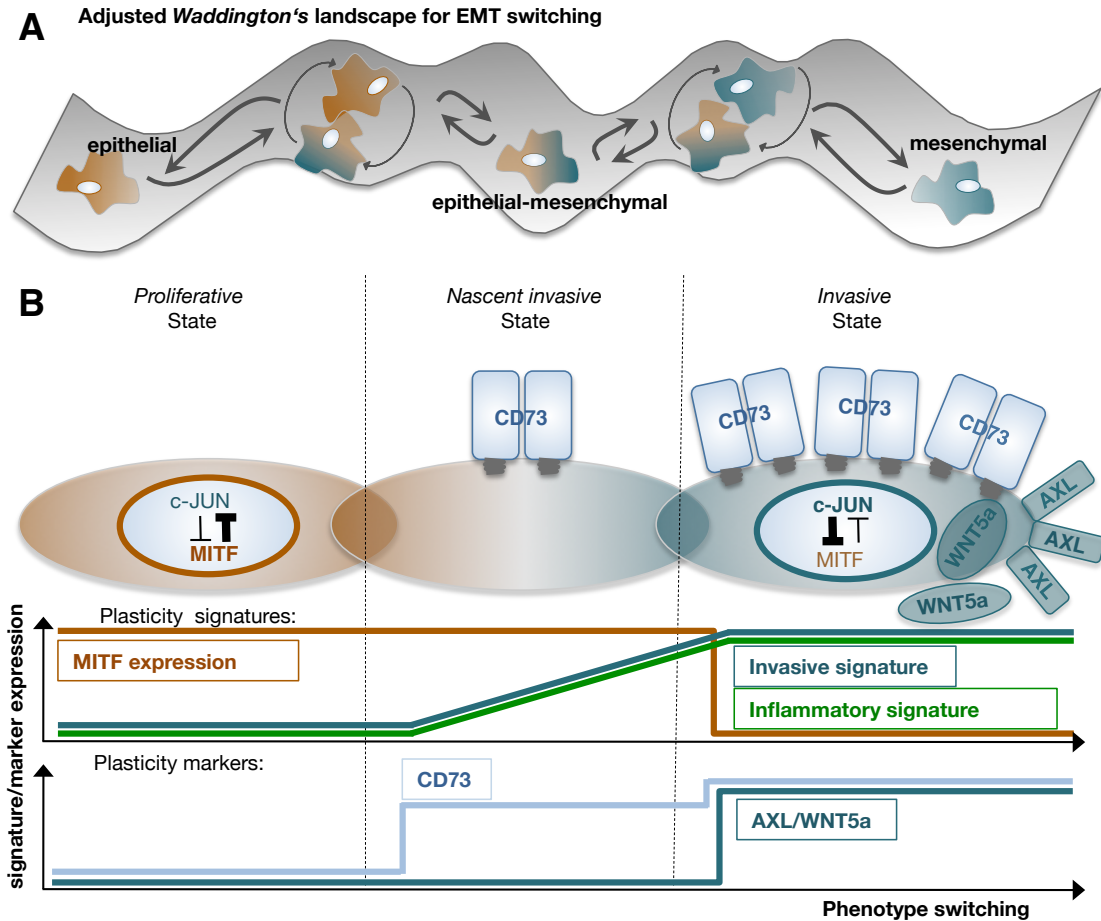


Figure 7.3: **A model of *Nascent invasive* phenotype switching in melanoma in comparison to the *Waddington's landscape* of partial EMT.** (A): Model of a *Waddington's landscape* for melanoma phenotype switching in the style of partial EMT of epithelial cancer. Stable phenotypes reside within valleys of a certain gene expression signature, interjacent hills represent the threshold that has to be overcome for phenotype switching, a process that is governed by environmental stress signals. Stable and metastable interstates are highlighted during the transition process. (B): Schematic representation on melanoma phenotype switching with implementation of the *nascent invasive* cell state marked by the expression of CD73, modified from Reinhardt *et al* [195].

Abbreviations

Prefixes

<i>p</i>	pico (10^{-12})
<i>n</i>	nano (10^{-9})
μ	micro (10^{-6})
<i>m</i>	milli (10^{-3})
<i>c</i>	centi (10^{-2})
<i>k</i>	kilo (10^3)

Units

A	ampere
Da	dalton
g	gram
h	hour
l	liter
m	meter
M	mol/l
min	minute
OD	optical density
s	second
U	unit
v/v	volume per volume
w/v	weight per volume
°C	degree celisius

Chemicals and solutions

APS	ammonium persulfate
DPBS	Dulbecco's phosphate-buffered saline
DMEM	Dulbecco's Modified Eagle's Medium
DMSO	dimethyl sulfoxide
DTT	dithiothreitol
EDTA	ethylenediaminetetraacetic acid
EtBr	ethidium bromide
LB	lysogeny broth

PMA	phorbol 12-myristate 13-acetate
SDS	sodium dodecyl sulfate
TEMED	tetramethylethylenediamine

Proteins, biomolecules and cell types

AMP	adenosine monophosphate
APC	antigen presenting cell
AP-1	activator protein-1
ATP	adenosine triphosphate
BSA	bovine serum albumin
Cas9	CRISPR-associated protein 9
C	cytosine
CAF	cancer-associated fibroblast
CSC	cancer stem cell
CTLA-4	cytotoxic T-lymphocyte-associated protein 4
DC	dendritic cell
ECM	extracellular matrix
EDN3	endothelin-3
ERK	extracellular signal?regulated kinase
<i>Escherichia coli</i>	<i>e. coli</i>
dNTP	desoxynucleoside triphosphate
FAK	focal adhesion kinase
FBS	fetal bovine serum
FGF	fibroblast growth factor
GFP	green fluorescence protein
GPCR	G protein coupled receptor
HEK	human embryonic kidney
HGF	hepatocyte growth factor
IFN	interferon
IL	interleukin
LPS	lipopolysaccharide
MAPK	mitogen-activated protein kinase
MEK	MAPK/ERK kinase
MDSC	myeloid derived suppressor cell
MITF	microphthalmia-associated transcription factor
mRNA	messenger RNA
NF- κ B	nuclear factor-kappa B
NGFR	nerve growth factor receptor
PBMC	peripheral blood mononuclear cell
PI3K	phosphatidylinositol-3-kinases
PD-1	programmed cell death protein 1
PD-L1	programmed cell death protein 1 ligand 1
RB	retinoblastoma protein

RNA	ribonucleic acid
RTK	receptor tyrosine kinase
sCD73	soluble CD73
TNF	tumor necrosis factor
TGF	transforming growth factor
VEGF	vascular endothelial growth factor
WNT	wingless Int 1

Other Abbreviations

ACT	adoptive T cell transfer
AP1	activator protein 1
bHLH	basic helix-loop-helix
BS	bottom strand
bp	base pair
BRAF	rapidly accelerated fibrosarcoma protein kinase B
BRAFi	BRAF inhibition
CAR	chimeric antigen receptor
CD	cluster of differentiation
ChIP	chromatin immunoprecipitation
ChIPseq	chromatin immunoprecipitation sequencing
CPD	cyclobutane pyrimidine dimer
CRISPR	clustered regularly interspaced short palindromic repeats
DNA	deoxyribonucleic acid
DOX	doxycycline
ECL	enhanced chemoluminescence
EMT	epithelial-mesenchymal transition
ERKi	ERK inhibition
FACS	fluorescence-activated cell sorting
FDR	false discovery rate
fwd	forward
gDNA	genomic DNA
GEO	gene expression omnibus
GSEA	gene set enrichment analysis
InDel	insertion and deletion
KO	knockout
MAPK	mitogen-activated protein kinases
MAPKi	MAPK inhibition
MEKi	MEK inhibition
MET	mesenchymal-epithelial transition
MFI	mean fluorescence intensity
MITF	microphthalmia-associated transcription factor
movAVG	moving average algorithm
MSigDB	Molecular Signature Database

NES	normalized enrichment score
NGS	next generation sequencing
NHEJ	non-homologous end joining
O/N	over night: 16-20 h
ORF	open reading frame
PAGE	polyacrylamide gelelectrophoresis
PAM	protospacer adjacent motif
PCR	polymerase chain reaction
PI3Ki	PI3K inhibition
qPCR	quantitative real-time PCR
PFA	paraformaldehyde
rev	reverse
RGF	radial growth phase
RNAseq	RNA sequencing
ROS	reactive oxygen species
RT	room temperature
rpm	rounds per minute
S1	security level 1
scRNA-seq	single cell RNA sequencing
sgRNA	single guide RNA molecule
SN	supernatant
T	thymidine
TF	transcription factor
TS	top strand
UV	ultraviolet
VGF	vertical growth phase
WT	wild type

Bibliography

- [1] J. Agudo, E. S. Park, S. A. Rose, E. Alibo, R. Sweeney, M. Dhainaut, K. S. Kobayashi, R. Sachidanandam, A. Baccarini, M. Merad, et al. Quiescent tissue stem cells evade immune surveillance. *Immunity*, 48(2):271–285, 2018.
- [2] F. Ahmed and N. K. Haass. Microenvironment-driven dynamic heterogeneity and phenotypic plasticity as a mechanism of melanoma therapy resistance. *Frontiers in oncology*, 8, 2018.
- [3] S. Aibar, C. B. González-Blas, T. Moerman, H. Imrichova, G. Hulselmans, F. Rambow, J.-C. Marine, P. Geurts, J. Aerts, J. van den Oord, et al. Scenic: single-cell regulatory network inference and clustering. *Nature methods*, 14(11):1083, 2017.
- [4] L. Airas, J. Niemelä, M. Salmi, T. Puurunen, D. J. Smith, and S. Jalkanen. Differential regulation and function of cd73, a glycosyl-phosphatidylinositol–linked 70-kd adhesion molecule, on lymphocytes and endothelial cells. *The Journal of cell biology*, 136(2):421–431, 1997.
- [5] R. Akbani, K. C. Akdemir, B. A. Aksoy, M. Albert, A. Ally, S. B. Amin, H. Arachchi, A. Arora, J. T. Auman, B. Ayala, et al. Genomic classification of cutaneous melanoma. *Cell*, 161(7):1681–1696, 2015.
- [6] L. B. Alexandrov, S. Nik-Zainal, D. C. Wedge, S. A. Aparicio, S. Behjati, A. V. Biankin, G. R. Bignell, N. Bolli, A. Borg, A.-L. Børresen-Dale, et al. Signatures of mutational processes in human cancer. *Nature*, 500(7463):415, 2013.
- [7] B. Allard, M. S. Longhi, S. C. Robson, and J. Stagg. The ectonucleotidases cd39 and cd73: novel checkpoint inhibitor targets. *Immunological reviews*, 276(1):121–144, 2017.
- [8] D. Allard, M. Turcotte, and J. Stagg. Targeting a2 adenosine receptors in cancer. *Immunology & Cell Biology*, 95(4):333–339, 2017.
- [9] L. Antonioli, C. Blandizzi, P. Pacher, and G. Haskó. Immunity, inflammation and cancer: a leading role for adenosine. *Nature Reviews Cancer*, 13(12):842, 2013.
- [10] L. Antonioli, S. V. Novitskiy, K. F. Sachsenmeier, M. Fornai, C. Blandizzi, and G. Haskó. Switching off cd73: a way to boost the activity of conventional and targeted antineoplastic therapies. *Drug discovery today*, 22(11):1686–1696, 2017.

- [11] L. Antonioli, G. G. Yegutkin, P. Pacher, C. Blandizzi, and G. Haskó. Anti-cd73 in cancer immunotherapy: awakening new opportunities. *Trends in cancer*, 2(2):95–109, 2016.
- [12] M. B. Atkins, M. T. Lotze, J. P. Dutcher, R. I. Fisher, G. Weiss, K. Margolin, J. Abrams, M. Sznol, D. Parkinson, M. Hawkins, et al. High-dose recombinant interleukin 2 therapy for patients with metastatic melanoma: analysis of 270 patients treated between 1985 and 1993. *Journal of clinical oncology*, 17(7):2105–2105, 1999.
- [13] T. Bald, T. Quast, J. Landsberg, M. Rogava, N. Glodde, D. Lopez-Ramos, J. Kohlmeyer, S. Riesenberger, D. Van Den Boorn-Konijnenberg, C. Hömig-Hölzel, et al. Ultraviolet-radiation-induced inflammation promotes angiotropism and metastasis in melanoma. *Nature*, 507(7490):109, 2014.
- [14] S. S. Banerjee and M. Harris. Morphological and immunophenotypic variations in malignant melanoma. *Histopathology*, 36(5):387–402, 2000.
- [15] S. Barrientos, O. Stojadinovic, M. S. Golinko, H. Brem, and M. Tomic-Canic. Growth factors and cytokines in wound healing. *Wound repair and regeneration*, 16(5):585–601, 2008.
- [16] B. C. Bastian. The molecular pathology of melanoma: an integrated taxonomy of melanocytic neoplasia. *Annual Review of Pathology: Mechanisms of Disease*, 9:239–271, 2014.
- [17] S. H. Baumeister, G. J. Freeman, G. Dranoff, and A. H. Sharpe. Coinhibitory pathways in immunotherapy for cancer. *Annual review of immunology*, 34:539–573, 2016.
- [18] P. A. Beavis, N. Milenkovski, M. A. Henderson, L. B. John, B. Allard, S. Loi, M. H. Kershaw, J. Stagg, and P. K. Darcy. Adenosine receptor 2a blockade increases the efficacy of anti-pd-1 through enhanced antitumor t-cell responses. *Cancer immunology research*, 3(5):506–517, 2015.
- [19] P. A. Beavis, C. Y. Slaney, N. Milenkovski, M. A. Henderson, S. Loi, J. Stagg, M. H. Kershaw, and P. K. Darcy. Cd73: A potential biomarker for anti-pd-1 therapy. *Oncoimmunology*, 4(11):e1046675, 2015.
- [20] I. Ben-Porath and R. A. Weinberg. The signals and pathways activating cellular senescence. *The international journal of biochemistry & cell biology*, 37(5):961–976, 2005.
- [21] J. C. Bendell, T. W. Kim, B. C. Goh, J. Wallin, D.-Y. Oh, S.-W. Han, C. B. Lee, M. D. Hellmann, J. Desai, J. H. Lewin, et al. Clinical activity and safety of cobimetinib (cobi) and atezolizumab in colorectal cancer (crc)., 2016.

- [22] G. Bergers, P. Graninger, S. Braselmann, C. Wrighton, and M. Busslinger. Transcriptional activation of the fra-1 gene by ap-1 is mediated by regulatory sequences in the first intron. *Molecular and cellular biology*, 15(7):3748–3758, 1995.
- [23] A. Bianchi-Smiraglia, A. Bagati, E. E. Fink, S. Moparthy, J. A. Wawrzyniak, E. K. Marvin, S. Battaglia, P. Jowdy, M. Kolesnikova, C. E. Foley, et al. Microphthalmia-associated transcription factor suppresses invasion by reducing intracellular gtp pools. *Oncogene*, 36(1):84, 2017.
- [24] M. Bittner, P. Meltzer, Y. Chen, Y. Jiang, E. Seftor, M. Hendrix, M. Radmacher, R. Simon, Z. Yakhini, A. Ben-Dor, et al. Molecular classification of cutaneous malignant melanoma by gene expression profiling. *Nature*, 406(6795):536, 2000.
- [25] A. D. Boiko, O. V. Razorenova, M. van de Rijn, S. M. Swetter, D. L. Johnson, D. P. Ly, P. D. Butler, G. P. Yang, B. Joshua, M. J. Kaplan, et al. Human melanoma-initiating cells express neural crest nerve growth factor receptor cd271. *Nature*, 466(7302):133, 2010.
- [26] A. Boni, A. P. Cogdill, P. Dang, D. Udayakumar, C.-N. J. Njauw, C. M. Sloss, C. R. Ferrone, K. T. Flaherty, D. P. Lawrence, D. E. Fisher, et al. Selective brafv600e inhibition enhances t-cell recognition of melanoma without affecting lymphocyte function. *Cancer research*, 70(13):5213–5219, 2010.
- [27] J. B. Boonyaratanakornkit, L. Yue, L. R. Strachan, K. J. Scalapino, P. E. LeBoit, Y. Lu, S. P. Leong, J. E. Smith, and R. Ghadially. Selection of tumorigenic melanoma cells using aldh. *Journal of Investigative Dermatology*, 130(12):2799–2808, 2010.
- [28] A. Breslow. Thickness, cross-sectional areas and depth of invasion in the prognosis of cutaneous melanoma. *Annals of surgery*, 172(5):902, 1970.
- [29] L. Buisseret, S. Pommey, B. Allard, S. Garaud, M. Bergeron, I. Cousineau, L. Ameye, Y. Bareche, M. Paesmans, J. Crown, et al. Clinical significance of cd73 in triple-negative breast cancer: multiplex analysis of a phase iii clinical trial. *Annals of Oncology*, 2017.
- [30] M. Burnet. Cancer—a biological approach: I. the processes of control. ii. the significance of somatic mutation. *British medical journal*, 1(5022):779, 1957.
- [31] M. K. Callahan, G. Masters, C. A. Pratilas, C. Ariyan, J. Katz, S. Kitano, V. Russell, R. A. Gordon, S. Vyas, J. Yuan, et al. Paradoxical activation of t cells via augmented erk signaling mediated by a raf inhibitor. *Cancer immunology research*, 2(1):70–79, 2014.
- [32] R. Calloni, E. A. A. Cordero, J. A. P. Henriques, and D. Bonatto. Reviewing and updating the major molecular markers for stem cells. *Stem cells and development*, 22(9):1455–1476, 2013.

- [33] J. Caramel, E. Papadogeorgakis, L. Hill, G. J. Browne, G. Richard, A. Wierinckx, G. Saldanha, J. Osborne, P. Hutchinson, G. Tse, et al. A switch in the expression of embryonic emt-inducers drives the development of malignant melanoma. *Cancer cell*, 24(4):466–480, 2013.
- [34] S. Carreira, J. Goodall, L. Denat, M. Rodriguez, P. Nuciforo, K. S. Hoek, A. Testori, L. Larue, and C. R. Goding. Mitf regulation of dia1 controls melanoma proliferation and invasiveness. *Genes & development*, 20(24):3426–3439, 2006.
- [35] R. D. Carvajal, C. R. Antonescu, J. D. Wolchok, P. B. Chapman, R.-A. Roman, J. Teitcher, K. S. Panageas, K. J. Busam, B. Chmielowski, J. Lutzky, et al. Kit as a therapeutic target in metastatic melanoma. *Jama*, 305(22):2327–2334, 2011.
- [36] L. Casalino, D. De Cesare, and P. Verde. Accumulation of fra-1 in ras-transformed cells depends on both transcriptional autoregulation and mek-dependent post-translational stabilization. *Molecular and cellular biology*, 23(12):4401–4415, 2003.
- [37] P. B. Chapman, A. Hauschild, C. Robert, J. B. Haanen, P. Ascierto, J. Larkin, R. Dummer, C. Garbe, A. Testori, M. Maio, et al. Improved survival with vemurafenib in melanoma with braf v600e mutation. *New England Journal of Medicine*, 364(26):2507–2516, 2011.
- [38] Y. Cheli, S. Giuliano, N. Fenouille, M. Allegra, V. Hofman, P. Hofman, P. Bahadoran, J. Lacour, S. Tartare-Deckert, C. Bertolotto, et al. Hypoxia and mitf control metastatic behaviour in mouse and human melanoma cells. *Oncogene*, 31(19):2461, 2012.
- [39] Y. Cheli, S. Guiliano, T. Botton, S. Rocchi, V. Hofman, P. Hofman, P. Bahadoran, C. Bertolotto, and R. Ballotti. Mitf is the key molecular switch between mouse or human melanoma initiating cells and their differentiated progeny. *Oncogene*, 30(20):2307, 2011.
- [40] L. Chin. The genetics of malignant melanoma: lessons from mouse and man. *Nature Reviews Cancer*, 3(8):559, 2003.
- [41] J. Chmielowiec, M. Borowiak, M. Morkel, T. Stradal, B. Munz, S. Werner, J. Wehland, C. Birchmeier, and W. Birchmeier. c-met is essential for wound healing in the skin. *The Journal of cell biology*, 177(1):151–162, 2007.
- [42] M. K. Chuk, J. T. Chang, M. R. Theoret, E. Sampene, K. He, S. L. Weis, W. S. Helms, R. Jin, H. Li, J. Yu, et al. Fda approval summary: accelerated approval of pembrolizumab for second-line treatment of metastatic melanoma. *Clinical Cancer Research*, 23(19):5666–5670, 2017.
- [43] W. H. Clark, D. E. Elder, and M. Van Horn. The biologic forms of malignant melanoma. *Human pathology*, 17(5):443–450, 1986.

- [44] S. P. Colgan, H. K. Eltzschig, T. Eckle, and L. F. Thompson. Physiological roles for ecto-5'-nucleotidase (cd73). *Purinergic signalling*, 2(2):351, 2006.
- [45] L. Cong, F. A. Ran, D. Cox, S. Lin, R. Barretto, N. Habib, P. D. Hsu, X. Wu, W. Jiang, L. Marraffini, et al. Multiplex genome engineering using crispr/cas systems. *Science*, page 1231143, 2013.
- [46] C. Coste, V. Neirinckx, A. Sharma, G. Agirman, B. Rogister, J. Foguene, F. Lallemand, A. Gothot, and S. Wislet. Human bone marrow harbors cells with neural crest-associated characteristics like human adipose and dermis tissues. *PloS one*, 12(7):e0177962, 2017.
- [47] L. M. Coussens and Z. Werb. Inflammation and cancer. *Nature*, 420(6917):860, 2002.
- [48] B. Csóka, Z. Selmeczy, B. Koscsó, Z. H. Németh, P. Pacher, P. J. Murray, D. Kepka-Lenhart, S. M. Morris, W. C. Gause, S. J. Leibovich, et al. Adenosine promotes alternative macrophage activation via a2a and a2b receptors. *The FASEB Journal*, 26(1):376–386, 2012.
- [49] C. L. Curchoe, J. Maurer, S. J. McKeown, G. Cattarossi, F. Cimadamore, M. Nilbratt, E. Y. Snyder, M. Bronner-Fraser, and A. V. Terskikh. Early acquisition of neural crest competence during hescs neuralization. *PloS one*, 5(11):e13890, 2010.
- [50] H. Davies, G. R. Bignell, C. Cox, P. Stephens, S. Edkins, S. Clegg, J. Teague, H. Woffendin, M. J. Garnett, W. Bottomley, et al. Mutations of the braf gene in human cancer. *Nature*, 417(6892):949, 2002.
- [51] A. Delmas, J. Cherier, M. Pohorecka, C. Medale-Giamarchi, N. Meyer, A. Casanova, O. Sordet, L. Lamant, A. Savina, A. Pradines, et al. The c-jun/rhob/akt pathway confers resistance of braf-mutant melanoma cells to mapk inhibitors. *Oncotarget*, 6(17):15250, 2015.
- [52] V. Delmas, F. Beermann, S. Martinozzi, S. Carreira, J. Ackermann, M. Kumasaka, L. Denat, J. Goodall, F. Luciani, A. Viros, et al. β -catenin induces immortalization of melanocytes by suppressing p16ink4a expression and cooperates with n-ras in melanoma development. *Genes & development*, 21(22):2923–2935, 2007.
- [53] G. Denecker, N. Vandamme, Ö. Akay, D. Koludrovic, J. Taminau, K. Lemeire, A. Gheldof, B. De Craene, M. Van Gele, L. Brochez, et al. Identification of a zeb2-mitf-zeb1 transcriptional network that controls melanogenesis and melanoma progression. *Cell death and differentiation*, 21(8):1250, 2014.
- [54] N. Dhomen, J. S. Reis-Filho, S. da Rocha Dias, R. Hayward, K. Savage, V. Delmas, L. Larue, C. Pritchard, and R. Marais. Oncogenic braf induces melanocyte senescence and melanoma in mice. *Cancer cell*, 15(4):294–303, 2009.

- [55] X. Ding, H. Pan, J. Li, Q. Zhong, X. Chen, S. M. Dry, and C.-Y. Wang. Epigenetic activation of ap1 promotes squamous cell carcinoma metastasis. *Sci. Signal.*, 6(273):ra28–ra28, 2013.
- [56] S. K. Dissanayake, P. B. Olkhanud, M. P. O’Connell, A. Carter, A. D. French, T. C. Camilli, C. D. Emeche, K. J. Hewitt, D. T. Rosenthal, P. D. Leotlela, et al. Wnt5a regulates expression of tumor-associated antigens in melanoma via changes in signal transducers and activators of transcription 3 phosphorylation. *Cancer research*, 68(24):10205–10214, 2008.
- [57] S. K. Dissanayake, M. Wade, C. E. Johnson, M. P. O’Connell, P. D. Leotlela, A. D. French, K. V. Shah, K. J. Hewitt, D. T. Rosenthal, F. E. Indig, et al. The wnt5a/protein kinase c pathway mediates motility in melanoma cells via the inhibition of metastasis suppressors and initiation of an epithelial to mesenchymal transition. *Journal of Biological Chemistry*, 282(23):17259–17271, 2007.
- [58] M. Dominici, K. Le Blanc, I. Mueller, I. Slaper-Cortenbach, F. Marini, D. Krause, R. Deans, A. Keating, D. Prockop, and E. Horwitz. Minimal criteria for defining multipotent mesenchymal stromal cells. the international society for cellular therapy position statement. *Cytotherapy*, 8(4):315–317, 2006.
- [59] G. P. Dunn, A. T. Bruce, H. Ikeda, L. J. Old, and R. D. Schreiber. Cancer immunoediting: from immunosurveillance to tumor escape. *Nature immunology*, 3(11):991, 2002.
- [60] G. P. Dunn, L. J. Old, and R. D. Schreiber. The three es of cancer immunoediting. *Annu. Rev. Immunol.*, 22:329–360, 2004.
- [61] M. M. D’Aloia, I. G. Zizzari, B. Sacchetti, L. Pierelli, and M. Alimandi. Car-t cells: the long and winding road to solid tumors. *Cell death & disease*, 9(3):282, 2018.
- [62] P. J. Ebert, J. Cheung, Y. Yang, E. McNamara, R. Hong, M. Moskalenko, S. E. Gould, H. Maecker, B. A. Irving, J. M. Kim, et al. Map kinase inhibition promotes t cell and anti-tumor activity in combination with pd-l1 checkpoint blockade. *Immunity*, 44(3):609–621, 2016.
- [63] R. Edwards, M. Ward, H. Wu, C. Medina, M. Brose, P. Volpe, S. Nussen-Lee, H. Haupt, A. Martin, M. Herlyn, et al. Absence of braf mutations in uv-protected mucosal melanomas. *Journal of medical genetics*, 41(4):270–272, 2004.
- [64] R. Eferl and E. F. Wagner. Ap-1: a double-edged sword in tumorigenesis. *Nature Reviews Cancer*, 3(11):859, 2003.
- [65] P. Ehrlich and F. Himmelweit. *Immunology and cancer research*. Pergamon Press, 1957.

- [66] M. Ennen, C. Keime, G. Gambi, A. Kieny, S. Coassolo, C. Thibault-Carpentier, F. Margerin-Schaller, G. Davidson, C. Vagne, D. Lipsker, et al. Mitf-high and mitf-low cells and a novel subpopulation expressing genes of both cell states contribute to intra-and intertumoral heterogeneity of primary melanoma. *Clinical Cancer Research*, 23(22):7097–7107, 2017.
- [67] F. Erdmann, J. Lortet-Tieulent, J. Schüz, H. Zeeb, R. Greinert, E. W. Breitbart, and F. Bray. International trends in the incidence of malignant melanoma 1953–2008—are recent generations at higher or lower risk? *International journal of cancer*, 132(2):385–400, 2013.
- [68] M. Fallahi-Sichani, V. Becker, B. Izar, G. J. Baker, J.-R. Lin, S. A. Boswell, P. Shah, A. Rotem, L. A. Garraway, and P. K. Sorger. Adaptive resistance of melanoma cells to raf inhibition via reversible induction of a slowly dividing de-differentiated state. *Molecular systems biology*, 13(1):905, 2017.
- [69] M. Fallahi-Sichani, N. J. Moerke, M. Niepel, T. Zhang, N. S. Gray, and P. K. Sorger. Systematic analysis of brafv600e melanomas reveals a role for jnk/c-jun pathway in adaptive resistance to drug-induced apoptosis. *Molecular Systems Biology*, 11(3):797, 2015.
- [70] P. Falletta, L. Sanchez-del Campo, J. Chauhan, M. Efferm, A. Kenyon, C. J. Kershaw, R. Siddaway, R. Lisle, R. Freter, M. J. Daniels, et al. Translation reprogramming is an evolutionarily conserved driver of phenotypic plasticity and therapeutic resistance in melanoma. *Genes & development*, 31(1):18–33, 2017.
- [71] D. Fang, T. K. Nguyen, K. Leishear, R. Finko, A. N. Kulp, S. Hotz, P. A. Van Belle, X. Xu, D. E. Elder, and M. Herlyn. A tumorigenic subpopulation with stem cell properties in melanomas. *Cancer research*, 65(20):9328–9337, 2005.
- [72] L. A. Fecher, R. K. Amaravadi, and K. T. Flaherty. The mapk pathway in melanoma. *Current opinion in oncology*, 20(2):183–189, 2008.
- [73] I. V. Fedorenko, E. V. Abel, J. M. Koomen, B. Fang, E. R. Wood, Y. A. Chen, K. J. Fisher, S. Iyengar, K. B. Dahlman, J. A. Wargo, et al. Fibronectin induction abrogates the braf inhibitor response of braf v600e/pten-null melanoma cells. *Oncogene*, 35(10):1225, 2016.
- [74] E. Feige, S. Yokoyama, C. Levy, M. Khaled, V. Igras, R. J. Lin, S. Lee, H. R. Widlund, S. R. Granter, A. L. Kung, et al. Hypoxia-induced transcriptional repression of the melanoma-associated oncogene mitf. *Proceedings of the National Academy of Sciences*, 108(43):E924–E933, 2011.
- [75] I. J. Fidler. Tumor heterogeneity and the biology of cancer invasion and metastasis. *Cancer research*, 38(9):2651–2660, 1978.
- [76] B. T. Fife and J. A. Bluestone. Control of peripheral t-cell tolerance and autoimmunity via the ctla-4 and pd-1 pathways. *Immunological reviews*, 224(1):166–182, 2008.

- [77] K. T. Flaherty, J. R. Infante, A. Daud, R. Gonzalez, R. F. Kefford, J. Sosman, O. Hamid, L. Schuchter, J. Cebon, N. Ibrahim, et al. Combined braf and mek inhibition in melanoma with braf v600 mutations. *New England Journal of Medicine*, 367(18):1694–1703, 2012.
- [78] K. T. Flaherty, C. Robert, P. Hersey, P. Nathan, C. Garbe, M. Milhem, L. V. Demidov, J. C. Hassel, P. Rutkowski, P. Mohr, et al. Improved survival with mek inhibition in braf-mutated melanoma. *New England Journal of Medicine*, 367(2):107–114, 2012.
- [79] W. A. Flavahan, E. Gaskell, and B. E. Bernstein. Epigenetic plasticity and the hallmarks of cancer. *Science*, 357(6348):eaal2380, 2017.
- [80] Y. Fu, J. D. Sander, D. Reyon, V. M. Cascio, and J. K. Joung. Improving crispr-cas nuclease specificity using truncated guide rnas. *Nature biotechnology*, 32(3):279, 2014.
- [81] S. Y. Fuchs, L. Dolan, R. J. Davis, and Z. Ronai. Phosphorylation-dependent targeting of c-jun ubiquitination by jun n-kinase. *Oncogene*, 13(7):1531–1535, 1996.
- [82] S. Gandini, F. Sera, M. S. Cattaruzza, P. Pasquini, R. Zanetti, C. Masini, P. Boyle, and C. F. Melchi. Meta-analysis of risk factors for cutaneous melanoma: lii. family history, actinic damage and phenotypic factors. *European journal of cancer*, 41(14):2040–2059, 2005.
- [83] C. Garbe, T. K. Eigentler, U. Keilholz, A. Hauschild, and J. M. Kirkwood. Systematic review of medical treatment in melanoma: current status and future prospects. *The oncologist*, 16(1):5–24, 2011.
- [84] C. Garbe, S. Krüger, C. E. Orfanos, P. Büttner, J. Weiß, H. P. Soyer, U. Stocker, M. Roser, J. Weckbecker, R. Panizzon, et al. Associated factors in the prevalence of more than 50 common melanocytic nevi, atypical melanocytic nevi, and actinic lentiginos: multicenter case-control study of the central malignant melanoma registry of the german dermatological society. *Journal of investigative dermatology*, 102(5):700–705, 1994.
- [85] C. Garbe and U. Leiter. Melanoma epidemiology and trends. *Clinics in dermatology*, 27(1):3–9, 2009.
- [86] L. A. Garraway, H. R. Widlund, M. A. Rubin, G. Getz, A. J. Berger, S. Ramaswamy, R. Beroukhi, D. A. Milner, S. R. Granter, J. Du, et al. Integrative genomic analyses identify mitf as a lineage survival oncogene amplified in malignant melanoma. *Nature*, 436(7047):117, 2005.
- [87] M. Gatti, A. Pattarozzi, A. Bajetto, R. Würth, A. Daga, P. Fiaschi, G. Zona, T. Florio, and F. Barbieri. Inhibition of cxcl12/cxcr4 autocrine/paracrine loop reduces viability of human glioblastoma stem-like cells affecting self-renewal activity. *Toxicology*, 314(2-3):209–220, 2013.

- [88] T. Gerber, E. Willscher, H. Loeffler-Wirth, L. Hopp, D. Schadendorf, M. Scharl, U. Anderegg, G. Camp, B. Treutlein, H. Binder, et al. Mapping heterogeneity in patient-derived melanoma cultures by single-cell rna-seq. *Oncotarget*, 8(1):846, 2017.
- [89] M. Gerlinger, A. J. Rowan, S. Horswell, J. Larkin, D. Endesfelder, E. Gronroos, P. Martinez, N. Matthews, A. Stewart, P. Tarpey, et al. Intratumor heterogeneity and branched evolution revealed by multiregion sequencing. *New England journal of medicine*, 366(10):883–892, 2012.
- [90] T. Golan, A. R. Messer, A. Amitai-Lange, Z. Melamed, R. Ohana, R. E. Bell, O. Kapitansky, G. Lerman, S. Greenberger, M. Khaled, et al. Interactions of melanoma cells with distal keratinocytes trigger metastasis via notch signaling inhibition of mitf. *Molecular cell*, 59(4):664–676, 2015.
- [91] J. Goodall, S. Carreira, L. Denat, D. Kobi, I. Davidson, P. Nuciforo, R. A. Sturm, L. Larue, and C. R. Goding. Brn-2 represses microphthalmia-associated transcription factor expression and marks a distinct subpopulation of microphthalmia-associated transcription factor-negative melanoma cells. *Cancer research*, 68(19):7788–7794, 2008.
- [92] J. G. Greger, S. D. Eastman, V. Zhang, M. R. Bleam, A. M. Hughes, K. N. Smitheman, S. H. Dickerson, S. G. Laquerre, L. Liu, and T. M. Gilmer. Combinations of braf, mek, and pi3k/mtor inhibitors overcome acquired resistance to the braf inhibitor gsk2118436 dabrafenib, mediated by nras or mek mutations. *Molecular cancer therapeutics*, 11(4):909–920, 2012.
- [93] N. K. Haass, K. S. Smalley, and M. Herlyn. The role of altered cell–cell communication in melanoma progression. *Journal of molecular histology*, 35(3):309–318, 2004.
- [94] N. K. Haass, K. S. Smalley, L. Li, and M. Herlyn. Adhesion, migration and communication in melanocytes and melanoma. *Pigment Cell & Melanoma Research*, 18(3):150–159, 2005.
- [95] A. C. Halpern, D. Guerry IV, D. E. Elder, B. Trock, and M. Synnestvedt. A cohort study of melanoma in patients with dysplastic nevi. *Journal of investigative dermatology*, 100(3):S346–S349, 1993.
- [96] R. Haq, S. Yokoyama, E. B. Hawryluk, G. B. Jönsson, D. T. Frederick, K. McHenry, D. Porter, T.-N. Tran, K. T. Love, R. Langer, et al. Bcl2a1 is a lineage-specific antiapoptotic melanoma oncogene that confers resistance to braf inhibition. *Proceedings of the National Academy of Sciences*, 110(11):4321–4326, 2013.
- [97] A. Hauschild, J.-J. Grob, L. V. Demidov, T. Jouary, R. Gutzmer, M. Millward, P. Rutkowski, C. U. Blank, W. H. Miller Jr, E. Kaempgen, et al. Dabrafenib

- in braf-mutated metastatic melanoma: a multicentre, open-label, phase 3 randomised controlled trial. *The Lancet*, 380(9839):358–365, 2012.
- [98] C. M. Hay, E. Sult, Q. Huang, K. Mulgrew, S. R. Fuhrmann, K. A. McGlinchey, S. A. Hammond, R. Rothstein, J. Rios-Doria, E. Poon, et al. Targeting cd73 in the tumor microenvironment with medi9447. *Oncoimmunology*, 5(8):e1208875, 2016.
- [99] E. D. Hay. An overview of epithelio-mesenchymal transformation. *Cells Tissues Organs*, 154(1):8–20, 1995.
- [100] M. J. Hendrix, E. A. Seftor, Y.-W. Chu, R. E. Seftor, R. B. Nagle, K. M. McDaniel, S. P. Leong, K. H. Yohem, A. M. Leibovitz, F. L. Meyskens Jr, et al. Coexpression of vimentin and keratins by human melanoma tumor cells: correlation with invasive and metastatic potential. *JNCI: Journal of the National Cancer Institute*, 84(3):165–174, 1992.
- [101] M. J. Hendrix, E. A. Seftor, P. S. Meltzer, L. M. Gardner, A. R. Hess, D. A. Kirschmann, G. C. Schatteman, and R. E. Seftor. Expression and functional significance of ve-cadherin in aggressive human melanoma cells: role in vasculogenic mimicry. *Proceedings of the National Academy of Sciences*, 98(14):8018–8023, 2001.
- [102] S. L. Highfill, Y. Cui, A. J. Giles, J. P. Smith, H. Zhang, E. Morse, R. N. Kaplan, and C. L. Mackall. Disruption of cxcr2-mediated mdsc tumor trafficking enhances anti-pd1 efficacy. *Science translational medicine*, 6(237):237ra67–237ra67, 2014.
- [103] E. Hirata, M. R. Girotti, A. Viros, S. Hooper, B. Spencer-Dene, M. Matsuda, J. Larkin, R. Marais, and E. Sahai. Intravital imaging reveals how braf inhibition generates drug-tolerant microenvironments with high integrin β 1/fak signaling. *Cancer cell*, 27(4):574–588, 2015.
- [104] F. S. Hodi, S. J. O’day, D. F. McDermott, R. W. Weber, J. A. Sosman, J. B. Haanen, R. Gonzalez, C. Robert, D. Schadendorf, J. C. Hassel, et al. Improved survival with ipilimumab in patients with metastatic melanoma. *New England Journal of Medicine*, 363(8):711–723, 2010.
- [105] E. Hodis, I. R. Watson, G. V. Kryukov, S. T. Arold, M. Imielinski, J.-P. Theurillat, E. Nickerson, D. Auclair, L. Li, C. Place, et al. A landscape of driver mutations in melanoma. *Cell*, 150(2):251–263, 2012.
- [106] K. S. Hoek, O. M. Eichhoff, N. C. Schlegel, U. Döbbeling, N. Kobert, L. Schaerer, S. Hemmi, and R. Dummer. In vivo switching of human melanoma cells between proliferative and invasive states. *Cancer research*, 68(3):650–656, 2008.
- [107] K. S. Hoek, N. C. Schlegel, P. Brafford, A. Sucker, S. Ugurel, R. Kumar, B. L. Weber, K. L. Nathanson, D. J. Phillips, M. Herlyn, et al. Metastatic potential of melanomas defined by specific gene expression profiles with no braf signature. *Pigment Cell & Melanoma Research*, 19(4):290–302, 2006.

- [108] M. Hölzel, A. Bovier, and T. Tüting. Plasticity of tumour and immune cells: a source of heterogeneity and a cause for therapy resistance? *Nature Reviews Cancer*, 13(5):365, 2013.
- [109] M. Hölzel, J. Landsberg, N. Glodde, T. Bald, M. Rogava, S. Riesenberger, A. Becker, G. Jönsson, and T. Tüting. A preclinical model of malignant peripheral nerve sheath tumor-like melanoma is characterized by infiltrating mast cells. *Cancer research*, 76(2):251–263, 2016.
- [110] M. Hölzel and T. Tüting. Inflammation-induced plasticity in melanoma therapy and metastasis. *Trends in immunology*, 37(6):364–374, 2016.
- [111] S. Hu-Lieskovan, S. Mok, B. H. Moreno, J. Tsoi, L. Robert, L. Goedert, E. M. Pinheiro, R. C. Koya, T. G. Graeber, B. Comin-Anduix, et al. Improved antitumor activity of immunotherapy with braf and mek inhibitors in brafv600e melanoma. *Science translational medicine*, 7(279):279ra41–279ra41, 2015.
- [112] W. E. Huber, E. R. Price, H. R. Widlund, J. Du, I. J. Davis, M. Wegner, and D. E. Fisher. A tissue-restricted camp transcriptional response sox10 modulates α -melanocyte-stimulating hormone-triggered expression of microphthalmia-associated transcription factor in melanocytes. *Journal of Biological Chemistry*, 278(46):45224–45230, 2003.
- [113] W. Hugo, J. M. Zaretsky, L. Sun, C. Song, B. H. Moreno, S. Hu-Lieskovan, B. Berent-Maoz, J. Pang, B. Chmielowski, G. Cherry, et al. Genomic and transcriptomic features of response to anti-pd-1 therapy in metastatic melanoma. *Cell*, 165(1):35–44, 2016.
- [114] R. Iannone, L. Miele, P. Maiolino, A. Pinto, and S. Morello. Adenosine limits the therapeutic effectiveness of anti-ctla4 mab in a mouse melanoma model. *American journal of cancer research*, 4(2):172, 2014.
- [115] M. Jafari, T. Papp, S. Kirchner, U. Kiener, D. Henschler, G. Burg, and D. Schiffmann. Analysis of ras mutations in human melanocytic lesions: activation of the ras gene seems to be associated with the nodular type of human malignant melanoma. *Journal of cancer research and clinical oncology*, 121(1):23–30, 1995.
- [116] D. Javelaud, V.-I. Alexaki, M.-J. Pierrat, K. S. Hoek, S. Dennler, L. Van Kempen, C. Bertolotto, R. Ballotti, S. Saule, V. Delmas, et al. Gli2 and m-mitf transcription factors control exclusive gene expression programs and inversely regulate invasion in human melanoma cells. *Pigment cell & melanoma research*, 24(5):932–943, 2011.
- [117] C. M. Johannessen, L. A. Johnson, F. Piccioni, A. Townes, D. T. Frederick, M. K. Donahue, R. Narayan, K. T. Flaherty, J. A. Wargo, D. E. Root, et al. A melanocyte lineage program confers resistance to map kinase pathway inhibition. *Nature*, 504(7478):138, 2013.

- [118] P. Johansson, S. Pavey, and N. Hayward. Confirmation of a braf mutation-associated gene expression signature in melanoma. *Pigment Cell & Melanoma Research*, 20(3):216–221, 2007.
- [119] M. Kappelmann, A. Bosserhoff, and S. Kuphal. Ap-1/c-jun transcription factors: regulation and function in malignant melanoma. *European journal of cell biology*, 93(1-2):76–81, 2014.
- [120] E. Katsuta, S. Tanaka, K. Mogushi, S. Shimada, Y. Akiyama, A. Aihara, S. Matsumura, Y. Mitsunori, D. Ban, T. Ochiai, et al. Cd73 as a therapeutic target for pancreatic neuroendocrine tumor stem cells. *International journal of oncology*, 48(2):657–669, 2016.
- [121] A. Kaur, M. R. Webster, K. Marchbank, R. Behera, A. Ndoye, C. H. Kugel, V. M. Dang, J. Appleton, M. P. O’Connell, P. Cheng, et al. sfrp2 in the aged microenvironment drives melanoma metastasis and therapy resistance. *Nature*, 532(7598):250, 2016.
- [122] W. J. Kent, C. W. Sugnet, T. S. Furey, K. M. Roskin, T. H. Pringle, A. M. Zahler, and D. Haussler. The human genome browser at ucsc. *Genome research*, 12(6):996–1006, 2002.
- [123] E. Kim, V. Rebecca, I. V. Fedorenko, J. L. Messina, R. Mathew, S. S. Maria-Engler, D. Basanta, K. S. Smalley, and A. R. Anderson. Senescent fibroblasts in melanoma initiation and progression: an integrated theoretical, experimental, and clinical approach. *Cancer research*, 73(23):6874–6885, 2013.
- [124] G. Kim, A. E. McKee, Y.-M. Ning, M. Hazarika, M. Theoret, J. R. Johnson, Q. C. Xu, S. Tang, R. Sridhara, X. Jiang, et al. Fda approval summary: vemurafenib for treatment of unresectable or metastatic melanoma with the brafv600e mutation. *Clinical Cancer Research*, 20(19):4994–5000, 2014.
- [125] I. S. Kim, S. Heilmann, E. R. Kansler, Y. Zhang, M. Zimmer, K. Ratnakumar, R. L. Bowman, T. Simon-Vermot, M. Fennell, R. Garippa, et al. Microenvironment-derived factors driving metastatic plasticity in melanoma. *Nature communications*, 8:14343, 2017.
- [126] J. E. Kim, E. Y. Leung, B. C. Baguley, and G. J. Finlay. Heterogeneity of expression of epithelial–mesenchymal transition markers in melanocytes and melanoma cell lines. *Frontiers in genetics*, 4:97, 2013.
- [127] J. M. Kirkwood, J. G. Ibrahim, V. K. Sondak, J. Richards, L. E. Flaherty, M. S. Ernstoff, T. J. Smith, U. Rao, M. Steele, and R. H. Blum. High-and low-dose interferon alfa-2b in high-risk melanoma: first analysis of intergroup trial e1690/s9111/c9190. *Journal of clinical oncology*, 18(12):2444–2458, 2000.

- [128] J. M. Kirkwood, M. H. Strawderman, M. S. Ernstoff, T. J. Smith, E. C. Borden, and R. H. Blum. Interferon alfa-2b adjuvant therapy of high-risk resected cutaneous melanoma: the eastern cooperative oncology group trial est 1684. *Journal of clinical oncology*, 14(1):7–17, 1996.
- [129] D. J. Konieczkowski, C. M. Johannessen, O. Abudayyeh, J. W. Kim, Z. A. Cooper, A. Piris, D. T. Frederick, M. Barzily-Rokni, R. Straussman, R. Haq, et al. A melanoma cell state distinction influences sensitivity to mapk pathway inhibitors. *Cancer discovery*, 4(7):816–827, 2014.
- [130] P. Koszałka, A. Prysłak, M. Gołńska, J. Kolasa, G. Stasiłojć, A. C. Składanowski, and J. J. Bigda. Inhibition of cd73 stimulates the migration and invasion of b16f10 melanoma cells in vitro, but results in impaired angiogenesis and reduced melanoma growth in vivo. *Oncology reports*, 31(2):819–827, 2014.
- [131] K. Kovary and R. Bravo. The jun and fos protein families are both required for cell cycle progression in fibroblasts. *Molecular and cellular biology*, 11(9):4466–4472, 1991.
- [132] M. Krauthammer, Y. Kong, A. Bacchiocchi, P. Evans, N. Pornputtpong, C. Wu, J. P. McCusker, S. Ma, E. Cheng, R. Straub, et al. Exome sequencing identifies recurrent mutations in nf1 and rasopathy genes in sun-exposed melanomas. *Nature genetics*, 47(9):996, 2015.
- [133] A. M. Krebs, J. Mitschke, M. L. Losada, O. Schmalhofer, M. Boerries, H. Busch, M. Boettcher, D. Mougiakakos, W. Reichardt, P. Bronsert, et al. The emt-activator zeb1 is a key factor for cell plasticity and promotes metastasis in pancreatic cancer. *Nature cell biology*, 19(5):518, 2017.
- [134] M. F. Krummel and J. P. Allison. Cd28 and ctla-4 have opposing effects on the response of t cells to stimulation. *Journal of Experimental Medicine*, 182(2):459–465, 1995.
- [135] P. M. Kulesa, J. C. Kasemeier-Kulesa, J. M. Teddy, N. V. Margaryan, E. A. Seftor, R. E. Seftor, and M. J. Hendrix. Reprogramming metastatic melanoma cells to assume a neural crest cell-like phenotype in an embryonic microenvironment. *Proceedings of the National Academy of Sciences of the United States of America*, 103(10):3752–3757, 2006.
- [136] J. Landsberg, J. Kohlmeyer, M. Renn, T. Bald, M. Rogava, M. Cron, M. Fatho, V. Lennerz, T. Wölfel, M. Hölzel, et al. Melanomas resist t-cell therapy through inflammation-induced reversible dedifferentiation. *Nature*, 490(7420):412, 2012.
- [137] J. Larkin, P. A. Ascierto, B. Dréno, V. Atkinson, G. Liskay, M. Maio, M. Mandalà, L. Demidov, D. Stroyakovskiy, L. Thomas, et al. Combined vemurafenib and cobimetinib in braf-mutated melanoma. *New England Journal of Medicine*, 371(20):1867–1876, 2014.

- [138] G. Lee, H. Kim, Y. Elkabetz, G. Al Shamy, G. Panagiotakos, T. Barberi, V. Tabar, and L. Studer. Isolation and directed differentiation of neural crest stem cells derived from human embryonic stem cells. *Nature biotechnology*, 25(12), 2007.
- [139] C. Levy, M. Khaled, and D. E. Fisher. Mitf: master regulator of melanocyte development and melanoma oncogene. *Trends in molecular medicine*, 12(9):406–414, 2006.
- [140] G. Li, H. Schaidler, K. Satyamoorthy, Y. Hanakawa, K. Hashimoto, and M. Herlyn. Downregulation of e-cadherin and desmoglein 1 by autocrine hepatocyte growth factor during melanoma development. *Oncogene*, 20(56):8125, 2001.
- [141] J. Lin, Y. Goto, H. Murata, K. Sakaizawa, A. Uchiyama, T. Saida, and M. Takata. Polyclonality of braf mutations in primary melanoma and the selection of mutant alleles during progression. *British journal of cancer*, 104(3):464, 2011.
- [142] W. M. Lin, A. C. Baker, R. Beroukhir, W. Winckler, W. Feng, J. M. Marmion, E. Laine, H. Greulich, H. Tseng, C. Gates, et al. Modeling genomic diversity and tumor dependency in malignant melanoma. *Cancer research*, 68(3):664–673, 2008.
- [143] L. Liu, P. A. Mayes, S. Eastman, H. Shi, S. Yadavilli, T. Zhang, J. Yang, L. Seestaller-Wehr, S.-Y. Zhang, C. Hopson, et al. The braf and mek inhibitors dabrafenib and trametinib: effects on immune function and in combination with immunomodulatory antibodies targeting pd-1, pd-l1, and ctla-4. *Clinical Cancer Research*, 2015.
- [144] S. Loi, S. Pommey, B. Haibe-Kains, P. A. Beavis, P. K. Darcy, M. J. Smyth, and J. Stagg. Cd73 promotes anthracycline resistance and poor prognosis in triple negative breast cancer. *Proceedings of the National Academy of Sciences*, 110(27):11091–11096, 2013.
- [145] G. V. Long, D. Stroyakovskiy, H. Gogas, E. Levchenko, F. De Braud, J. Larkin, C. Garbe, T. Jouary, A. Hauschild, J.-J. Grob, et al. Dabrafenib and trametinib versus dabrafenib and placebo for val600 braf-mutant melanoma: a multicentre, double-blind, phase 3 randomised controlled trial. *The Lancet*, 386(9992):444–451, 2015.
- [146] P. Lopez-Bergami, C. Huang, J. S. Goydos, D. Yip, M. Bar-Eli, M. Herlyn, K. S. Smalley, A. Mahale, A. Eroshkin, S. Aaronson, et al. Rewired erk-jnk signaling pathways in melanoma. *Cancer cell*, 11(5):447–460, 2007.
- [147] J. M. López-Novoa and M. A. Nieto. Inflammation and emt: an alliance towards organ fibrosis and cancer progression. *EMBO molecular medicine*, 1(6-7):303–314, 2009.

- [148] M. Lupia, F. Angiolini, G. Bertalot, S. Freddi, K. F. Sachsenmeier, E. Chisci, B. Kutryb-Zajac, S. Confalonieri, R. T. Smolenski, R. Giovannoni, et al. Cd73 regulates stemness and epithelial-mesenchymal transition in ovarian cancer-initiating cells. *Stem cell reports*, 10(4):1412–1425, 2018.
- [149] J. B. Macdonald, A. C. Dueck, R. J. Gray, N. Wasif, D. L. Swanson, A. Sekulic, and B. A. Pockaj. Malignant melanoma in the elderly: different regional disease and poorer prognosis. *Journal of Cancer*, 2:538, 2011.
- [150] N. Maddodi and V. Setaluri. Role of uv in cutaneous melanoma. *Photochemistry and photobiology*, 84(2):528–536, 2008.
- [151] T. Maj, W. Wang, J. Crespo, H. Zhang, W. Wang, S. Wei, L. Zhao, L. Vatan, I. Shao, W. Szeliga, et al. Oxidative stress controls regulatory t cell apoptosis and suppressor activity and pd-l1-blockade resistance in tumor. *Nature immunology*, 18(12):1332, 2017.
- [152] A. J. Maniotis, R. Folberg, A. Hess, E. A. Seftor, L. M. Gardner, J. Pe'er, J. M. Trent, P. S. Meltzer, and M. J. Hendrix. Vascular channel formation by human melanoma cells in vivo and in vitro: vasculogenic mimicry. *The American journal of pathology*, 155(3):739–752, 1999.
- [153] S. N. Markovic, L. A. Erickson, R. D. Rao, R. R. McWilliams, L. A. Kottschade, E. T. Creagan, R. H. Weenig, J. L. Hand, M. R. Pittelkow, B. A. Pockaj, et al. Malignant melanoma in the 21st century, part 1: epidemiology, risk factors, screening, prevention, and diagnosis. In *Mayo Clinic Proceedings*, volume 82, pages 364–380. Elsevier, 2007.
- [154] R. Marks. Epidemiology of melanoma. *Clinical and Experimental Dermatology*, 25(6):459–463, 2000.
- [155] A. Marusyk, V. Almendro, and K. Polyak. Intra-tumour heterogeneity: a looking glass for cancer? *Nature Reviews Cancer*, 12(5):323, 2012.
- [156] Y. Matsumura and H. N. Ananthaswamy. Molecular mechanisms of photocarcinogenesis. *Frontiers in bioscience: a journal and virtual library*, 7:d765–83, 2002.
- [157] G. A. McArthur, P. B. Chapman, C. Robert, J. Larkin, J. B. Haanen, R. Dummer, A. Ribas, D. Hogg, O. Hamid, P. A. Ascierto, et al. Safety and efficacy of vemurafenib in brafv600e and brafv600k mutation-positive melanoma (brim-3): extended follow-up of a phase 3, randomised, open-label study. *The lancet oncology*, 15(3):323–332, 2014.
- [158] K. A. McBride, M. L. Ballinger, E. Killick, J. Kirk, M. H. Tattersall, R. A. Eeles, D. M. Thomas, and G. Mitchell. Li-fraumeni syndrome: cancer risk assessment and clinical management. *Nature Reviews Clinical Oncology*, 11(5):260, 2014.

- [159] N. McGranahan and C. Swanton. Biological and therapeutic impact of intratumor heterogeneity in cancer evolution. *Cancer cell*, 27(1):15–26, 2015.
- [160] A. Mehta, Y. J. Kim, L. Robert, J. Tsoi, B. Comin-Anduix, B. Berent-Maoz, A. J. Cochran, J. Economou, P. C. Tumeh, C. Puig-Saus, et al. Immunotherapy resistance by inflammation-induced dedifferentiation. *Cancer discovery*, pages CD–17, 2018.
- [161] L. M. Merlo, J. W. Pepper, B. J. Reid, and C. C. Maley. Cancer as an evolutionary and ecological process. *Nature Reviews Cancer*, 6(12):924, 2006.
- [162] D. Mittal, D. Sinha, D. Barkauskas, A. Young, M. Kalimutho, K. Stannard, F. Caramia, B. Haibe-Kains, J. Stagg, K. K. Khanna, et al. Adenosine 2b receptor expression on cancer cells promotes metastasis. *Cancer research*, 76(15):4372–4382, 2016.
- [163] D. Mittal, A. Young, K. Stannard, M. Yong, M. W. Teng, B. Allard, J. Stagg, and M. J. Smyth. Antimetastatic effects of blocking pd-1 and the adenosine a2a receptor. *Cancer research*, 74(14):3652–3658, 2014.
- [164] E. Monzani, F. Facchetti, E. Galmozzi, E. Corsini, A. Benetti, C. Cavazzin, A. Gritti, A. Piccinini, D. Porro, M. Santinami, et al. Melanoma contains cd133 and abcg2 positive cells with enhanced tumourigenic potential. *European journal of cancer*, 43(5):935–946, 2007.
- [165] W. Mooi and D. Peeper. Oncogene-induced cell senescence—halting on the road to cancer. *New England Journal of Medicine*, 355(10):1037–1046, 2006.
- [166] S. Morello, M. Capone, C. Sorrentino, D. Giannarelli, G. Madonna, D. Mallardo, A. M. Grimaldi, A. Pinto, and P. A. Ascierto. Soluble cd73 as biomarker in patients with metastatic melanoma patients treated with nivolumab. *Journal of translational medicine*, 15(1):244, 2017.
- [167] J. Müller, O. Krijgsman, J. Tsoi, L. Robert, W. Hugo, C. Song, X. Kong, P. A. Possik, P. D. Cornelissen-Steijger, M. H. G. Foppen, et al. Low mitf/axl ratio predicts early resistance to multiple targeted drugs in melanoma. *Nature communications*, 5:5712, 2014.
- [168] E. Nevedomskaya, R. Perryman, S. Solanki, N. Syed, O. A. Mayboroda, and H. C. Keun. A systems oncology approach identifies nt5e as a key metabolic regulator in tumor cells and modulator of platinum sensitivity. *Journal of proteome research*, 15(1):280–290, 2015.
- [169] M. A. Nieto. Context-specific roles of emt programmes in cancer cell dissemination. *Nature cell biology*, 19(5):416, 2017.
- [170] M. A. Nieto, R. Y.-J. Huang, R. A. Jackson, and J. P. Thiery. Emt: 2016. *Cell*, 166(1):21–45, 2016.

- [171] C. L. Nigro, M. Monteverde, S. Lee, L. Lattanzio, D. Vivenza, A. Comino, N. Syed, A. McHugh, H. Wang, C. Proby, et al. 5m CpG island methylation is a favourable breast cancer biomarker. *British journal of cancer*, 107(1):75, 2012.
- [172] S. V. Novitskiy, S. Ryzhov, R. Zaynagetdinov, A. E. Goldstein, Y. Huang, O. Y. Tikhomirov, M. R. Blackburn, I. Biaggioni, D. P. Carbone, I. Feoktistov, et al. Adenosine receptors in regulation of dendritic cell differentiation and function. *Blood*, 112(5):1822–1831, 2008.
- [173] P. C. Nowell. The clonal evolution of tumor cell populations. *Science*, 194(4260):23–28, 1976.
- [174] T. S. Nowicki, S. Hu-Lieskovan, and A. Ribas. Mechanisms of resistance to pd-1 and pd-l1 blockade. *The Cancer Journal*, 24(1):47–53, 2018.
- [175] A. C. Obenauf, Y. Zou, A. L. Ji, S. Vanharanta, W. Shu, H. Shi, X. Kong, M. C. Bosenberg, T. Wiesner, N. Rosen, et al. Therapy-induced tumour secretomes promote resistance and tumour progression. *Nature*, 520(7547):368, 2015.
- [176] M. P. O’Connell, K. Marchbank, M. R. Webster, A. A. Valiga, A. Kaur, A. Vultur, L. Li, M. Herlyn, J. Villanueva, Q. Liu, et al. Hypoxia induces phenotypic plasticity and therapy resistance in melanoma via the tyrosine kinase receptors ror1 and ror2. *Cancer discovery*, 3(12):1378–1393, 2013.
- [177] A. Ohta and M. Sitkovsky. Role of g-protein-coupled adenosine receptors in downregulation of inflammation and protection from tissue damage. *Nature*, 414(6866):916, 2001.
- [178] A. Ohta and M. Sitkovsky. Extracellular adenosine-mediated modulation of regulatory t cells. *Frontiers in immunology*, 5:304, 2014.
- [179] K. Opdecamp, A. Nakayama, M. Nguyen, C. A. Hodgkinson, W. J. Pavan, and H. Arnheiter. Melanocyte development in vivo and in neural crest cell cultures: crucial dependence on the mitf basic-helix-loop-helix-zipper transcription factor. *Development*, 124(12):2377–2386, 1997.
- [180] S. Paget. The distribution of secondary growths in cancer of the breast. *The Lancet*, 133(3421):571–573, 1889.
- [181] S. M. Pagnotta, C. Laudanna, M. Pancione, L. Sabatino, C. Votino, A. Remo, L. Cerulo, P. Zoppoli, E. Manfrin, V. Colantuoni, et al. Ensemble of gene signatures identifies novel biomarkers in colorectal cancer activated through ppar γ and tnfa signaling. *PloS one*, 8(8):e72638, 2013.
- [182] D. Pan, S. Roy, P. Gascard, J. Zhao, C. Chen-Tanyolac, and T. D. Tlsty. Sox2, oct3/4 and nanog expression and cellular plasticity in rare human somatic cells requires cd73. *Cellular signalling*, 28(12):1923–1932, 2016.

- [183] K. H. Paraiso, Y. Xiang, V. W. Rebecca, E. V. Abel, Y. A. Chen, A. C. Munko, E. Wood, I. V. Fedorenko, V. K. Sondak, A. R. Anderson, et al. Pten loss confers braf inhibitor resistance to melanoma cells through the suppression of bim expression. *Cancer research*, 71(7):2750–2760, 2011.
- [184] E. E. Patton, H. R. Widlund, J. L. Kutok, K. R. Kopani, J. F. Amatruda, R. D. Murphey, S. Berghmans, E. A. Mayhall, D. Traver, C. D. Fletcher, et al. Braf mutations are sufficient to promote nevi formation and cooperate with p53 in the genesis of melanoma. *Current Biology*, 15(3):249–254, 2005.
- [185] C. C. Pinnix, J. T. Lee, Z.-J. Liu, R. McDaid, K. Balint, L. J. Beverly, P. A. Brafford, M. Xiao, B. Himes, S. E. Zabierowski, et al. Active notch1 confers a transformed phenotype to primary human melanocytes. *Cancer research*, 69(13):5312–5320, 2009.
- [186] E. Piskounova, M. Agathocleous, M. M. Murphy, Z. Hu, S. E. Huddlestun, Z. Zhao, A. M. Leitch, T. M. Johnson, R. J. DeBerardinis, and S. J. Morrison. Oxidative stress inhibits distant metastasis by human melanoma cells. *Nature*, 527(7577):186, 2015.
- [187] P. M. Pollock, U. L. Harper, K. S. Hansen, L. M. Yudt, M. Stark, C. M. Robbins, T. Y. Moses, G. Hostetter, U. Wagner, J. Kakareka, et al. High frequency of braf mutations in nevi. *Nature genetics*, 33(1):19, 2003.
- [188] M. Potrony, C. Badenas, P. Aguilera, J. A. Puig-Butille, C. Carrera, J. Malveyh, and S. Puig. Update in genetic susceptibility in melanoma. *Annals of translational medicine*, 3(15), 2015.
- [189] E. R. Price, M. A. Horstmann, A. G. Wells, K. N. Weilbaecher, C. M. Takemoto, M. W. Landis, and D. E. Fisher. α -melanocyte-stimulating hormone signaling regulates expression of microphthalmia, a gene deficient in waardenburg syndrome. *Journal of Biological Chemistry*, 273(49):33042–33047, 1998.
- [190] B.-Z. Qian and J. W. Pollard. Macrophage diversity enhances tumor progression and metastasis. *Cell*, 141(1):39–51, 2010.
- [191] E. Quintana, M. Shackleton, M. S. Sabel, D. R. Fullen, T. M. Johnson, and S. J. Morrison. Efficient tumour formation by single human melanoma cells. *Nature*, 456(7222):593, 2008.
- [192] R. Ramsdale, R. N. Jorissen, F. Z. Li, S. Al-Obaidi, T. Ward, K. E. Sheppard, P. E. Bukczynska, R. J. Young, S. E. Boyle, M. Shackleton, et al. The transcription cofactor c-jun mediates phenotype switching and braf inhibitor resistance in melanoma. *Sci. Signal.*, 8(390):ra82–ra82, 2015.
- [193] T. Raskovalova, X. Huang, M. Sitkovsky, L. C. Zacharia, E. K. Jackson, and E. Gorelik. Gs protein-coupled adenosine receptor signaling and lytic function of activated nk cells. *The Journal of Immunology*, 175(7):4383–4391, 2005.

- [194] J. Reinhardt, M. Effer, and M. H¹zel. Molecular mechanisms governing melanoma cell plasticity in response to therapy-induced stress. *British journal of cancer*, x(x):x, under revision.
- [195] J. Reinhardt, J. Landsberg, J. L. Schmid-Burgk, B. B. Ramis, T. Bald, N. Glodde, D. Lopez-Ramos, A. Young, S. F. Ngiow, D. Nettersheim, et al. Mapk signaling and inflammation link melanoma phenotype switching to induction of cd73 during immunotherapy. *Cancer research*, 77(17):4697–4709, 2017.
- [196] R. Rezzonico, K. Yeow, A. Loubat, B. Ferrua, G. Lenegrata, L. Turchi, A. A. Chassot, J. P. Ortonne, and G. Ponzio. Dynamic characterization of the molecular events during in vitro epidermal wound healing. *Journal of Investigative Dermatology*, 119(1):56–63, 2002.
- [197] A. D. Rhim, E. T. Mirek, N. M. Aiello, A. Maitra, J. M. Bailey, F. McAllister, M. Reichert, G. L. Beatty, A. K. Rustgi, R. H. Vonderheide, et al. Emt and dissemination precede pancreatic tumor formation. *Cell*, 148(1):349–361, 2012.
- [198] A. Ribas, M. Butler, J. Lutzky, D. P. Lawrence, C. Robert, W. Miller, G. P. Linette, P. A. Ascierto, T. Kuzel, A. P. Algazi, et al. Phase i study combining anti-pd-l1 (medi4736) with braf (dabrafenib) and/or mek (trametinib) inhibitors in advanced melanoma., 2015.
- [199] A. Ribas, F. S. Hodi, M. Callahan, C. Konto, and J. Wolchok. Hepatotoxicity with combination of vemurafenib and ipilimumab. *New England Journal of Medicine*, 368(14):1365–1366, 2013.
- [200] A. Ribas and J. D. Wolchok. Cancer immunotherapy using checkpoint blockade. *Science*, 359(6382):1350–1355, 2018.
- [201] S. Riesenberger, A. Groetchen, R. Siddaway, T. Bald, J. Reinhardt, D. Smorra, J. Kohlmeyer, M. Renn, B. Phung, P. Aymans, et al. Mitf and c-jun antagonism interconnects melanoma dedifferentiation with pro-inflammatory cytokine responsiveness and myeloid cell recruitment. *Nature communications*, 6:8755, 2015.
- [202] C. Robert, G. V. Long, B. Brady, C. Dutriaux, M. Maio, L. Mortier, J. C. Hassel, P. Rutkowski, C. McNeil, E. Kalinka-Warzocha, et al. Nivolumab in previously untreated melanoma without braf mutation. *New England journal of medicine*, 372(4):320–330, 2015.
- [203] C. Robert, J. Schachter, G. V. Long, A. Arance, J. J. Grob, L. Mortier, A. Daud, M. S. Carlino, C. McNeil, M. Lotem, et al. Pembrolizumab versus ipilimumab in advanced melanoma. *New England Journal of Medicine*, 372(26):2521–2532, 2015.

- [204] S. A. Rosenberg, J. C. Yang, R. M. Sherry, U. S. Kammula, M. S. Hughes, G. Q. Phan, D. E. Citrin, N. P. Restifo, P. F. Robbins, J. R. Wunderlich, et al. Durable complete responses in heavily pretreated patients with metastatic melanoma using t-cell transfer immunotherapy. *Clinical Cancer Research*, 17(13):4550–4557, 2011.
- [205] M. Ruscetti, B. Quach, E. L. Dadashian, D. J. Mulholland, and H. Wu. Tracking and functional characterization of epithelial–mesenchymal transition and mesenchymal tumor cells during prostate cancer metastasis. *Cancer research*, 75(13):2749–2759, 2015.
- [206] S. Ryzhov, S. V. Novitskiy, A. E. Goldstein, A. Biktasova, M. R. Blackburn, I. Biaggioni, M. M. Dikov, and I. Feoktistov. Adenosinergic regulation of the expansion and immunosuppressive activity of cd11b+ gr1+ cells. *The Journal of Immunology*, 187(11):6120–6129, 2011.
- [207] R. Sadej, J. Spychala, and A. C. Skladanowski. Expression of ecto-5'-nucleotidase (en, cd73) in cell lines from various stages of human melanoma. *Melanoma research*, 16(3):213–222, 2006.
- [208] M. Sáez-Ayala, M. F. Montenegro, L. Sánchez-del Campo, M. P. Fernández-Pérez, S. Chazarra, R. Freter, M. Middleton, A. Piñero-Madrona, J. Cabezas-Herrera, C. R. Goding, et al. Directed phenotype switching as an effective antimelanoma strategy. *Cancer cell*, 24(1):105–119, 2013.
- [209] D. Sarrió, S. M. Rodríguez-Pinilla, D. Hardisson, A. Cano, G. Moreno-Bueno, and J. Palacios. Epithelial-mesenchymal transition in breast cancer relates to the basal-like phenotype. *Cancer research*, 68(4):989–997, 2008.
- [210] D. Schadendorf, D. E. Fisher, C. Garbe, J. E. Gershenwald, J.-J. Grob, A. Halpern, M. Herlyn, M. A. Marchetti, G. McArthur, A. Ribas, et al. Melanoma. *Nature reviews Disease primers*, 1:15003, 2015.
- [211] D. Schadendorf, N. Haas, M. Worm, H. Ostmeier, C. Kohlmus, J. Gottschalk, B. Algermissen, G. Jautzke, and B. Czarnetzki. Amelanotic malignant melanoma presenting as malignant schwannoma. *British Journal of Dermatology*, 129(5):609–614, 1993.
- [212] D. Schadendorf, F. S. Hodi, C. Robert, J. S. Weber, K. Margolin, O. Hamid, D. Patt, T.-T. Chen, D. M. Berman, and J. D. Wolchok. Pooled analysis of long-term survival data from phase ii and phase iii trials of ipilimumab in unresectable or metastatic melanoma. *Journal of clinical oncology*, 33(17):1889, 2015.
- [213] T. Schatton, G. F. Murphy, N. Y. Frank, K. Yamaura, A. M. Waaga-Gasser, M. Gasser, Q. Zhan, S. Jordan, L. M. Duncan, C. Weishaupt, et al. Identification of cells initiating human melanomas. *Nature*, 451(7176):345, 2008.

- [214] M. J. Schliekelman, A. Taguchi, J. Zhu, X. Dai, J. Rodriguez, M. Celiktas, Q. Zhang, A. Chin, C.-H. Wong, H. Wang, et al. Molecular portraits of epithelial, mesenchymal and hybrid states in lung adenocarcinoma and their relevance to survival. *Cancer research*, pages canres–2535, 2015.
- [215] J. L. Schmid-Burgk, T. Schmidt, M. M. Gaidt, K. Pelka, E. Latz, T. S. Ebert, and V. Hornung. Outknocker: a web tool for rapid and simple genotyping of designer nuclease edited cell lines. *Genome research*, 24(10):1719–1723, 2014.
- [216] S. Schwitalla, A. A. Fingerle, P. Cammareri, T. Nebelsiek, S. I. Göktuna, P. K. Ziegler, O. Canli, J. Heijmans, D. J. Huels, G. Moreaux, et al. Intestinal tumorigenesis initiated by dedifferentiation and acquisition of stem-cell-like properties. *Cell*, 152(1):25–38, 2013.
- [217] E. A. Seftor, K. M. Brown, L. Chin, D. A. Kirschmann, W. W. Wheaton, A. Protopopov, B. Feng, Y. Balagurunathan, J. M. Trent, B. J. Nickoloff, et al. Epigenetic transdifferentiation of normal melanocytes by a metastatic melanoma microenvironment. *Cancer research*, 65(22):10164–10169, 2005.
- [218] M. Sensi, M. Catani, G. Castellano, G. Nicolini, F. Alciato, G. Tragni, G. De Santis, I. Bersani, G. Avanzi, A. Tomassetti, et al. Human cutaneous melanomas lacking mitf and melanocyte differentiation antigens express a functional axl receptor kinase. *Journal of Investigative Dermatology*, 131(12):2448–2457, 2011.
- [219] M. Sensi, G. Nicolini, C. Petti, I. Bersani, F. Lozupone, A. Molla, C. Vegetti, D. Nonaka, R. Mortarini, G. Parmiani, et al. Mutually exclusive nras q61r and braf v600e mutations at the single-cell level in the same human melanoma. *Oncogene*, 25(24):3357, 2006.
- [220] M. Shackleton, E. Quintana, E. R. Fearon, and S. J. Morrison. Heterogeneity in cancer: cancer stem cells versus clonal evolution. *Cell*, 138(5):822–829, 2009.
- [221] S. M. Shaffer, M. C. Dunagin, S. R. Torborg, E. A. Torre, B. Emert, C. Krepler, M. Beqiri, K. Sproesser, P. A. Brafford, M. Xiao, et al. Rare cell variability and drug-induced reprogramming as a mode of cancer drug resistance. *Nature*, 546(7658):431, 2017.
- [222] M. Shah, A. Bhoumik, V. Goel, A. Dewing, W. Breitwieser, H. Kluger, S. Krajewski, M. Krajewska, J. DeHart, E. Lau, et al. A role for atf2 in regulating mitf and melanoma development. *PLoS genetics*, 6(12):e1001258, 2010.
- [223] S. V. Sharma, D. Y. Lee, B. Li, M. P. Quinlan, F. Takahashi, S. Maheswaran, U. McDermott, N. Azizian, L. Zou, M. A. Fischbach, et al. A chromatin-mediated reversible drug-tolerant state in cancer cell subpopulations. *Cell*, 141(1):69–80, 2010.
- [224] E. Shaulian and M. Karin. Ap-1 in cell proliferation and survival. *Oncogene*, 20(19):2390, 2001.

- [225] H. Shi, W. Hugo, X. Kong, A. Hong, R. C. Koya, G. Moriceau, T. Chodon, R. Guo, D. B. Johnson, K. B. Dahlman, et al. Acquired resistance and clonal evolution in melanoma during braf inhibitor therapy. *Cancer discovery*, 4(1):80–93, 2014.
- [226] A. Sica and A. Mantovani. Macrophage plasticity and polarization: in vivo veritas. *The Journal of clinical investigation*, 122(3):787–795, 2012.
- [227] R. L. Siegel, K. D. Miller, and A. Jemal. Cancer statistics, 2015. *CA: a cancer journal for clinicians*, 65(1):5–29, 2015.
- [228] A. Slipicevic, R. Holm, M. T. Nguyen, P. J. Bøhler, B. Davidson, and V. A. Flørenes. Expression of activated akt and pten in malignant melanomas: relationship with clinical outcome. *American journal of clinical pathology*, 124(4):528–536, 2005.
- [229] K. S. Smalley, M. Lioni, M. Dalla Palma, M. Xiao, B. Desai, S. Egyhazi, J. Hansson, H. Wu, A. J. King, P. Van Belle, et al. Increased cyclin d1 expression can mediate braf inhibitor resistance in braf v600e-mutated melanomas. *Molecular cancer therapeutics*, 7(9):2876–2883, 2008.
- [230] M. P. Smith, H. Brunton, E. J. Rowling, J. Ferguson, I. Arozarena, Z. Miskolczi, J. L. Lee, M. R. Girotti, R. Marais, M. P. Levesque, et al. Inhibiting drivers of non-mutational drug tolerance is a salvage strategy for targeted melanoma therapy. *Cancer cell*, 29(3):270–284, 2016.
- [231] R. Somasundaram and D. Herlyn. Chemokines and the microenvironment in neuroectodermal tumor–host interaction. *Seminars in cancer biology*, 19(2):92–96, 2009.
- [232] L. Song, W. Ye, Y. Cui, J. Lu, Y. Zhang, N. Ding, W. Hu, H. Pei, Z. Yue, and G. Zhou. Ecto-5'-nucleotidase (cd73) is a biomarker for clear cell renal carcinoma stem-like cells. *Oncotarget*, 8(19):31977, 2017.
- [233] B. Spangler, M. Kappelmann, B. Schitteck, S. Meierjohann, L. Vardimon, A. K. Bosserhoff, and S. Kuphal. Ets-1/rhoc signaling regulates the transcription factor c-jun in melanoma. *International journal of cancer*, 130(12):2801–2811, 2012.
- [234] B. Spangler, L. Vardimon, A. Bosserhoff, and S. Kuphal. Post-transcriptional regulation controlled by e-cadherin is important for c-jun activity in melanoma. *Pigment cell & melanoma research*, 24(1):148–164, 2011.
- [235] J. Stagg, U. Divisekera, H. Duret, T. Sparwasser, M. W. Teng, P. K. Darcy, and M. J. Smyth. Cd73-deficient mice have increased antitumor immunity and are resistant to experimental metastasis. *Cancer research*, 71(8):2892–2900, 2011.
- [236] S. M. Steinberg, T. B. Shabaneh, P. Zhang, V. Martyanov, Z. Li, B. T. Malik, T. A. Wood, A. Boni, A. Molodtsov, C. V. Angeles, et al. Myeloid cells that impair immunotherapy are restored in melanomas with acquired resistance to braf inhibitors. *Cancer research*, 77(7):1599–1610, 2017.

- [237] R. Strauss, P. Sova, Y. Liu, Z. Y. Li, S. Tuve, D. Pritchard, P. Brinkkoetter, T. Möller, O. Wildner, S. Pesonen, et al. Epithelial phenotype confers resistance of ovarian cancer cells to oncolytic adenoviruses. *Cancer research*, 69(12):5115–5125, 2009.
- [238] R. Straussman, T. Morikawa, K. Shee, M. Barzily-Rokni, Z. R. Qian, J. Du, A. Davis, M. M. Mongare, J. Gould, D. T. Frederick, et al. Tumour micro-environment elicits innate resistance to raf inhibitors through hgf secretion. *Nature*, 487(7408):500, 2012.
- [239] M. Suarez-Carmona, J. Lesage, D. Cataldo, and C. Gilles. Emt and inflammation: inseparable actors of cancer progression. *Molecular oncology*, 2017.
- [240] A. Subramanian, P. Tamayo, V. K. Mootha, S. Mukherjee, B. L. Ebert, M. A. Gillette, A. Paulovich, S. L. Pomeroy, T. R. Golub, E. S. Lander, et al. Gene set enrichment analysis: a knowledge-based approach for interpreting genome-wide expression profiles. *Proceedings of the National Academy of Sciences*, 102(43):15545–15550, 2005.
- [241] K. Takeda, K.-i. Yasumoto, R. Takada, S. Takada, K.-i. Watanabe, T. Uono, H. Saito, K. Takahashi, and S. Shibahara. Induction of melanocyte-specific microphthalmia-associated transcription factor by wnt-3a. *Journal of Biological Chemistry*, 275(19):14013–14016, 2000.
- [242] F. Talotta, T. Mega, G. Bossis, L. Casalino, J. Basbous, I. Jariel-Encontre, M. Piechaczyk, and P. Verde. Heterodimerization with fra-1 cooperates with the erk pathway to stabilize c-jun in response to the ras oncoprotein. *Oncogene*, 29(33):4732, 2010.
- [243] L. Y. Tan, C. Martini, Z. G. Fridlender, C. S. Bonder, M. P. Brown, and L. M. Ebert. Control of immune cell entry through the tumour vasculature: a missing link in optimising melanoma immunotherapy? *Clinical & translational immunology*, 6(3), 2017.
- [244] E. Theveneau and R. Mayor. Neural crest delamination and migration: from epithelium-to-mesenchyme transition to collective cell migration. *Developmental biology*, 366(1):34–54, 2012.
- [245] J. P. Thiery, H. Acloque, R. Y. Huang, and M. A. Nieto. Epithelial-mesenchymal transitions in development and disease. *cell*, 139(5):871–890, 2009.
- [246] J. P. Thiery and J. P. Sleeman. Complex networks orchestrate epithelial–mesenchymal transitions. *Nature reviews Molecular cell biology*, 7(2):131, 2006.
- [247] A. J. Thomas and C. A. Erickson. The making of a melanocyte: the specification of melanoblasts from the neural crest. *Pigment cell & melanoma research*, 21(6):598–610, 2008.

- [248] I. Tirosh, B. Izar, S. M. Prakadan, M. H. Wadsworth, D. Treacy, J. J. Trombetta, A. Rotem, C. Rodman, C. Lian, G. Murphy, et al. Dissecting the multicellular ecosystem of metastatic melanoma by single-cell rna-seq. *Science*, 352(6282):189–196, 2016.
- [249] B. Titz, A. Lomova, A. Le, W. Hugo, X. Kong, J. Ten Hoeve, M. Friedman, H. Shi, G. Moriceau, C. Song, et al. Jun dependency in distinct early and late braf inhibition adaptation states of melanoma. *Cell discovery*, 2:16028, 2016.
- [250] M. Todaro, M. P. Alea, A. B. Di Stefano, P. Cammareri, L. Vermeulen, F. Iovino, C. Tripodo, A. Russo, G. Gulotta, J. P. Medema, et al. Colon cancer stem cells dictate tumor growth and resist cell death by production of interleukin-4. *Cell stem cell*, 1(4):389–402, 2007.
- [251] S. L. Topalian, M. Sznol, D. F. McDermott, H. M. Kluger, R. D. Carvajal, W. H. Sharfman, J. R. Brahmer, D. P. Lawrence, M. B. Atkins, J. D. Powderly, et al. Survival, durable tumor remission, and long-term safety in patients with advanced melanoma receiving nivolumab. *Journal of clinical oncology*, 32(10):1020, 2014.
- [252] H. D. Tran, K. Luitel, M. Kim, K. Zhang, G. D. Longmore, and D. D. Tran. Transient snail1 expression is necessary for metastatic competence in breast cancer. *Cancer research*, 74(21):6330–6340, 2014.
- [253] S. Tsai, C. Balch, and J. Lange. Epidemiology and treatment of melanoma in elderly patients. *Nature reviews Clinical oncology*, 7(3):148, 2010.
- [254] H. Tsao, M. B. Atkins, and A. J. Sober. Management of cutaneous melanoma. *New England Journal of Medicine*, 351(10):998–1012, 2004.
- [255] J. Tsoi, L. Robert, K. Paraiso, C. Galvan, K. M. Sheu, J. Lay, D. J. Wong, M. Atefi, R. Shirazi, X. Wang, et al. Multi-stage differentiation defines melanoma subtypes with differential vulnerability to drug-induced iron-dependent oxidative stress. *Cancer cell*, 33(5):890–904, 2018.
- [256] A. Tuccitto, M. Tazzari, V. Beretta, F. Rini, C. Miranda, A. Greco, M. Santinami, R. Patuzzo, B. Vergani, A. Villa, et al. Immunomodulatory factors control the fate of melanoma tumor initiating cells. *Stem Cells*, 34(10):2449–2460, 2016.
- [257] M. Turcotte, K. Spring, S. Pommey, G. Chouinard, I. Cousineau, J. George, G. M. Chen, D. M. Gendoo, B. Haibe-Kains, T. Karn, et al. Cd73 is associated with poor prognosis in high-grade serous ovarian cancer. *Cancer research*, 75(21):4494–4503, 2015.
- [258] S. Ugurel, R. Hildenbrand, A. Zimpfer, P. La Rosee, P. Paschka, A. Sucker, P. Keikavoussi, J. Becker, W. Rittgen, A. Hochhaus, et al. Lack of clinical efficacy of imatinib in metastatic melanoma. *British journal of cancer*, 92(8):1398, 2005.

- [259] S. Ugurel, R. K. Thirumaran, S. Bloethner, A. Gast, A. Sucker, J. Mueller-Berghaus, W. Rittgen, K. Hemminki, J. C. Becker, R. Kumar, et al. B-raf and n-ras mutations are preserved during short time in vitro propagation and differentially impact prognosis. *PLoS one*, 2(2):e236, 2007.
- [260] E. M. Van Allen, N. Wagle, A. Sucker, D. J. Treacy, C. M. Johannessen, E. M. Goetz, C. S. Place, A. Taylor-Weiner, S. Whittaker, G. V. Kryukov, et al. The genetic landscape of clinical resistance to raf inhibition in metastatic melanoma. *Cancer discovery*, 4(1):94–109, 2014.
- [261] F. A. Vargas, A. J. Furness, I. Solomon, K. Joshi, L. Mekkaoui, M. H. Lesko, E. M. Rota, R. Dahan, A. Georgiou, A. Sledzinska, et al. Fc-optimized anti-cd25 depletes tumor-infiltrating regulatory t cells and synergizes with pd-1 blockade to eradicate established tumors. *Immunity*, 46(4):577–586, 2017.
- [262] A. Verfaillie, H. Imrichova, Z. K. Atak, M. Dewaele, F. Rambow, G. Hulselmans, V. Christiaens, D. Svetlichnyy, F. Luciani, L. Van den Mooter, et al. Decoding the regulatory landscape of melanoma reveals teads as regulators of the invasive cell state. *Nature communications*, 6:6683, 2015.
- [263] E. Vial and C. J. Marshall. Elevated erk-map kinase activity protects the fos family member fra-1 against proteasomal degradation in colon carcinoma cells. *Journal of cell science*, 116(24):4957–4963, 2003.
- [264] N. Wagle, E. M. Van Allen, D. J. Treacy, D. T. Frederick, Z. A. Cooper, A. Taylor-Weiner, M. Rosenberg, E. M. Goetz, R. J. Sullivan, D. N. Farlow, et al. Map kinase pathway alterations in braf-mutant melanoma patients with acquired resistance to combined raf/mek inhibition. *Cancer discovery*, 4(1):61–68, 2014.
- [265] T. L. Walunas, D. J. Lenschow, C. Y. Bakker, P. S. Linsley, G. J. Freeman, J. M. Green, C. B. Thompson, and J. A. Bluestone. Ctl4 can function as a negative regulator of t cell activation. *Immunity*, 1(5):405–413, 1994.
- [266] P. T. Wan, M. J. Garnett, S. M. Roe, S. Lee, D. Niculescu-Duvaz, V. M. Good, C. M. Jones, C. J. Marshall, C. J. Springer, D. Barford, et al. Mechanism of activation of the raf-erk signaling pathway by oncogenic mutations of b-raf. *Cell*, 116(6):855–867, 2004.
- [267] H. Wang, S. Lee, C. L. Nigro, L. Lattanzio, M. Merlano, M. Monteverde, R. Matin, K. Purdie, N. Mladkova, D. Bergamaschi, et al. Nt5e (cd73) is epigenetically regulated in malignant melanoma and associated with metastatic site specificity. *British journal of cancer*, 106(8):1446, 2012.
- [268] L. Wang, J. Fan, L. F. Thompson, Y. Zhang, T. Shin, T. J. Curiel, and B. Zhang. Cd73 has distinct roles in nonhematopoietic and hematopoietic cells to promote tumor growth in mice. *The Journal of clinical investigation*, 121(6):2371–2382, 2011.

- [269] I. R. Watson, C.-J. Wu, L. Zou, J. E. Gershenwald, and L. Chin. Genomic classification of cutaneous melanoma, 2015.
- [270] E. J. Wherry. T cell exhaustion. *Nature immunology*, 12(6):492, 2011.
- [271] D. S. Widmer, K. S. Hoek, P. F. Cheng, O. M. Eichhoff, T. Biedermann, M. I. Raaijmakers, S. Hemmi, R. Dummer, and M. P. Levesque. Hypoxia contributes to melanoma heterogeneity by triggering hif1 α -dependent phenotype switching. *Journal of Investigative Dermatology*, 133(10):2436–2443, 2013.
- [272] B. J. Wilson, K. R. Saab, J. Ma, T. Schatton, P. Putz, Q. Zhan, G. F. Murphy, M. Gasser, A. M. Waaga-Gasser, N. Y. Frank, et al. Abcb5 maintains melanoma-initiating cells through a pro-inflammatory cytokine signaling circuit. *Cancer research*, pages canres–0582, 2014.
- [273] K.-K. Wong, Y. T. Tsang, M. T. Deavers, S. C. Mok, Z. Zu, C. Sun, A. Malpica, J. K. Wolf, K. H. Lu, and D. M. Gershenson. Braf mutation is rare in advanced-stage low-grade ovarian serous carcinomas. *The American journal of pathology*, 177(4):1611–1617, 2010.
- [274] C. Yan, W. A. Grimm, W. L. Garner, L. Qin, T. Travis, N. Tan, and Y.-P. Han. Epithelial to mesenchymal transition in human skin wound healing is induced by tumor necrosis factor- α through bone morphogenic protein-2. *The American journal of pathology*, 176(5):2247–2258, 2010.
- [275] G. G. Yegutkin, F. Marttila-Ichihara, M. Karikoski, J. Niemelä, J. P. Laurila, K. Elima, S. Jalkanen, and M. Salmi. Altered purinergic signaling in cd73-deficient mice inhibits tumor progression. *European journal of immunology*, 41(5):1231–1241, 2011.
- [276] A. Young, S. F. Ngiow, D. S. Barkauskas, E. Sult, C. Hay, S. J. Blake, Q. Huang, J. Liu, K. Takeda, M. W. Teng, et al. Co-inhibition of cd73 and a2ar adenosine signaling improves anti-tumor immune responses. *Cancer Cell*, 30(3):391–403, 2016.
- [277] A. Young, S. F. Ngiow, J. Madore, J. Reinhardt, J. Landsberg, A. Chitsazan, J. Rautela, T. Bald, D. S. Barkauskas, E. Ahern, et al. Targeting adenosine in braf-mutant melanoma reduces tumor growth and metastasis. *Cancer research*, 77(17):4684–4696, 2017.
- [278] H. L. Young, E. J. Rowling, M. Bugatti, E. Giurisato, N. Luheshi, I. Arozarena, J.-C. Acosta, J. Kamarashev, D. T. Frederick, Z. A. Cooper, et al. An adaptive signaling network in melanoma inflammatory niches confers tolerance to mapk signaling inhibition. *Journal of Experimental Medicine*, pages jem–20160855, 2017.

-
- [279] M. Yu, A. Bardia, B. S. Wittner, S. L. Stott, M. E. Smas, D. T. Ting, S. J. Isakoff, J. C. Ciciliano, M. N. Wells, A. M. Shah, et al. Circulating breast tumor cells exhibit dynamic changes in epithelial and mesenchymal composition. *science*, 339(6119):580–584, 2013.
- [280] L. H. Zapico, M. Parodi, C. Cantoni, C. Lavarello, J. L. Fernández-Martínez, A. Petretto, E. J. DeAndrés-Galiana, M. Balsamo, A. López-Soto, G. Pietra, et al. Nk cell editing mediates epithelial to mesenchymal transition via phenotypic and proteomic changes in melanoma cell lines. *Cancer research*, pages canres–1891, 2018.
- [281] P. E. Zarek, C.-T. Huang, E. R. Lutz, J. Kowalski, M. R. Horton, J. Linden, C. G. Drake, and J. D. Powell. A 2a receptor signaling promotes peripheral tolerance by inducing t-cell anergy and the generation of adaptive regulatory t cells. *Blood*, 111(1):251–259, 2008.
- [282] B. Zhang. Cd73: a novel target for cancer immunotherapy. *Cancer research*, 70(16):6407–6411, 2010.
- [283] X. Zheng, J. L. Carstens, J. Kim, M. Scheible, J. Kaye, H. Sugimoto, C.-C. Wu, V. S. LeBleu, and R. Kalluri. Epithelial-to-mesenchymal transition is dispensable for metastasis but induces chemoresistance in pancreatic cancer. *Nature*, 527(7579):525, 2015.
- [284] H. Zimmermann. 5'-nucleotidase: molecular structure and functional aspects. *Biochemical Journal*, 285(Pt 2):345, 1992.

Acknowledgment / Danksagung

Zu allererst und vor allem möchte ich mich bei meinem Doktorvater, Prof. Dr. Michael Hölzel, bedanken. Sowohl fachlich, als auch menschlich, war er mir zu jeder Zeit des Projektes ein guter Ansprechpartner, ich habe mich durch ihn optimal gefördert, gefordert und unterstützt gefühlt. Vielen Dank für die tollen Diskussionen, die zahlreichen Ideen und Vorschläge für die Durchführung dieser Arbeit! Ich würde mir nichts anders wünschen in der Rückschau. Vielen Dank für diese prägenden Jahre.

Auch meinem Zweitkorrektor, Prof. Dr. Waldemar Kolanus, möchte ich besonderen Dank aussprechen. Nicht nur für die Zeit, die es in Anspruch nimmt eine solche Arbeit zu bewerten und abzuschließen, sondern auch für seine Beratung und Hilfe auf dem Weg dahin.

Der ganzen AG Hölzel möchte ich danken für den Zusammenhalt, die Hilfsbereitschaft und das tolle Arbeitsklima. Ich habe mich sehr wohlgeföhlt die Jahre hindurch.

Auch bei allen anderen die mich auf diesem Weg begleitet haben möchte ich mich bedanken, insbesondere bei Jonathan und Stefan. Ihr habt mich unterstützt, jeder auf die eigene Art. Zum erfolgreichen Abschluss habt ihr maßgeblich beigetragen.

Ein großer Dank von ganzem Herzen gilt meinen Eltern und meiner Familie, die mir immer Rückhalt gegeben haben so gut sie es konnten und vor allem nie den Glauben verloren haben, dass gelingt was ich mir vornehme. Sehr viel meiner Energie und Durchhaltevermögen erhalte ich von ihnen.

Zu aller letzt aber danke ich meinem wunderbaren Sohn Elias, der trotz aller Strapazen und zeitlichen Engpässen, die er durch diese Arbeit wegstecken musste, nie den Mut verloren hat und sich zu einem tollen Menschen entwickelt. Er ist es, der mir die Augen aufhält für die wirklich wichtigen Dinge.

List of publications

0. **Reinhardt J**, Effern M, Hölzel M. Molecular mechanisms governing melanoma cell plasticity in response to therapy-induced stress. *Br J Cancer*. 2018 [under revision].
1. Breitbach M, Kimura K, Luis TC, Fuegemann CJ, Woll PS, Hesse M, Facchini R, Rieck S, Jobin K, **Reinhardt J**, Ohneda O, Wenzel D, Geisen C, Kurts C, Kastenmüller W, Hölzel M, Jacobsen SEW, Fleischmann BK. In Vivo Labeling by CD73 Marks Multipotent Stromal Cells and Highlights Endothelial Heterogeneity in the Bone Marrow Niche. *Cell Stem Cell*. 2018 Feb 1;22(2):262-276.
2. **Reinhardt J**, Landsberg J, Schmid-Burgk JL, Bibiloni Ramis B, Bald T, Glodde N, Lopez-Ramos D, Young A, Ngiow SF, Nettersheim D, Schorle H, Quast T, Kolanus W, Schadendorf D, Long GV, Madore J, Scolyer RA, Ribas A, Smyth MJ, Tumeh PC, Tuting T, Hölzel M. MAPK signaling and inflammation link melanoma phenotype switching to induction of CD73 during immunotherapy. *Cancer Res*. 2017 Sep 1;77(17):4697-4709.
3. Young A, Ngiow SF, Madore J, **Reinhardt J**, Landsberg J, Chitsazan A, Rautela J, Bald T, Barkauskas D, Ahern E, Huntington N, Schadendorf D, Long GV, Boyle GM, Hölzel M, Scolyer RA, Smyth MJ. Targeting adenosine in BRAF-mutant melanoma reduces tumor growth and metastasis. *Cancer Res*. 2017 Sep 1;77(17):4684-4696.
4. Schmid-Burgk JL, Chauhan D, Schmidt T, Ebert TS, **Reinhardt J**, Endl E, Hornung V. A Genome-wide CRISPR (Clustered Regularly Interspaced Short Palindromic Repeats) Screen Identifies NEK7 as an Essential Component of NLRP3 Inflammasome Activation. *J Biol Chem*. 2016 Jan 1;291(1):103-9.
5. Riesenberger S, Groetchen A, Siddaway R, Bald T, **Reinhardt J**, Smorra D, Kohlmeyer J, Renn M, Phung B, Aymans P, Schmidt T, Hornung V, Davidson I, Goding CR, JXnsson G, Landsberg J, Tüting T, Hölzel M. MITF and c-Jun antagonism interconnects melanoma dedifferentiation with pro-inflammatory cytokine responsiveness and myeloid cell recruitment. *Nat Commun*. 2015 Nov 4;6:8755.
6. Kopatz J, Beutner C, Welle K, Bodea LG, **Reinhardt J**, Claude J, Linnartz-Gerlach B, Neumann H. Siglec-h on activated microglia for recognition and engulfment of glioma cells. *Glia*. 2013 Jul 61(7):1122-33.